UNIVERSITÉ DE MONTRÉAL

MÉCANISMES PHYSIQUES ET FONDEMENTS THÉORIQUES DE LA RÉCUPÉRATION D'ÉNERGIE MICRO-ONDES AMBIANTE POUR LES DISPOSITIFS SANS FIL À FAIBLE CONSOMMATION

CARLOS HENRIQUE PETZL LORENZ

DÉPARTEMENT DE GÉNIE ÉLECTRIQUE

ÉCOLE POLYTECHNIQUE DE MONTRÉAL

MÉMOIRE PRÉSENTÉ EN VUE DE L'OBTENTION

DU DIPLÔME DE MAÎTRISE ÈS SCIENCES APPLIQUÉES

(GÉNIE ÉLECTRIQUE)

DÉCEMBRE 2015

UNIVERSITÉ DE MONTRÉAL

ÉCOLE POLYTECHNIQUE DE MONTRÉAL

Ce mémoire intitulé :

MÉCANISMES PHYSIQUES ET FONDEMENTS THÉORIQUES DE LA RÉCUPÉRATION D'ÉNERGIE MICRO-ONDES AMBIANTE POUR LES DISPOSITIFS SANS FIL À FAIBLE CONSOMMATION

présenté par : PETZL LORENZ Carlos Henrique

en vue de l'obtention du diplôme de : Maîtrise ès Sciences Appliquées

a été dûment accepté par le jury d'examen constitué de :

M. LAURIN Jean-Jacques, Ph. D., président

M. WU Ke, Ph. D., membre et directeur de recherche

M. CONSTANTIN Nicolas, Ph. D., membre

DÉDICACE

À mon épouse Antonia Yume Eiri Trebien Lorenz, qui m'a appuyé inconditionnellement pendant la maîtrise,

à mes parents Curt et Cristina Lorenz, qui m'ont enseigné l'importance de persévérer et de me dévouer au travail, mais aussi de garder du temps pour la famille et les amis,

à Simon Hemour pour m'avoir guidé pendant ce travail de recherche et pour toujours avoir été présent pour discuter de nouvelles idées.

REMERCIEMENTS

Je tiens à remercier en premier lieu à Dieu pour toutes ses bénédictions qu'il m'a offertes.

Je tiens aussi à exprimer mes remerciements sincères à mon directeur de recherche, professeur Ke Wu, par son soutien et ses conseils donnés au cours de mes travaux de recherches; aussi comme par son soutien lors de mes moments de doute.

Un gros merci à Simon Hemour, qui était toujours présent pour discuter de nouvelles idées et méthodes pour résoudre les problèmes auxquelles j'ai fait face. Je suis certain que sans ton aide ce travail ne serait pas arrivé si loin.

Je voulais aussi remercier à tous les membres de l'équipe technique de Poly GRAMES, par leur soutien dans les fabrication et caractérisation des prototypes, aussi bien que par leur support informatique, à savoir Jules Gauthier, Traian Antonescu, Maxime Thibault, Steve Dubé et Jean-Sébastien Décarie. Je tiens aussi à remercier à Nathalie Levesque de l'École Polytechnique qui m'a toujours aidé lorsque des problèmes administratifs apparaissaient.

Je veux également remercier les membres du jury pour le temps qu'ils ont passé à la révision de ce mémoire. Et aux collègues de Poly GRAMES qui ont contribué directement ou indirectement au bon déroulement de ma maîtrise.

Je tiens finalement à exprimer ma plus profonde gratitude à mon épouse Antonia Yume Eiri Trebien Lorenz pour son soutien inconditionnel tout au long de ces années de maîtrise, et aussi à mes parents Curt et Cristina Lorenz qui ont mis plusieurs de leurs années de vie à ma formation, ce qui m'a permis arriver là où je suis maintenant.

RÉSUMÉ

La récupération d'énergie micro-ondes ambiantes (REMA) pour alimenter de circuits à faible consommation et faible rapport cyclique a été le sujet de plusieurs publications au cours des dernières années. L'intérêt par ce sujet a été poussé principalement par les diverses applications prévues par l'Internet des Objets, l'Immotique et les nouveaux développements des dispositifs pour les « *Body Area Netwoks* ». Un des besoins récurrents que l'on retrouve parmi plusieurs de ces applications est une source d'énergie intégrée, qui ne nécessiterait pas de maintenance régulière, qui serait de petite taille et d'un faible poids. Pour beaucoup d'applications à venir, les piles sont trop encombrantes et demandent un plan de maintenance pour les recharger ou les remplacer, ce qui n'est pas possible. Dans ce contexte, un autre type de source d'énergie est nécessaire. La récupération d'énergie ambiante est ici proposée comme une source alternative de puissance pour ces circuits à faible consommation. Ce travail explore plus spécifiquement la récupération d'énergie micro-ondes ambiantes par l'utilisation centrale de circuits redresseurs à diodes.

Un modèle mathématique a tout d'abord été développé pour décrire les mécanismes qui contribuent au processus de redressement d'énergie micro-ondes aux niveaux de puissance que l'on retrouve dans l'ambiant. Ce modèle est évalué en utilisant des résultats de simulation et de mesures réalisées sur trois prototypes fabriqués dans le cadre de cette maîtrise. Le modèle développé inclut les pertes dans les composants parasitiques de l'élément non linéaire utilisé pour le redressement d'énergie ainsi que les pertes d'insertion du réseau d'adaptation d'impédance.

Partant de ce modèle, deux possibilités sont explorées pour améliorer l'efficacité de conversion de puissance des redresseurs micro-ondes actuels, particulièrement pour ceux fonctionnant à des niveaux de puissance trouvés dans la REMA. On considèrera dans ce travail que la plage de puissance correspondant à la REMA se situe à une valeur de crête de -30 dBm, et à des niveaux de puissance moyenne bien en dessous de ce seuil.

Un circuit hybride coopératif de récupération d'énergie ambiante va ensuite être proposé. Celui-ci présente la particularité de n'être basé que sur un seul composant non linéaire pour redresser l'énergie micro-ondes et l'énergie mécanique de façon coopérative. La théorie, les simulations ainsi que les mesures montrent que la puissance totale récupérée par ce schéma est jusqu'à deux fois plus forte que la puissance combinée de deux circuits indépendants, utilisés pour exploiter les deux sources séparément.

L'aspect *composant non linéaire* a aussi été développé dans ce travail, à travers une étude sur le rôle critique que joue la responsivité en courant du composant sur les performances globale du circuit de redressement. On démontre ainsi pour la première fois que l'utilisation de diodes tunnel ayant une responsivité en courant plus élevée que la valeur atteignable avec des diodes Schottky permet de dépasser l'efficacité de récupération d'énergie micro-ondes atteignable avec ces dernières diodes. L'efficacité de récupération de puissance mesurée pour un signal RF d'entrée de -30 dBm à 2.4 GHz est de 18.2 %, tandis que l'efficacité de conversion pour un circuit similaire utilisant des diodes Schottky, telle que ceux présentés dans la première partie de ce travail, ne dépasse pas 11 % dans de conditions similaires de fréquence et de puissance. Notons par ailleurs que jusqu'à la date de publication des articles présentés dans ce mémoire de maîtrise la plus haute efficacité de récupération de puissance micro-ondes publiée était proche de 5 % pour une puissance à l'entrée de -30 dBm et une fréquence proche de 2 GHz.

Enfin, les compétences acquises lors des études ci-dessus ont été mises à profit pour une application de transfert de puissance par micro-ondes. Une rectenne opérant à 94 GHz est ainsi présentée, dont l'efficacité de conversion de puissance égale à 37.7 % a été obtenue pour une puissance à l'entrée de 3 dBm. Cette rectenne est proposée comme source alternative de puissance pour les microrobots, qui en raison de leur taille et leur poids limités ne peuvent pas embarquer de piles.

ABSTRACT

Powering low consumption and low duty cycle devices and circuits using Ambient Microwave Energy Harvesting (AMEH) has been the subject of several investigations in recent years. The interest for this research topic has been promoted mainly by various and new applications driven mainly by the Internet of things, Building Automation and new developments in devices for the Body Area Netwoks. A common characteristic among several of these applications is the need for a wireless source which does not require regular maintenance, and has a small size and low weight. Batteries are often too cumbersome and require a maintenance plan to recharge or replace them, which is not always possible. A new source of energy is thus necessary. Ambient energy harvesting is proposed as an alternative source of power to these low power consumption devices and circuits. This M.A.Sc. work is developed to explore the microwave ambient energy harvesting using diode rectifier circuits.

A mathematical model is first developed to explain the mechanisms that contribute to the process of recovery of microwave energy in the range of power found in the ambient microwave energy harvesting applications. An evaluation of this model is made using simulation results and then measurements results from three prototypes developed under this M.A.Sc. program. The results show an excellent agreement between the three methods. The developed model includes losses in the parasitic components of the non-linear element used for the rectification of energy as well as the impedance matching network insertion losses.

Based on this model, two possible ways of improving the efficiency of ambient microwave power rectifiers at the power levels found in the AMEH are explored. In this work, it is considered that the AMEH takes place within the range of powers with a peak value of -30 dBm, however at average power levels well below this threshold.

First, a cooperative hybrid circuit of ambient energy harvesting is presented where collected microwave and mechanical energies are converted in a cooperative manner through a single non-linear component. Theory, simulations and measurements show that the total power recovered by the proposed scheme can provide up to twice the efficiency of a circuit combining the output of two independent harvesters.

Then, a work demonstrating for the first time that the limitations of a Schottky diode harvester can be overcome by using backward tunnel diodes is presented. It is shown that the

limitation reached by the Schottky diodes half a century ago can be overcome thanks to a higher current responsivity obtained through tunneling transport. The measured power recovery efficiency was equal to 18.2% when a -30 dBm signal at 2.4 GHz was applied to the input of the microwave energy harvesting circuit. The efficiency of conversion for a similar circuit using Schottky diodes, which is presented in the first chapter together with the mathematical model, does not exceed 11% at the same input power level and similar frequency. On the date of publication of the articles presented in this thesis, the highest published microwave power conversion efficiency was close to 5% for input power levels equal to -30 dBm and frequency close to 2 GHz.

Finally, an application of microwave power transfer is presented. A rectenna operating at 94 GHz is built and measured, an energy conversion efficiency equal to 37.7% was obtained for an input power equal to 3 dBm. This rectenna is proposed as an alternative power source for microrobots, which may not use batteries due to their small size and light weight.

TABLE DES MATIÈRES

LISTE DES TABLEAUX

LISTE DES FIGURES

LISTE DES SIGLES ET ABRÉVIATIONS

L'abréviation utilisée en anglais est donnée à droite entre parenthèses.

BAN	Body Area Network
ca	Courant alternatif (*ac*)
cc	Courant continu (*dc*)
CPW	Ligne de transmission coplanaire (*CPW*)
ECP	Efficacité de conversion de puissance (*PCE*)
IdO	Internet d'objets (*IoT*)
RECTENNE	Circuit composé par une antenne et un circuit de redressement (*RECTENNA*)
REM	Récupération d'énergie micro-ondes (*MPH*)
REMA	Récupération d'énergie micro-ondes ambiantes (*AMPH*)
RF	Radiofréquence
ROS	Rapport d'onde stationnaire (*SWR*)
TEM	Transmission d'énergie par micro-ondes (*MPT*)

LISTE DES SYMBOLES

α	Constante d'atténuation de la ligne de transmission
α_r	Constante équivalente d'atténuation de la ligne de transmission
β	Constante de phase de la ligne de transmission
γ	Exposant de propagation de la ligne de transmission
η_m	Efficacité du réseau d'adaptation d'impédances
η_p	Efficacité parasitique de la diode
η_{RFDC}	Efficacité de conversion de puissance RF/Micro-Ondes en cc
η_{SL}	Efficacité du transfert de puissance cc de la source à la charge
$\mathcal{R}_I$	Responsivité en courant
$\mathcal{R}_{I0}$	Responsivité en courant avec un courant de polarisation nul
C_j	Capacitance de jonction
C_{j0}	Capacitance de jonction avec un courant de polarisation nul
k	Constante de Boltzmann
N	Facteur d'idéalité de la diode
q	Charge élémentaire
Q	Facteur de qualité
Qr	Facteur de qualité requis
Qm	Facteur de qualité obtenu avec le réseau d'adaptation d'impédances
R_j	Résistance de jonction
R_{j0}	Résistance de jonction avec un courant de polarisation nul
R_s	Résistance série
V_t	Tension thermique

CHAPITRE 1 INTRODUCTION

L'utilisation à grande échelle de dispositifs sans-fils à faible consommation; comme les capteurs de température, de mouvement et de sollicitation mécanique; est la base des nouveaux schémas proposés par l'IdO (Internet des Objets), les bâtiments intelligents (aussi connu sous le nom d'Immotique) et des dispositifs de suivi vestimentaires ou implantables utilisés dans le BAN (*Body Area Network*) [1, 2]. Une limitation commune à plusieurs de ces technologies est la source d'énergie qui doit être sans fil, petite, légère et qui ne doit pas nécessiter une maintenance régulière – caractéristiques qui souvent excluent les piles et les sources plus traditionnelles. La récupération d'énergie ambiante a déjà été proposée dans plusieurs travaux comme une solution pour ce problème [1-5], dans lesquels l'énergie solaire, les vibrations mécaniques ou les micro-ondes présentes autour de nous sont utilisés pour alimenter de petits dispositifs à faible consommation.

Ce travail de M.Sc.A. explore de nouveaux moyens pour augmenter l'efficacité de récupération d'énergie micro-ondes ambiantes (REMA). La REMA est très similaire à la transmission d'énergie par micro-ondes (TEM), avec une nuance importantes en ce qui concerne la différence de plage de puissances d'opération de ces applications. Dans ce mémoire nous allons considérer comme REMA les travaux dans lesquels la puissance micro-ondes à l'entrée du circuit de récupération ne dépasse pas -30 dBm, ce qui correspond typiquement à la puissance crête maximale souvent disponible dans les environnements urbain selon des études réalisées à Tokyo, Atlanta et Londres [6-8] (ces travaux montrent de puissances crête allant jusqu'à -20 dBm dans certains emplacements, toutefois l'incidence de puissances si élevées est trop rare et n'est pas considérée comme une source possible dans ce travail). Ce seuil de puissance a été estimé pour une antenne omnidirectionnelle avec un gain de 0 dBi.

Le redressement efficace des micro-ondes dans les puissances en dessous de -30 dBm est un des plus grands défis à résoudre pour que la REMA puisse être utilisée pour des applications commerciales. L'état de l'art des circuits de récupération et de transmission des micro-ondes ne dépasse pas 5% d'efficacité de conversion de puissance RF en cc (courant continu) quand il s'agit de puissances de l'ordre de -30 dBm à l'entrée du circuit de redressement [9]. Le manque d'un modèle mathématique pour expliquer les mécanismes de pertes et de conversion de puissance à ces faibles puissances limite aussi les efforts pour trouver une solution qui augmenterait l'efficacité de conversion de puissance (ECP) [10].

Ce travail débute par la proposition d'un modèle mathématique pour expliquer les mécanismes liés à la conversion d'énergie micro-ondes en cc par les circuits de redressement à diodes. Ce modèle comprend une étude de l'impact de l'impédance du circuit non-linéaire utilisé pour le redressement dans la bande maximale qui peut être adaptée et dans les pertes d'insertion du circuit d'adaptation d'impédance. Trois prototypes sont présentés et comparés aux prévisions du modèle mathématique développé avec une très bonne concordance entre les résultats prévus, mesurés, et simulés. Dans cette même étude, une comparaison du modèle mathématique proposé avec d'autres modèles déjà publiés est présentée, où les points forts et les faiblesses de chaque méthode sont discutés.

Ensuite dans le chapitre 3 un système coopératif de récupération d'énergie ambiante est proposé. En utilisant une extension du modèle mathématique, où deux signaux sont considérés à l'entrée du circuit, il y est démontré que l'efficacité de conversion de puissance peut être augmentée par la combinaison de différentes sources dans le même élément non-linéaire de redressement de puissance. Un circuit hybride coopératif dans lequel la puissance micro-ondes et la puissance provenant de la vibration mécanique sont combinées dans le même élément non-linéaire, est utilisé pour démontrer le gain dans l'ECP prévu par la théorie. Des résultats de simulation et de mesures confirment les résultats prévus par la théorie, où la puissance récupérée par le système coopératif peut atteindre un gain proche de 3 dB, si comparée à la puissance recueillie par des circuits de redressement isolés et postérieurement combinés en cc. Ce gain diminue graduellement à mesure que la puissance d'entrée monte à cause d'un effet de mixage entre les deux signaux d'entrée dans le dispositif non linéaire. Toutefois la méthode se montre très efficace dans la plage de puissances d'opération de la REMA.

Dans le chapitre 4 l'effet de la responsivité en courant du dispositif non linéaire utilisé pour le redressement est étudié. Il y est démontré que l'ECP des circuits de récupération d'énergie micro-ondes basés sur les dispositifs utilisant l'effet thermo-ionique, comme est le cas des diodes Schottky, est limité par la tension thermique V_t. Dans ce chapitre l'utilisation de diodes tunnel, qui n'ont pas leur responsivité limitée par la tension thermique, est proposée pour la première fois pour les circuits de REMA. L'utilisation d'une diode tunnel ayant une responsivité 12% plus élevée que le maximum atteignable par les dispositifs thermo-ioniques, résulte en une ECP mesurée proche de 18% pour une puissance à l'entrée égale à -30 dBm. Cela signifie une amélioration de 65 % par

rapport aux meilleurs résultats mesurés pour les prototypes construits utilisant les diodes Schottky, lesquels sont présentés dans le chapitre 2.

Une application de transmission de puissance par micro-ondes est ensuite présentée. L'utilisation d'une rectenne à 94 GHz comme source de puissance pour de micro-robots est proposée. Ces robots d'une taille très petite ont aussi le besoin d'une source d'énergie sans fil, légère et de taille réduite. Toutefois les niveaux de puissance disponibles dans la REMA ne sont pas assez élevés pour garantir le fonctionnement fiable et continu de ces petits robots. Par conséquent un schéma de transmission d'énergie sans fils est proposé. Une ECP de 37.7 % est mesurée pour une puissance de 3 dBm à l'entrée du circuit de redressement. La taille totale de la rectenne comprise de circuit de redressement et antenne est de 5.62 mm^2.

Finalement, ce mémoire se conclu par une présentation des nouveaux concepts développés et une discussion de leurs possibles évolutions.

Les principales contributions originales apportées par ce mémoire de maîtrise sont les suivants :

- Développement d'un modèle mathématique qui décrit le mécanisme de redressement de puissance micro-ondes en cc dans les faibles puissances où la REMA prend place, y incluant une estimation des pertes dans le réseau d'adaptation d'impédances.
- Proposition et démonstration de la récupération d'énergie ambiante hybride coopérative. Une démonstration a été présentée où la puissance provenant de la vibration mécanique et des micro-ondes ambiantes ont été combinées dans le même élément non linéaire. La puissance récupérée par l'approche hybride a présenté un gain allant jusqu'à 3 dB dans la puissance de sortie pour les puissances d'entrée proches de -40 dBm, quand comparé à la puissance récupérée par deux circuits indépendants et postérieurement combinée. Un autre grand avantage du circuit proposé est la combinaison de la puissance rectifiée par l'élément non linéaire de redressement sans le besoin d'un circuit supplémentaire, lequel ajouterait des pertes dans le circuit et augmenterais son coût et complexité.
- Proposition et démonstration d'un circuit de REMA utilisant de diodes Tunnel avec une responsivité en courant plus élevée que celle atteignable avec les diodes Schottky. L'ECP mesurée à -30 dBm et 2.4 GHz a atteint 18.2 %, soit une multiplication par un facteur 3

pour les circuits de REMA opérant dans de bandes de fréquences similaires et publiés jusqu'à la date d'obtention de ce résultat, et un gain de 61 % quand comparé au meilleur résultat obtenu avec une diode Schottky, lequel a été présenté dans le Chapitre 2.

Ce mémoire est présenté par articles et reprend trois articles dont je suis l'auteur principal, présentés dans l'ordre suivant :

a. Carlos H. P. Lorenz; Simon Hemour; Ke Wu. (2015). "Physical Mechanism and Theoretical Foundation of Ambient RF Power Harvesting for Wireless Devices." IEEE Transactions on Microwave Theory and Techniques.

b. Carlos H. P. Lorenz; Simon Hemour; Weiqun Liu; Adrien Badel; Fabien Formosa, Ke Wu. (2015). "Hybrid Power Harvesting for Increased Power Conversion Efficiency". IEEE Microwave and Wireless Components Letters

c. Lorenz, C. H. P.; Hemour, S.; Wenjun Li; Yi Xie; Gauthier, J.; Fay, P.; Ke Wu. (2015). "Breaking the efficiency barrier for Ambient Microwave Power Harvesting with Heterojunction Backward Tunnel Diodes." IEEE Transactions on Microwave Theory and Techniques.

L'article (a) a été soumis dans le 1er septembre 2015 et est présentement en révision. L'article (b) a été accepté et est disponible depuis le 18 août 2015. L'article (c) a été soumis le 1er juillet 2015 et a été accepté le 13 octobre 2015. Ce dernier article est une extension d'un travail présenté à la conférence IMS 2015, lequel n'est pas repris dans ce travail.

Un quatrième article est aussi repris dans la fin de ce mémoire de maîtrise, dont je suis le premier co-auteur ("*Equally Contributing Authors*"), ayant développé le circuit, réalisé les mesures et contribué dans la rédaction de la partie de présentation des résultats obtenus. L'article est nommé ci-dessous :

d. Hemour, S.; Lorenz, Carlos HP; Wu, Ke. (2015). "Small-Footprint Wideband 94GHz Rectifier for Swarm Micro-Robotics." in IEEE MTT-S International Microwave Symposium (IMS). Phoenix, AZ, USA.

Les travaux listés ci-dessous ont aussi été réalisés dans le cadre de cette maîtrise, mais ne sont pas inclus dans ce mémoire, vu que je ne suis pas leur auteur principal ou pour éviter la répétition de contenu.

e. Lorenz, C. H. P.; Hemour, S.; Wu, Ke. (2015). "Modeling and Influence of Matching Network Insertion Losses on Ambient Microwave Power Harvester." in IEEE MTT-S International Conference on Numerical Electromagnetic and Multiphysics Modeling and Optimization (NEMO). Ottawa (ON) Canada.

f. Lorenz, C. H. P.; Hemour, S.; Wenjun Li; Yi Xie; Gauthier, J.; Fay, P.; Ke Wu, (2015). "Overcoming the efficiency limitation of low microwave power harvesting with backward tunnel diodes," in IEEE MTT-S International Microwave Symposium (IMS). Phoenix, AZ USA.

g. Hemour, S., et al. (2014). "Towards Low-Power High-Efficiency RF and Microwave Energy Harvesting." IEEE Transactions on Microwave Theory and Techniques 62(4) : 965-976.

h. Application de brevet de la propriété intellectuelle déposée avec le numéro P142583. Relié au travail de récupération hybride coopérative d'énergie ambiante.

CHAPITRE 2 MODÉLISATION MATHÉMATIQUE DU REDRESSEMENT D'ÉNERGIE MICRO-ONDES AMBIENTES

2.1 Introduction

La compréhension des mécanismes liés aux processus de récupération de puissance est primordiale pour pouvoir proposer des méthodes permettant d'améliorer l'efficacité des circuits de récupération de puissance micro-ondes ambiantes. Dans la majorité des articles publiés à ce jour, on essaye d'obtenir les meilleurs résultats possibles grâce à des simulations réalisées avant la fabrication de prototypes, sans toutefois expliquer les raisons pour lesquelles une topologie présente de meilleurs résultats qu'une autre.

Il faut ajouter à cet état des lieux que les modèles mathématiques proposés jusqu'à maintenant ne permettent pas de faire de bonnes prédictions aux faibles puissances où la REMA prend place. Dans ces modèles, les diodes sont considérées comme des interrupteurs parfaits, dont l'impédance s'approche de zéro quand la tension de seuil est dépassée, et d'infinie quand la tension reste en dessous de ce seuil. L'étude présentée ici montre que cette simplification ne peut pas être utilisée dans les faibles puissances, vu que les tensions d'opération restent souvent en dessous ou très proches des tensions de conduction des diodes.

De plus, notre modèle mathématique inclue pour la première fois les pertes dues au réseau d'adaptation d'impédance. La théorie dérivée pour calculer les pertes dans le réseau d'adaptation d'impédances peut facilement être utilisée dans d'autres applications (autres que les circuits de récupération d'énergie micro-ondes ambiantes).

Dans ce chapitre, présenté dans un format d'article, la dérivation du modèle mathématique est premièrement présentée. Dans la suite une comparaison des prévisions est faite avec les résultats obtenus dans les simulations réalisées avec le logiciel Keysight ADS et les résultats mesurés sur trois prototypes développés utilisant la méthode proposée. Une comparaison entre le modèle proposé et les prévisions d'autres modèles déjà publiés est faite dans la conclusion du chapitre, où les points forts et les faiblesses de chaque modèle sont mis en évidence.

2.2 Article 1 – Physical Mechanism and Theoretical Foundation of Ambient RF Power Harvesting for Wireless Devices

Carlos H. P. Lorenz, *Student Member, IEEE,* Simon Hemour, *Member, IEEE,*

Ke Wu, *Fellow, IEEE*.

Soumis le 6 Septembre 2015 à « *IEEE Transactions on Microwave Theory and Techniques* ».

***Abstract* — Estimating the amount of harvestable ambient RF and microwave power from the omnipresent electromagnetic sources is of vital importance when designing a wireless device that makes use of ambient microwave power harvesting (AMPH) as a power source. This work studies and looks into the underlying RF and microwave rectification mechanism at low input ambient power levels, specifically -30 dBm and below. A fundamental theory is formulated and developed, which is able to correctly predict the rectifier efficiency including the effects of matching network insertion losses through an easy-to-understand analytical model. The suggested model provides a direct design guideline in determining and choosing the optimal diode for a predetermined application. Based on the developed theoretical framework, the diode characteristics that have a direct impact on the microwave power conversion efficiency are discussed in detail. The theory highlights the influences of critical diode parameters on the performance of three different Schottky diode rectifiers which are designed, fabricated and characterized theoretically and experimentally. Measured results are then compared with those obtained by the proposed analytical model and state-of-the-art microwave power rectifiers, showing a good model accuracy and also a 10% improvement in the rectifying efficiency for low input power levels.**

Index Terms — Ambient energy harvesting, RF and microwave power transmission, Schottky diodes, rectifier, rectenna.

2.2.1 Introduction

The use of RF and microwaves to transmit and receive electrical energy has successfully been demonstrated by W. C. Brown and R. M. Dickinson in the decades of 1960 [11] and 1970 [12], following early attempts of N. Tesla. Those early wireless experiments reached maximum RF-to-dc power conversion efficiencies of 82.5% for nearly 8W of input power [12]. However, a good efficiency was not possible at lower input power levels because of the limitation of technologies available at that time. Improvements in Schottky diode technology have led to an increased RF-to-dc power conversion efficiency (PCE) at lower input powers [13], approaching 5% at -30 dBm input power and 40% at -10 dBm or 70% at 10 dBm input powers [9]. Recent progress on the development and deployment of heterojunction backward diodes have made the ambient microwave power harvesting a closer reality by outperforming Schottky diodes, with a PCE of 18%, measured at -30dBm input power, and a theoretical efficiency of almost 40% at the same input power level if matching network insertion losses were eliminated from the circuit [10]. This considerable difference verified between the maximum calculated PCE in a lossless circuit and the real obtainable PCE, which is reduced because of the matching network insertion losses, is one of the fundamental limitations in the design and development of ambient microwave power harvesters (AMPH). It is one of the topics further explored and investigated by this work.

AMPH generally operates in a power range below -30 dBm, which can be considered as the peak available power for AMPH in urban environments [3, 6]. With the ever-decreasing of the power consumption of electronic components and devices, as described by Koomey's law [14, 15]; AMPH becomes an interesting power source for driving the operation of low-power distributed wireless devices such as sensors or actuators nodes in distributed wireless networks as proposed in the Internet of Things (IoT) schemes, body area networks and building automation & structure monitoring [3]. Some examples of the proposed applications include the health monitoring of bridges and buildings using batteryless sensors embedded into the structures, and distributed wireless sensor systems to monitor air, water and noise pollution in cities, just to cite a few [16]. In fact, the wireless powering through the harvesting of ambient electromagnetic sources will be one of the most critical enabling technologies for future wireless systems and applications including the upcoming deployment of the 5^{th} generation (5G) technologies.

Given the typical low peak power densities that take place in ambient microwave power harvesting applications, the analysis presented in this paper will focus on a description of the rectification mechanisms over the power range going up to few microwatts of input power. After depicting the specificities of Schottky diode microwave rectifiers, the effects of matching network insertion losses on the power conversion efficiency is studied and modeled mathematically. The microwatt model is subsequently extended to the case of higher power levels using a pre-generated deviation matrix.

After the theory presentation, this paper exemplifies the use of the proposed model to determine the optimum Schottky diode and synthesize an ambient microwave power harvester exploring the GSM-1900 frequency band. Off-the-shelf Schottky diodes are evaluated using the proposed methodology to estimate the maximum power conversion efficiency that each diode is able to provide for a matched input and a given output load. This information together with a study on the maximum attainable matched bandwidth is used to define which prototypes are built and evaluated. Finally, the measured RF-to-dc power conversion efficiency of the three selected prototypes is presented and compared to state-of-the-art published results, simulation results and the theoretical model predictions. A very good agreement between the simulated, predicted and measured results is shown.

At the end, a comparison between the proposed model and previously published models is made, showing the advantages and disadvantages of each method.

2.2.2 Power Conversion Efficiency Chain

To simplify the understanding of the various power loss mechanisms that take place in the process of microwave power rectification, the efficiency chain shown below is used [9]. It is important to note that single diode parameters may have impact on each separate block in a different manner.

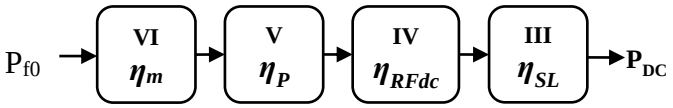

Figure 2-1: Microwave power rectification efficiency chain

In Figure 2-1 η_m stands for the matching efficiency, η_p for the diode's parasitic efficiency, η_{RFdc} for the RF-to-dc power conversion efficiency, and η_{SL} for the dc source to load power transfer efficiency. The numbers refer to the sections of this paper where the theoretical modeling of each block is developed and presented. The diode's mathematical focuses on η_p, η_{RFdc} and η_{SL} while the matching efficiency η_m will later be discussed from both the maximum bandwidth and matching network insertion losses perspectives. It is shown in this work that the matching network insertion loss is of major importance when determining the optimum operation point of a microwave power harvester. This will be discussed in detail during the development of the mathematical model.

The Shockley diode model with added packaging parasitic components presented in Figure 2-2 is considered during the development done in this work [17]. In this model, R_s is the series linear resistance, R_j is the nonlinear junction resistance whose current can be calculated by using (2.1) [18], C_j is the nonlinear junction capacitance and C_p and L_p are the packaging parasitic capacitance and inductance, respectively. The packaging parasitic components are only considered in the matching calculations. Although C_j may be bias-dependent, it is considered to be constant for the low-power evaluation described in this paper.

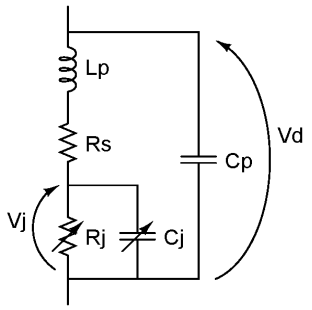

Figure 2-2: Diode model considered in the developments described in this article

$$I_j\left(V_j\right) = I_s\left(e^{\frac{V_j}{V_T}} - 1\right) \tag{2.1}$$

where $V_T = \frac{N \cdot k \cdot T}{q}$ is the thermal voltage, with the diode's ideality factor N already embedded for simplification purposes, q is the electron charge, k is the Boltzmann constant, T is the temperature of operation, I_s is the diode's reverse saturation current, and V_j is the voltage applied to the diode's junction.

2.2.3 DC source-to-load power transfer efficiency

To evaluate the dc behavior, the diode junction can be modeled through the use of the Thévenin or Norton equivalent circuits as shown in Figure 2-3.

In the Norton equivalent circuit, the total rectified current I_{jdc} is divided between the dc load R_L which is in series with the diode's series resistance R_s, and the parallel diode's junction resistance R_j. The dc current at the load, I_{load}, can be calculated by the following equation:

$$I_{load}\left(V_{jf0}\right) = \frac{R_j\left(I_{load}\right)}{R_S + R_j\left(I_{load}\right) + R_L}.I_{jdc}\left(V_{jf0}\right) \tag{2.2}$$

where V_{jf0} is the excitation voltage over the diode's junction at the fundamental frequency *f0* and I_{jdc} is the total dc current rectified by the diode junction.

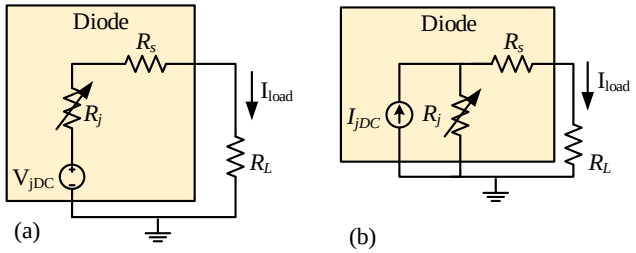

Figure 2-3: (a) Thévenin and (b) Norton equivalent circuits for the diode junction working as a dc power supply.

The total dc power generated by the diode, P_{dc}, is calculated using I_{load} (2.2) and the resistive loads at the dc current path. This can be calculated through the diode model given in Figure 2-2 and the series load R_L, as given by circuit in Figure 2-3 (a).

$$P_{dc} = \left[R_L + R_s + R_j\left(I_{load}\right)\right].I_{load}\left(V_{jf0}\right)^2 \tag{2.3}$$

And the dc power delivered to the load, P_{load}, by:

$$P_{load} = R_L.I_{load}\left(V_{jf0}\right)^2 \tag{2.4}$$

So the DC source-to-load power transfer efficiency can be calculated by:

$$\eta_{SL} = \frac{P_{load}}{P_{dc}} = \frac{R_L}{R_L + R_s + R_j(I_{load})} \tag{2.5}$$

2.2.4 RF-to-dc power conversion efficiency

Most of the published RF and microwave power harvester models, which describe the RF-to-dc power conversion efficiency, consider the diode as a perfect switch whose impedance approaches R_S, the diode's series resistance when directly polarized, and infinity when reversely polarized [17, 19]. This method delivers good results when the input signal is relatively large, usually in the mW range and above, and the investigated diode has a high barrier leading to a large zero-bias resistance (ZBR) R_{j0}. However, this method does not hold for very low input power levels, or for low barrier diodes which present a small ZBR in the order of tens of kΩ and below. As it may be seen in Figure 2-4 where the simulated junction resistance of the Skyworks SMS7630 [20] diode at -40 dBm is presented, the assumption that the diode works as a perfect switch is not true anymore. In such a typical low power driving condition, the diode's impedance varies between 2 kΩ and 20 kΩ over time, not reaching neither a 0 Ω neither an infinitely large impedance state.

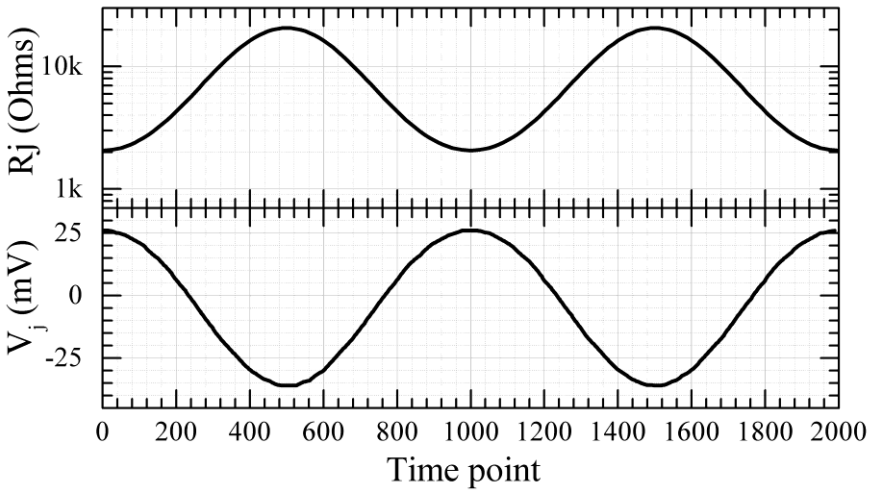

Figure 2-4: Simulation result of the junction resistance of a SMS7630 diode, input power is -40 dBm and load is 5 kΩ. R_j is calculated using δV/δI.

To model this non-linearity of R_j, the zero bias current responsivity $\Re_{I_0}$ will be used in this work. The current responsivity (2.6) is defined as the ratio between the output dc current I_{jdc} and the input RF power P_{f0} [18] for a 0Ω load. The usual derivations of $\Re_{I_0}$ however may only be used in the diode's square law region. Thus, an extended version of the current responsivity that will be denoted by $\Re_I^*$ and may be used out of the diode's square-law region is proposed here.

$$\Re_I = \frac{I_{jDC}}{P_{f0}} \tag{2.6}$$

To find its extended form, the diode's I-V characteristic, given by (2.1) is extended in a Taylor series. In a Taylor expansion around the 0 V point:

$$I_j\left(V_j\right) = I_s.\left[\frac{1}{1!}\frac{V_j}{V_T} + \frac{1}{2!}\left(\frac{V_j}{V_T}\right)^2 + \ldots + \frac{1}{n!}\left(\frac{V_j}{V_T}\right)^n\right] \tag{2.7}$$

Assuming that the applied signal is a constant sinusoidal wave with fundamental frequency f_0, one can write V_j as

$$V_j = V_{jf0}\,\sin\left(2\pi.f_0.t\right) \tag{2.8}$$

Substituting (2.8) into (2.7), and isolating only the terms in dc and in the fundamental frequency, one can find the dc current generated at the junction, I_{jdc}, and the current at the fundamental frequency, I_{jf0}. The power that reaches the diode junction at the fundamental frequency, P_{jf0}, can then be found using equation (2.9).

$$\begin{aligned} P_{jf0}\left(V_{f0}\right) &= f_0 \int_0^{1/f_0} V_j.I_{jf0}dt \;= \\ &= \frac{V_{jf0}^2}{2\cdot V_T}\left[1 + \frac{1}{8}\left(\frac{V_{jf0}}{V_T}\right)^2 + \frac{1}{192}\left(\frac{V_{jf0}}{V_T}\right)^4 + \frac{1}{9216}\left(\frac{V_{jf0}}{V_T}\right)^6 + \ldots\right] \end{aligned} \tag{2.9}$$

Using I_{jdc} and casting (2.9) into (2.6), one can obtain the extended current responsivity, which can be written as

$$\begin{aligned} \Re_I^*\left(V_{jf0}\right) &= \frac{1}{2\cdot V_T}\frac{\left[1 + \frac{1}{16}\left(\frac{V_{jf0}}{V_T}\right)^2 + \frac{1}{576}\left(\frac{V_{jf0}}{V_T}\right)^4 + \ldots\right]}{\left[1 + \frac{1}{8}\left(\frac{V_{jf0}}{V_T}\right)^2 + \frac{1}{192}\left(\frac{V_{jf0}}{V_T}\right)^4 + \ldots\right]} = \\ &= \frac{1}{2\cdot V_T}\Delta_{\Re_{I_0}} = \Re_{I_0}.\Delta_{\Re_{I_0}} \end{aligned} \tag{2.10}$$

where $\Re_{I_0}$ is the diode's zero-bias current responsivity. This extended responsivity equation results from the current-voltage relationship given in (2.1). What's remarkable about (2.10) is that the only diode intrinsic characteristic having an impact on the current responsivity is the diode's

ideality factor *N*, embedded into V_T. $\Re_{I_0}$. This is inversely proportional to *N* and has a maximum equal to 19.34 A/W at 300K. This is the maximum current responsivity that any Schottky diode can reach at the ambient temperature, thereby standing for an important limitation in the use of Schottky diodes for low power energy harvesters. A recently published microwave power rectifier using heterojunction backward tunnel diodes with current responsivities in the order of 22 A/W has demonstrated how such a technology can be used to break through this Schottky diode limitation, thus greatly improving the microwave power harvester efficiency [10].

Equation (2.10) also depends upon the external parameter V_{jf0}. As the denominators from the lower polynomial are smaller than the counterpart from the upper polynomial, $\Re_I^*$ decreases when V_{jf0} increases, thus, when the input power increases. This decrease in responsivity can be understood by looking at Figure 2-5 where the simulated SMS7630 current responsivity is given together with two different amplitude V_j signals. The smaller amplitude signal remains in a maximum $\Re_I$ region. When the applied signal amplitude increases, the diode starts to operate in regions with a reduced $\Re_I$. If one thinks of the total $\Re_I^*$ as an average responsivity for the voltages through which the junction is excited, the average $\Re_I$ would then decrease with the increasing excitation amplitude. This variation of $\Re_I^*$ as a function of the external excitation is represented by $\Delta_{\Re_{I_0}}$ in equation (2.10).

In order to calculate the total dc current generated at the diode junction I_{jdc}, equations (2.10) and (2.6) are used for a given junction voltage V_{jf0}. The junction power P_{jf0} is then found by using (2.9) for this same value of V_{jf0}. This method can be used for low input power levels, ranging up to few μW of input power. The model becomes less accurate for an increasing power because of the simplification assumed in (2.8) where the harmonics and dc bias in the diode junction voltage were ignored. This range, however, is enough for ambient microwave energy harvesting aplications and can be extended as it will be further presented in section 2.2.8.

The presented equations can be used to calculate the total dc current generated by the diode junction, I_{jdc} given the power arriving at the diode's non-linear junction. In order to calculate the

total dc power delivered to the load, the effects of the dc source-to-load power transfer have to be considered as shown in section 2.2.3.

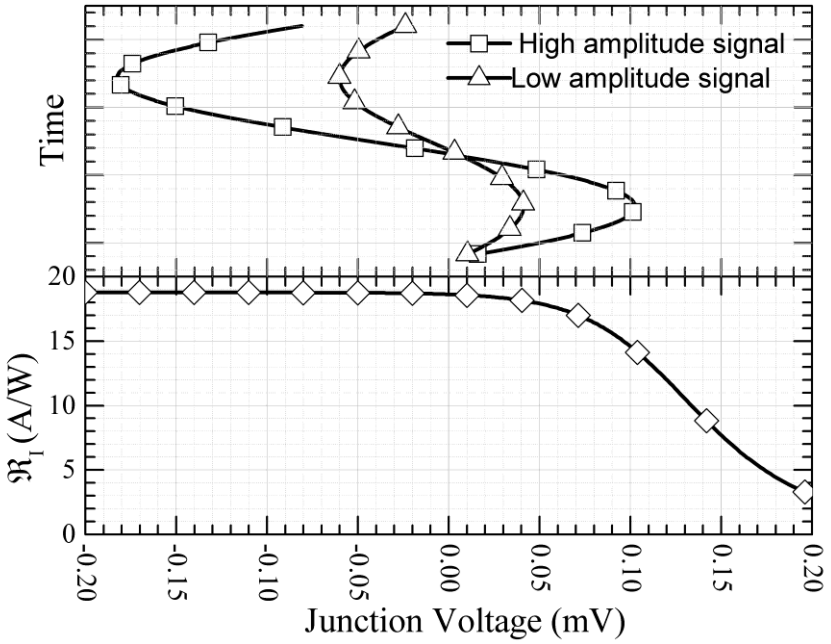

Figure 2-5: Top part: Two sine waves, representing the voltage applied to the diode terminals. Bottom part: Simulated current responsivity of the SMS7630 diode for a voltage sweep near the zero-bias condition.

The total dc power generated by the diode, P_{dc}, can then be calculated using I_{load} (2.2) and the equivalent resistance at the dc current path. This can be calculated using the Thévenin equivalent circuit in which the diode is in series with the load, as described by (2.3). Defining the RF-to-dc power conversion efficiency as the total dc generated power divided by the power that reaches the junction, one can write the following,

$$\eta_{RFdc} = \frac{P_{DC}}{P_{jf\,0}} = \frac{R_j^2(I_{load})}{R_L + R_s + R_j(I_{load})} \cdot \left(\Re_{I_0} \cdot \Delta_{\Re_{I_0}}\right)^2 \cdot P_{jf\,0} \tag{2.11}$$

Equations (2.5) and (2.11) may be used to determine the optimum load value with which the maximum efficiency in the RF-to-dc power conversion efficiency is reached. In Annex A, it is shown that the load value for which the maximum efficiency is obtained is equal to $R_s+R_j(I_{load})$. This can be simplified to $R_j(I_{load})$ within the square-law operation limits as R_s is much smaller than $R_j(I_{load})$.

2.2.5 Parasitic Efficiency

Due to the low-pass filter effect of the diode's junction capacitance C_{j0}, some of the RF current that reaches the diode is shunted, therefore dissipating power in the series resistance R_s. The total RF power that is delivered to the diode may be calculated by adding the power that reaches its junction (2.9) to the power that is dissipated by the diode's series resistance R_s. The later may be calculated using equation (2.12), which can be derived by using simple linear circuit theory.

$$P_{R_s} = \frac{1}{2} R_s . \left| 2 . \frac{P_{jf\,0}}{V_{jf\,0}} + j.2.\pi . f_0 . C_{j0} . V_{jf\,0} \right|^2 \tag{2.12}$$

The parasitic efficiency can be defined as the ratio between the total power supplied to the diode and the power that reaches the nonlinear junction, which may be expressed by

$$\eta_{parasitics} = \frac{P_{jf\,0}}{P_{jf\,0} + P_{R_s}} \tag{2.13}$$

Equations (2.12) and (2.13) can be simplified for the square-law region, where the junction resistance is considered to be constant and equal to R_{j0}, the resulting equation is given in (2.14) and was already given in [9, 18].

$$\eta_{parasitics} = \left(\frac{1}{1 + \left(2\pi \cdot f_0 \cdot C_{j0} \right)^2 \cdot R_{j0} \cdot R_s} \right)^2 \tag{2.14}$$

Equations (2.5), (2.11) and (2.13), which are used to calculate η_{SL}, η_{RFdc} and $\eta_{parasitics}$ respectively, describe the power conversion efficiencies related to the diode parasitic components and non-linearity. Assuming that the optimum load is chosen such that $\eta_{RFDC} \cdot \eta_{SL}$ is maximized, one can assume from equation (2.11) that diodes with higher R_j will reach higher efficiencies. In equation (2.14), however, the impact of a higher R_{j0} is seen to decrease efficiency. Finally, as it will be shown subsequently, the zero bias resistance value also plays a key role in the matching network losses. Those three tendencies will be analysed in the next session and the matching network insertion losses impact on the total rectifier PCE is evaluated in detail.

2.2.6 Matching Efficiency

The matching network insertion loss, or in turn, matching efficiency η_m, plays a significant role when determining the optimum diode for an ambient microwave power harvester. While (2.11)

indicates that a diode with a high R_{j0} is expected to deliver a higher RF-to-dc power conversion efficiency, it is shown that η_m is inversely proportional to R_{j0}. Using the given model, an optimum R_{j0} where $\eta_m \cdot \eta_{RFdc} \cdot \eta_{SL}$ is maximized can be suggested, indicating the optimum diode's zero-bias junction resistance.

A prior knowledge of the matching network technology in terms of transmission line attenuation and propagation constants as well as lumped components quality factors, can be used to estimate the matching efficiency η_m as follows [21],

$$\eta_m = \frac{1}{1+\frac{Q_r}{Q_m}} \tag{2.15}$$

$$Q_r = \sqrt{\frac{R_{HIGH}}{R_{LOW}} - 1} \tag{2.16}$$

where R_{HIGH} and R_{LOW} are the highest and lowest real impedances chosen from the source or the load, being typically the source impedance and R_j, respectively, when matching a diode. Q_r is called the required quality factor while Q_m is the matching network quality factor that is actually obtained.

Finding the value of Q_m can be simplified by approximating the diode by a parallel R_d//C_d circuit at the operation point of interest, which is determined by the input power and f_0. In this case, R_d is the equivalent parallel diode resistance to which the power is delivered and the equivalent parallel capacitance C_d will be absorbed into the matching network losses and bandwidth calculations. For a center frequency of interest, R_d and C_d may be calculated using the equations below, while maintaining the equivalent load quality factor [21]:

$$R_d = \mathrm{Re}[Z_{diode}] \cdot (1 + Q_{diode}{}^2) \tag{2.17}$$

$$C_d = \left| \frac{\mathrm{Im}[Z_{diode}]}{2\pi f_0} \right| \cdot (1 + Q_{diode}{}^{-2}) \tag{2.18}$$

where Zdiode is the input impedance of the diode alone at f0 and the input power level of interest, and Qdiode is the quality factor of the diode, calculated at the same frequency and power. For frequencies far below the diode cut-off frequency, it can be approximated by:

$$Q_{diode} = \frac{\mathrm{Im}[Z_{diode}]}{\mathrm{Re}[Z_{diode}]} \tag{2.19}$$

To obtain the quality factor of the matching network, its input impedance as a function of frequency $Z_{match}(f)$ needs to be calculated, with the first component of the matching network being C_d. Once this equation is known, Q_m may be calculated using one of the two equations below [22]:

$$Q_m(f) = \frac{1}{2} \frac{\mathrm{Im}[Y_{match}(f)] + f \frac{d\,\mathrm{Im}[Y_{match}(f)]}{df}}{\mathrm{Re}[Y_{match}(f)]} \tag{2.20}$$

$$Q_m(f) = \frac{1}{2} \frac{\mathrm{Im}[Z_{match}(f)] + f \frac{d\,\mathrm{Im}[Z_{match}(f)]}{df}}{\mathrm{Re}[Z_{match}(f)]} \tag{2.21}$$

where $Y_{match}(f)$ is the input admittance of the matching network, given by $1/Z_{match}(f)$. Equation (2.20) is used when the matching network behaves as a parallel resonator near f_0, while equation (2.21) is used when the behaviour resembles a series resonator.

Every component used in the matching network's $Z_{match}(f)$ calculation needs to have its contributing parasitic parts included. When transmission line distributed components are used, the complex characteristic impedance of the line Z_c needs to be used. In [23], for example, it is shown that the quality factor of a short stub can vary by a factor of 2 if a simplified real impedance is used instead of the complex impedance of the transmission line.

When transmission lines are used as components of the matching network, it is important to take into account the effect that the standing waves have on losses. The increased voltage and current that appear on the line would introduce higher losses to the system. In [24], it is shown that an equivalent transmission line attenuation constant α_r can be calculated, which will account for these increased losses. α_r is related to the matched transmission line attenuation constant α_m by the following equation:

$$\alpha_r = \alpha_m \frac{r^2 + 1}{2r} \tag{2.22}$$

where r is the standing wave ratio sustained by the transmission line, which is usually calculated using (2.23), where Γ_L is the reflection coefficient at the load side.

$$r = \frac{1 + |\Gamma_L|}{1 - |\Gamma_L|} \tag{2.23}$$

However, since transmission lines used in the design of matching networks are usually shorter than half-wavelength, it is not possible to assume that both maximum and minimum current and

voltage nodes will appear in the standing wave sustained in the transmission line under consideration. For this reason, equation (2.23) cannot be used.

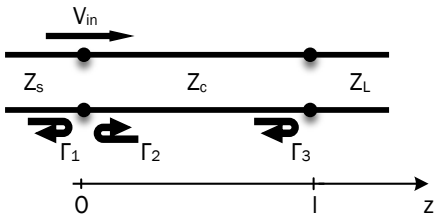

Figure 2-6: Travelling wave approach used to calculate the standing wave ratio in a transmission line of length *l*.

Using the travelling wave formulation, one can calculate the voltage at a short length of transmission line with reflection at both ends. Assuming a transmission line with propagation constant γ, characteristic impedance Zc and length l, connected to a source with impedance Z_S and a load with impedance Z_L, as shown in Figure 2-6, one can write the voltage on the transmission line V_l as a function of the position *z* as given by equation (2.24).

$$V_l(z) = V_{in}\begin{pmatrix} e^{-\gamma z} + \Gamma_3 e^{-2\gamma l} e^{\gamma z} + \Gamma_2\Gamma_3 e^{-2\gamma l} e^{-\gamma z} + \ldots \\ +\Gamma_2\Gamma_3^2 e^{-4\gamma l} e^{\gamma z} + \Gamma_2^2\Gamma_3^2 e^{-4\gamma l} e^{-\gamma z} + \ldots \end{pmatrix} \tag{2.24}$$

which can then be simplified to (2.26) by using (2.25).

$$\sum_{n=0}^{\infty} x^n = \frac{1}{1-x} \text{ for } |x| < 1 \tag{2.25}$$

$$V_l(z) = V_{in}\left[\frac{\left(e^{-\gamma z} + \Gamma_3 e^{\gamma z} e^{-2\gamma l}\right)}{1-\Gamma_2\Gamma_3 e^{-2\gamma l}}\right] \tag{2.26}$$

Using the points where the first derivative of (2.26) with respect to *z* equals 0, one can find the positions where $|V_l(z)|$ has a maximum or a minimum point. In Annex B, it is shown that this happens for:

$$z = \frac{n\pi + \text{atan}(-D/C)}{2\beta} \tag{2.27}$$

where $\Gamma_3 e^{-2\gamma l} = (C + Di)$, β is the transmission line's phase constant and *n* is an integer equal or greater than 0.

If a z value is found to be within the limits of the transmission line length, a standing voltage maximum or minimum is found at this position. For short transmission lines, the maximum and minimums must also be verified at the transmission line ends when less than two valid values of z are obtained from equation (2.27). Having the maximum and minimum standing wave voltages that occur within the transmission line boundaries, equation (2.28) is used to calculate the maximum to minimum voltage ratio found in the transmission line.

$$r = \frac{|V_l(z)|_{\max}}{|V_l(z)|_{\min}} \tag{2.28}$$

This value of r is used in conjunction with (2.22) to calculate the equivalent attenuation constant α_r for the transmission line, which is used to construct the $Z_{match}(f)$ matching network input impedance equation.

Adding the matching network insertion loss effects to the microwave power rectification model creates a model where the total trade-off between the diode's junction resistance and the maximum microwave power rectification efficiency can be studied.

Such a tradeoff is shown in the bottom graph depicted in Figure 2-7 for an input power equal to -30 dBm, using a hypothetical parasitic-less diode. The rectifier power conversion efficiencies and insertion losses are calculated by considering that a microstrip L-Matching network is used, which is composed by a series transmission line and a parallel short-circuited stub, which lengths are optimized to minimize reflections for every new value of R_j. Low loss Rogers RT/Duroid 6002 substrate with 30 mil thickness and 18 μm copper cladding is used for the matching network insertion losses calculations. The microstrip line is 76 mil wide and the transmission line's propagation constant and complex characteristic impedance functions are extracted by using the method proposed in [25]. This evaluation provides the range of junction resistances where the highest rectification efficiencies can be obtained by using the proposed matching network. It is clear from this graph that for a parasitic-less diode, a maximum could be obtained near 17kΩ, however close-to-the maximum efficiencies could be achieved with diodes that have an R_{j0} ranging from 5kΩ up to 50kΩ. The parasitic components will later reduce the maximum efficiency and play an important role in the maximum bandwidth that can be matched to the diode. This will be shown in the next section.

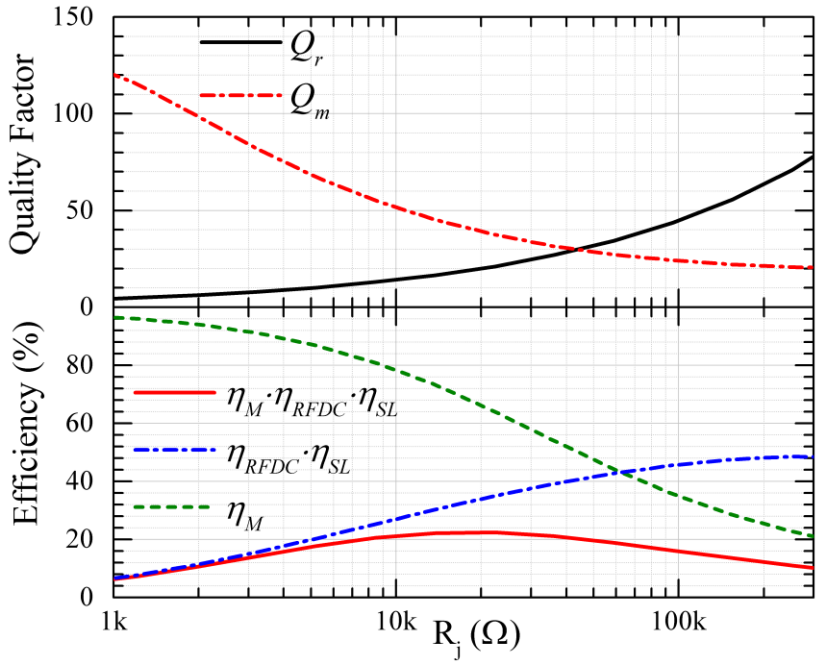

Figure 2-7: Top: Calculated required quality factor Qr and obtained matching network quality factor Qm. Bottom: Calculated matching network efficiency, diode's $\boldsymbol{\eta}_{\mathrm{RFdc}} \cdot \boldsymbol{\eta}_{\mathrm{SL}}$ and total efficiency at -30 dBm 1.95GHz. Load value equal to Rj.

2.2.7 Maximum Bandwidth

The relationship between the load impedance and the maximum attainable matching bandwidth was described by Bode [26] and Fano [27], being known as the Bode-Fano criteria [28]. It gives the maximum bandwidth that can be matched to a load, given the load's equivalent circuit and the maximum desired reflection coefficient.

Equation (2.29) can be used to calculate ΔB, the maximum obtainable fractional bandwidth. It is derived using the Bode-Fano criterion for a parallel RC circuit.

$$\Delta B \leq \frac{\pi}{R_d \cdot 2\pi f_0 C_d} \cdot \frac{1}{\ln \frac{1}{|\Gamma_{inband}|}} \tag{2.29}$$

where f_0 is the frequency of interest, corresponding to the central frequency of the band, and Γ_{inband} is the desired reflection coefficient.

It is important to bear in mind that this equation is derived by assuming that the reflection coefficient is flat and equal to $|\Gamma_{inband}|$ for the matched band, and equal to one outside of this band.

In this derivation, there are also other implicit assumptions, namely the availability of lossless matching networks and wideband lossless impedance transformers. As one knows, matching networks always introduce losses to the system, and wideband impedance transformers are difficult to obtain over microwave frequency range for very different source and load impedances.

This means that in a real circuit design scenario, the maximum attainable bandwidth is actually lower than the calculated by the Bode-Fano criteria, as such sharp transitions and flat passband are impossible to obtain. The out of band reflection coefficient will also not be equal to one for the whole frequency spectrum, thus reducing even more the maximum bandwidth that may be obtained for the passband.

However, the Bode-Fano criteria can be used to establish an upper bound to the maximum bandwidth that can be matched to a diode at a given frequency and estimated input power. It will be shown that, despite that high R_{j0} diodes show an increased η_{RFdc} at low power level according to (2.11), the maximum bandwidth that can be matched to them is usually very narrow.

2.2.8 Extension of the Low Power Model

The aforementioned method can be used to evaluate the RF-to-dc power conversion mechanism and understand where the power conversion inefficiencies originate. Even though equations (2.7) to (2.10) are limited in power to a few μW, this analysis can be extended to a larger power range by means of pre-generated V_{j0} as function of the junction power and load resistor $V_{j0}(P_{jf0},R_l)$, and current responsivity delta as function of the junction voltage and normalized load $\Delta_{\Re_{I_0}}(V_{j0}, R_l/R_{j0})$ matrixes, which are calculated with the aid of an Harmonic Balance algorithm implemented in MATLAB [29]. The $\Delta_{\Re_{I_0}}$ matrix contours are given in Figure 2-8. These may be used for Schottky diodes operating below the breakdown voltage, however, the V_{j0} contours which are shown in Figure 2-9 are diode dependent and need to be obtained for each different diode to be evaluated in higher input powers. All inductive and capacitive parasitic elements are removed during the contours generation to make them frequency independent. In this way, any further analysis may be done quickly and the results may be extrapolated to any frequency using only the previously presented linear equations. This procedure can be used to quickly evaluate and optimize microwave rectifiers at different frequencies or evaluate different matching network topologies.

The results of the extended method are compared to the low power model in the next section, where five commercial diodes are evaluated for a given microwave power harvesting application. In addition to the insight about the power loss and power conversion mechanisms, the extended model is simpler and less resource-consuming as all non-linear dependences are already contained in the presented contours. Given these lower computational requirements, this method could be used to determine the optimum load in a maximum power point tracking algorithm embedded in the final dc-dc converter, so the optimum dc load can be presented to the microwave power harvester.

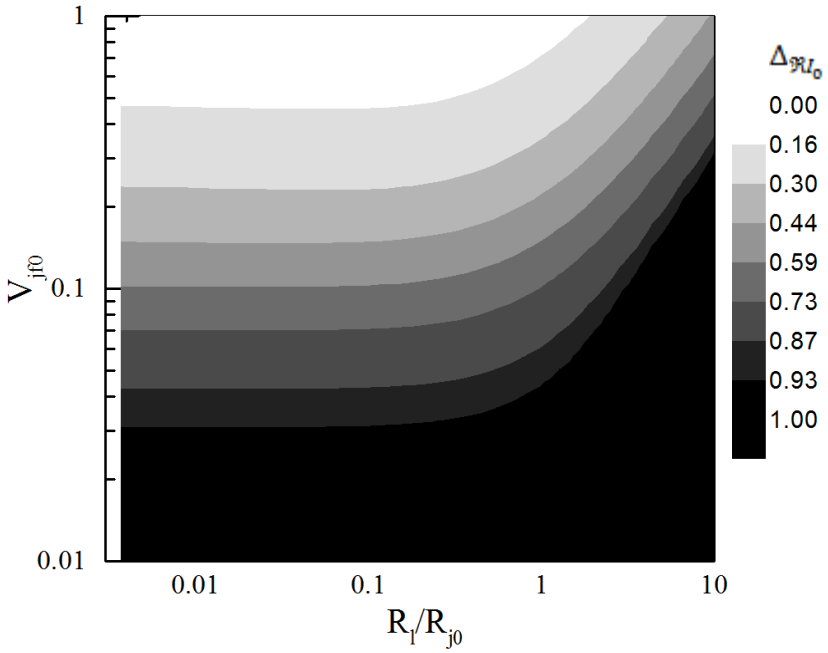

Figure 2-8: Example of $\Delta_{\Re_{I_0}}$ contours generated using the model of the SMS7630 diode.

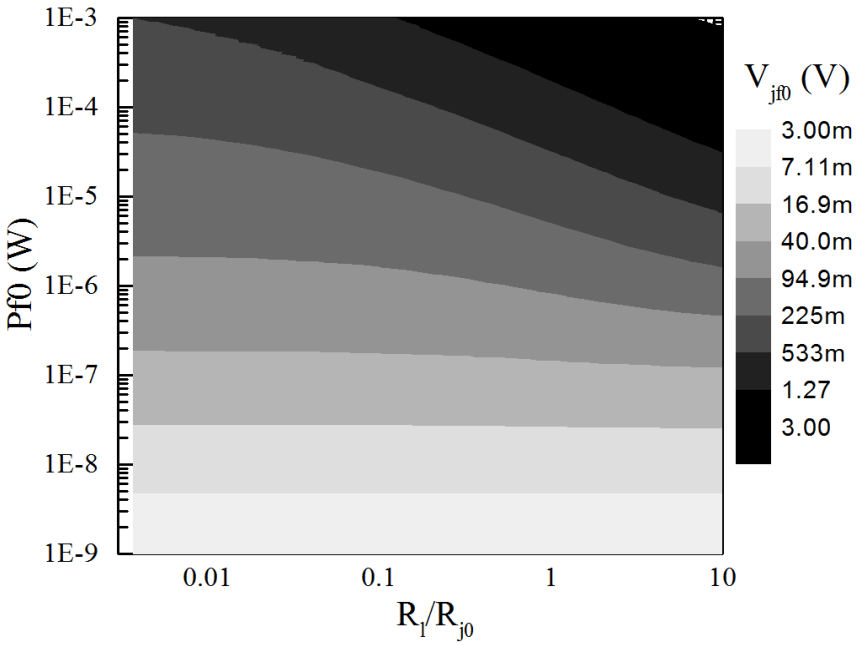

Figure 2-9: Junction voltage as function of the normalized load and of the input power for the SMS7630 diode.

2.2.9 Evaluation of schottky diodes using the proposed method

The following commercially available Schottky diodes are selected and compared using the proposed method: Skyworks SMS7630 [20], Infineon BAT15 [30], Avago HSMS-2860 [31], Avago HSMS-2850 [32] and VDI W-Band ZBD [33]. These diodes present very different saturation currents and R_{j0} within the boundaries given in Figure 2-7, so the effects of a high, medium or low barrier Schottky diode can be verified.

The proposed microwave power harvester operates in the GSM-1900 frequency band, covering from 1850 MHz to 1990 MHz, as this is found to be one of the bands with a higher microwave power density in measurements done within the Poly GRAMES research center environment. The operational input power range is optimized within the -45 dBm to -30 dBm range. The load to which the power will be delivered is a 5.1 kΩ resistive load.

In order to estimate the matching network insertion losses even before defining the final matching network topology, all rectifier calculations were done considering the use of a microstrip L-matching network composed of a series transmission line and a parallel short-circuited stub,

which is also used as the dc current path. The same substrate and line impedances presented in the previous section that discussed the matching network insertion losses estimation model are used.

Using the proposed method and the diodes' characteristics given in the datasheets, the total RF-to-dc power conversion efficiency and the losses that take place in this conversion have been estimated. The result is given in Figure 2-10 for the five proposed diodes. The results are organized from the diode with the highest R_{j0} on the top, to the lowest R_{j0} at the bottom. The stacked areas are calculated with the extended model, using the pre-generated $V_{j0}(P_{jf0},R_l)$ and $\Delta_{\Re_{I_0}}(V_{j0}, R_l/R_{j0})$ matrices. The red triangles correspond to the low power model, while the blue squares make use of an extended version of the low power model that does not need the deviation matrices. In this case, I_L is calculated as the average of (2.2) and (2.30). This last method is found empirically and extends the range of power levels in which the low power model may be used up to nearly -20 dBm.

$$I_{load}\left(V_{jf\,0}\right)=\frac{R_{j0}}{R_S+R_{j0}+R_l}.I_{jDC}\left(V_{jf\,0}\right) \tag{2.30}$$

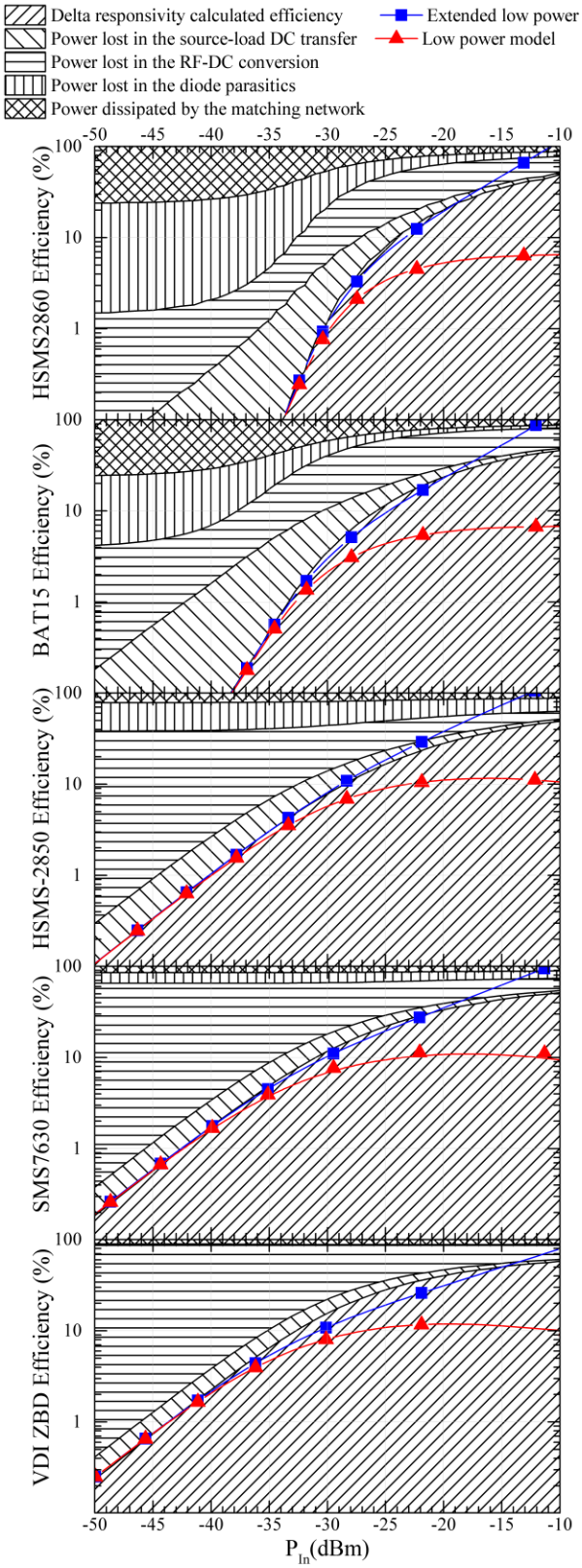

Figure 2-10: RF-to-dc conversion efficiency for multiple diodes, frequency = 1.9 GHz, load = 5.1 kOhms

The effect of the variation of R_{j0} is obvious from the evaluation of Figure 2-10, the first remarkable difference is the power dissipated by the matching network when higher barrier diodes are used, reaching 75% of the total power. This effect has already been shown and explained in Figure 2-7, and is verified here again with real diode models. The higher R_{j0} also increases the total parasitic losses, as the low-pass filter effect from the parallel circuit composed of $R_j//C_j$ becomes more pronounced. This is true for low input power levels in the range of -30 dBm and lower, usually found in ambient microwave power harvesting (MPH) applications. At higher power levels, the decrease in R_j improves the matching and parasitic efficiencies. However, this may not be explored in MPH because of the low ambient power densities that are available [13].

The best predicted efficiencies are given by the low barrier SMS7630 and VDI W-Band ZBD diodes, which present respectively 4.7% and 6.7% power conversion efficiencies at -35 dBm input power level. Because of the higher C_{j0}, the HSMS-2850 diode dissipates nearly 40% of the available power in diode parasitic losses. The medium to high barrier height diodes, BAT15 and HSMS-2860 present two main limitations at this power region. First, the parasitic losses are very high, as R_j is still large when compared to the parallel capacitance C_j impedance, much of the junction current is shunted through C_j and dissipated by R_s. Second, because of the large R_j, nearly 75% of the power is dissipated in the matching network, even though the low loss material Rogers RT/Duroid 6002 is used. Also as shown by equation (2.5), nearly all of the rectified power would be lost because of the low source-to-load power transfer efficiency in the proposed application. This last efficiency could be raised by increasing the load to a value near the diode's zero-bias junction resistance. Nevertheless, this would not reduce the high matching and parasitic efficiency problems. The maximum power that can be harvested with the higher barrier diodes in the square-law operation region can be calculated by using equation (2.5) with the efficiency value given by the stacked area given by the recovered power and the power lost in the source-to-load dc power transfer. The resulting maximum recoverable power is 50% of the value given by these two stacked areas if a load equal to R_{j0} is chosen. Having this in mind Figure 2-10 shows that the high barrier diodes won't reach higher efficiencies even if a larger load is used in the AMPH power range.

Another limitation appears when studying the higher barrier diodes for low ambient power harvesting applications. As shown in Figure 2-11, the maximum fractional bandwidth for the medium and high barrier diodes, calculated by using equation (2.29), is below the minimum

required fractional bandwidth of 7.4%. So, even having the possibility of slightly increasing the efficiency using a higher load, the desired bandwidth would only be partially covered.

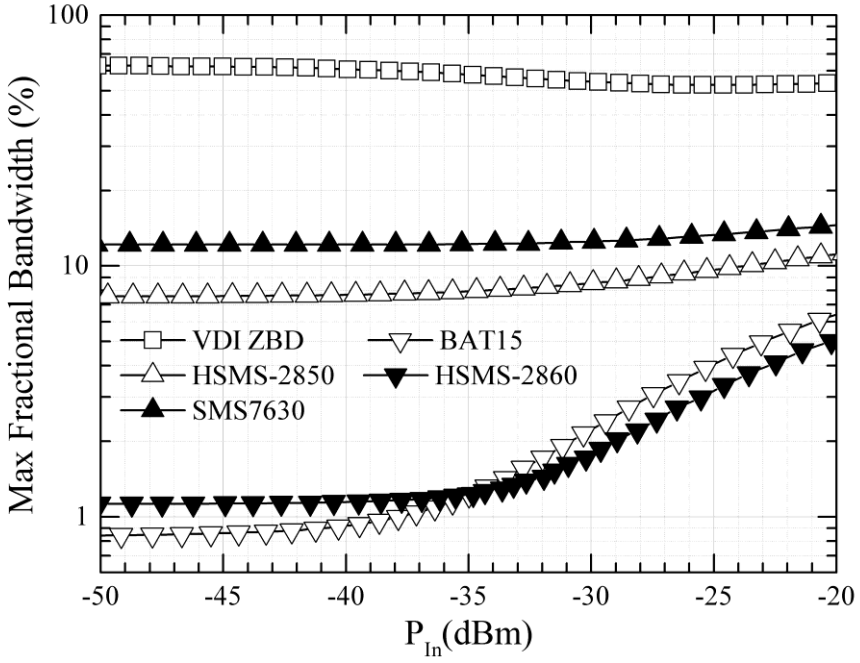

Figure 2-11: Maximum obtainable fractional bandwidth for the proposed diodes, given a -12 dB return loss requirement.

One important remark about the Bode-Fano criteria is that it considers the fact that lossless matching networks and broadband impedance transformers are available at any frequency, and for any source-load impedance mismatch [34]. Due to these assumptions, it yields the maximum bandwidth that would be available, provided that these requirements were actually met. As wideband impedance transformers are difficult to obtain, the realizable maximum bandwidth may be lower than the indicated in Figure 2-11.

2.2.10 Prototypes

In order to verify the proposed methodology, three prototypes were built, each using a different diode, and the rectifier's specifications proposed in section 2.2.9. As already shown in Figure 2-11, the SMS7630-061 and the VDI W-Band ZBD diodes can be matched to the whole GSM-1900 frequency band when working at ambient RF power levels, while the HSMS-2850 diode could cover the whole bandwidth, however with lower efficiency and leaving no margin for deviations. Even though the higher barrier diodes do not comply with the bandwidth requirement and present

lower RF-to-dc power conversion efficiency due to high matching network insertion losses, a third prototype using the BAT15 diode is presented in order to verify the model's predictions. The methodology used in this work to build the prototypes is described hereunder.

1st: The diode's input impedance is calculated using the diode datasheet information and, when available, SPICE model parameters. The input power used during the matching circuit development is -35 dBm and the load is 5.1 kΩ.

2nd: An initial matching network, covering at least the frequency band ranging from 1.84 GHz to 1.99 GHz is generated using the Simplified Real Frequency Technique (SRFT) [35, 36]. The minimum desired return loss is 12 dB.

3rd: The lumped components matching networks are converted into mixed matching networks, both lumped and distributed components are optimized afterwards using Keysight ADS LSSP and Momentum co-simulation.

The prototypes are then built using microstrip technology over a 30 mil Rogers RT/Duroid 6002 substrate, the same substrate is used in the model calculations given in Figure 2-10. A picture of the circuits is shown in Figure 2-13.

For the efficiency measurement, the output of a RF generator is calibrated and then connected to the prototypes. The dc voltage V_{dc} over the output 5.1 kΩ load resistor is measured by a HP 34401A precision voltmeter. With the voltage values in hand, the measured total efficiency is calculated using equation (2.31).

$$\eta_{meas} = \frac{V_{dc}^2}{R_l . P_{in}} \tag{2.31}$$

The simulated and measured S11 for a -35 dBm input signal, as well as the measured and calculated power conversion efficiency for a -30 dBm input signal, are shown in Figure 2-12.

The maximum bandwidth for a -12 dB return loss, calculated using the Bode-Fano criteria, is shown as a grayed out area for the SMS7630 and BAT15 diodes. The obtained bandwidths are near-to-the maximum predicted value, considering that the measured return loss is lower than -12 dB for some frequencies, and not flat as considered in the Bode-Fano criteria derivations.

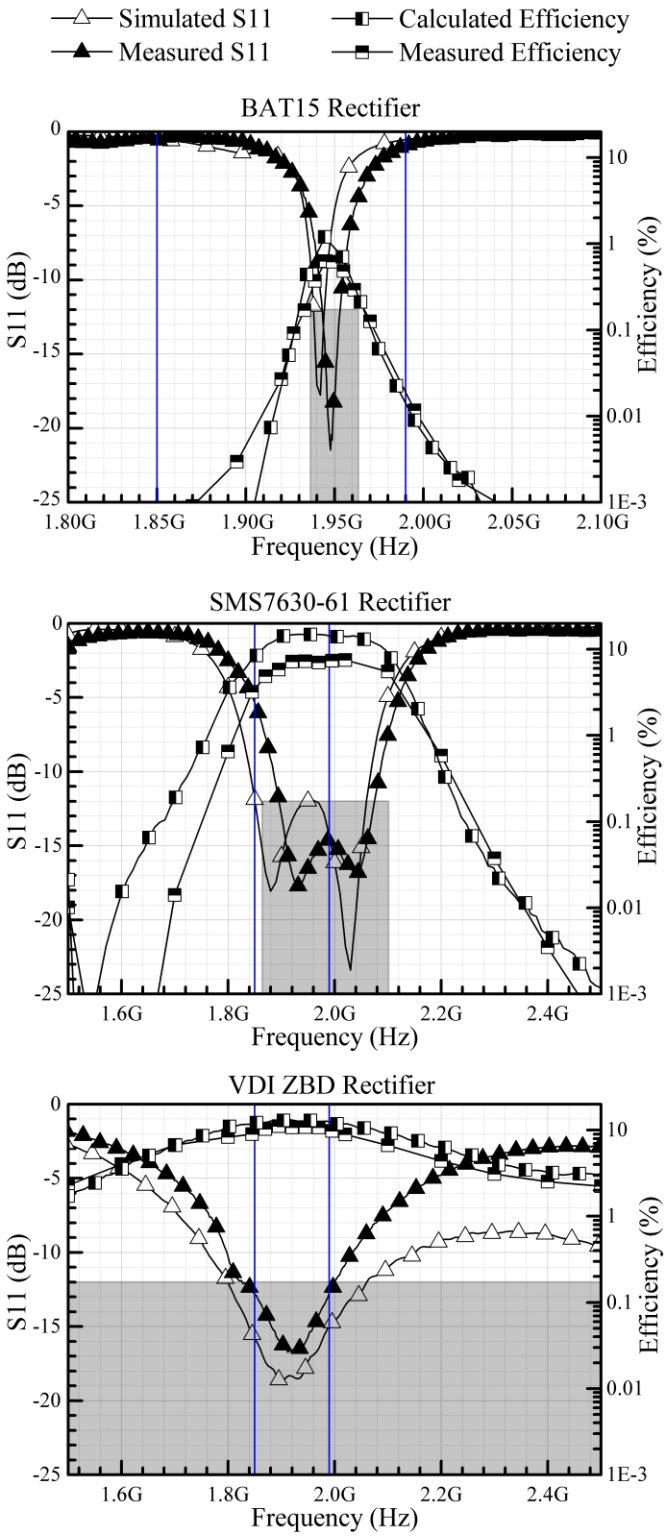

Figure 2-12: Measured and calculated S11 (at -35 dBm) and power conversion efficiency (at -30 dbm). The theoretical maximum bandwidth for -12 dB return loss is indicated by the grayed out area. The proposed prototipes bandwidth is indicated by the parallel blue line.

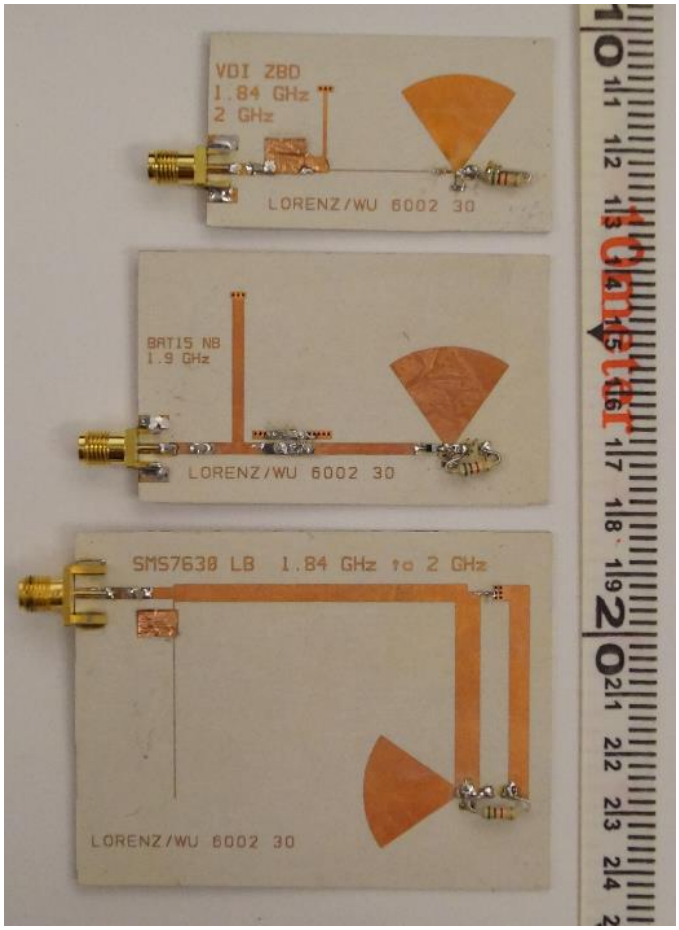

Figure 2-13: Picture of the circuits built for this paper. Top: SMS7630. Middle: VDI ZBD. Bottom: BAT15.

As shown in the results, the agreement between the simulated and measured S11 is very good for the SMS7630 and BAT15 diodes. However, a difference is observed between the initially simulated and measured S11 values for the VDI prototype. This happened mainly because of a large tolerance that this diode presents for the value of I_s, reflecting on a junction resistance that may vary from 2.5 k**Ω** to 6 k**Ω**. It was initially assumed in this work an I_s value equal to 11 **μ**A; however from the measurements it was found that the used sample presents an I_s near to 7 **μ**A. The measured S11 values presented in Figure 2-12 are obtained after tuning the matching network, which was done by using a copper tape as can be seen in Figure 2-13.

The measured power conversion efficiencies agree very well with the predicted values, which are calculated using the $\Delta_{\Re_{I_0}}$ extended mathematical model. η_m is calculated using the measured reflection coefficient and the matching network insertion loss, estimated using Keysight ADS

Momentum software package, as the wider band matching networks become too complicated to be modeled mathematically.

After the bandwidth measurement, a power sweep is done to verify the model power conversion efficiency prediction at different power levels. The power distribution, calculated using the $\Delta_{\Re_{I_0}}$ mathematical model and simulated matching network insertion loss is shown in Figure 2-14 for the three built prototypes, together with the measured results. A very good agreement between the model predictions and measurements is found and verified for the BAT15 and VDI prototypes. A small difference is observed between the measured and predicted power conversion efficiencies of the SMS7630, this difference shown in Figure 2-12 and Figure 2-14 is believed to be the result of an underestimation of the used diode model parasitic components, or in the diode package parasitic components.

As expected from the previous discussions, the higher initial mismatch between source and load for the diodes with higher R_{j0} results in a very high loss of P_{in} in connection with the increased matching network insertion losses. For the SMS7630 diode, this loss accounts for 18% of P_{in}, while for the BAT15 diode this raises to nearly 82% of P_{in}. The increase in the matching network insertion losses for the BAT15 prototype, when compared to the predictions given inFigure 2-10, is mainly caused by the use of a longer transmission line between the diode and the parallel capacitor, when compared to the transmission line used with a parallel shorted stub solution, which allows a larger standing wave ratio to be sustained increasing losses.

Despite the fact that the SMS7630 diode has a slightly higher R_j than the VDI ZBD diode, the larger diode parasitic losses decrease the final efficiency, as nearly 18.8% of the total input power is lost in the diode's parasitic components. This results in a total efficiency very near for both rectifiers, with the VDI ZBD rectifier delivering the best performance, reaching 11.29% at -30 dBm compared to 8.08% measured on the SMS7630 rectifier.

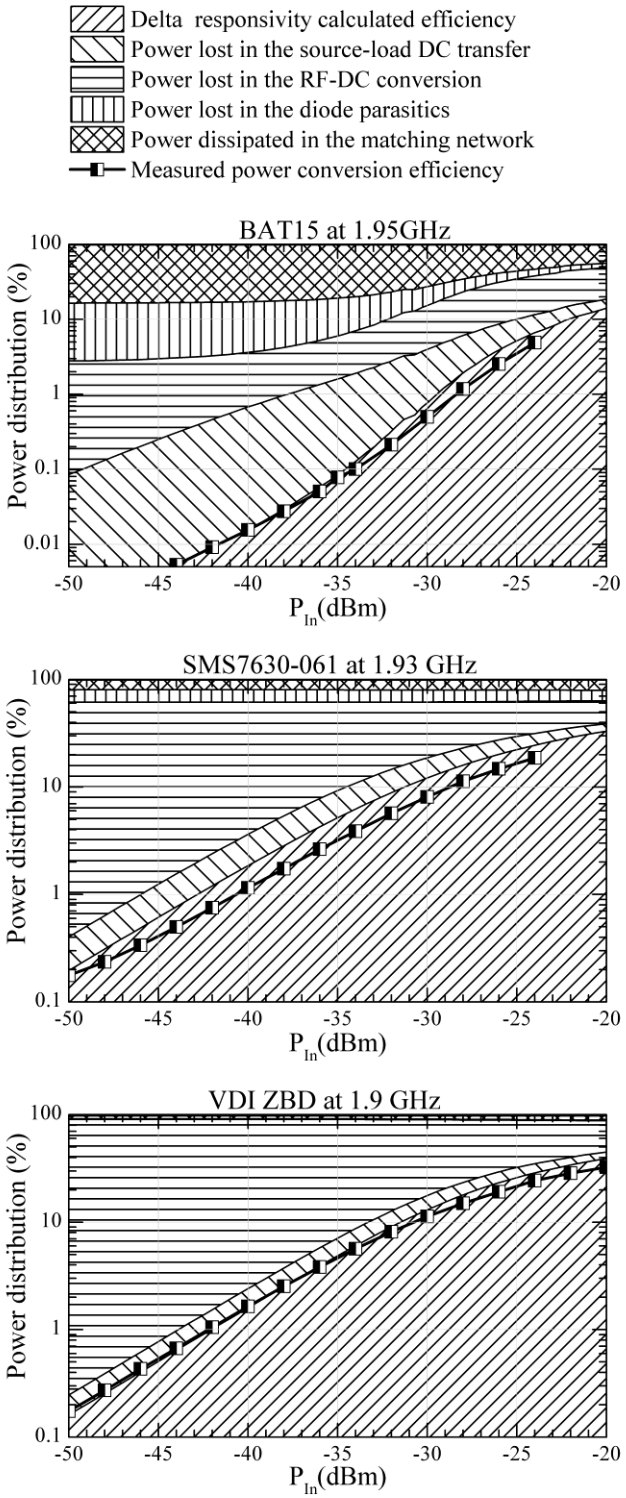

Figure 2-14: Measured and calculated microwave power harvester efficiency, with power distribution. f = 1.9 GHz, Load = 5.1 kΩ.

2.2.11 Conclusion

In this paper, a mathematical model has been presented and verified, in which the power conversion efficiency-related physical mechanisms of microwave power harvesters using Schottky diodes are explained and formulated. Knowing where the power is dissipated enables the design and development of a new class of rectifiers with maximized conversion efficiency. The modeled efficiencies, calculated in conjunction with the matching network losses, are in a close agreement with the measured results. Even though the matching network insertion losses are approximated by a simpler L-matching network, the results show a good agreement with the final wider band matching network calculated and measured results, thus substantiating the claim that the proposed model can be used as a trustworthy approximation of the maximum attainable power conversion efficiencies, even before having the rectifier circuit designed.

Figure 2-15 shows a comparison between the three proposed models: the low power model presented in the beginning of this paper, the extended low power model using (2.30) and the delta-responsivity matrix model described in item 2.2.8. The matching efficiency was removed to compare the proposed models to previously published mathematical models, so the power ranges and scenarios where each method delivers the best results could be highlighted, these models are: the diode operating as a switch [19], and the Ritz-Galerkin solution for the diode non-linear equations [37]. The Keysight ADS Harmonic Balance result was added as reference. Since the Ritz-Galerkin model uses a given source voltage and impedance instead of the power arriving at the diode to calculate the output dc voltage and power, the reflection coefficient at the source-diode interface is used to calculate the power delivered to the diode and hence the power conversion efficiency. This reflection coefficient has to be pre-generated using a harmonic balance, as the non-linear diode input impedance is unknown.

The limitation in the low power models for higher input powers is evident from Figure 2-15. Nevertheless, the result at input power levels up to few microwatts makes the low power and the extended low power models very good tools to predict the performance of ambient microwave power harvesters. The delta-responsivity matrix model delivers an exact result when compared to the Keysight ADS simulation results, even at higher input power levels. The Ritz-Galerkin model has a shift up in the efficiency for the SMS7630 and the BAT15 diodes, as the result of a simplification in the model derivation where the parasitic capacitances are ignored, this effect is

not seen for the VDI ZBD diode due to its very low parasitic capacitances. As expected, the switch diode model works well for higher input powers and higher R_{j0} diodes, as is seen in the BAT15 diode results, but cannot be used in ambient microwave power harvesting applications.

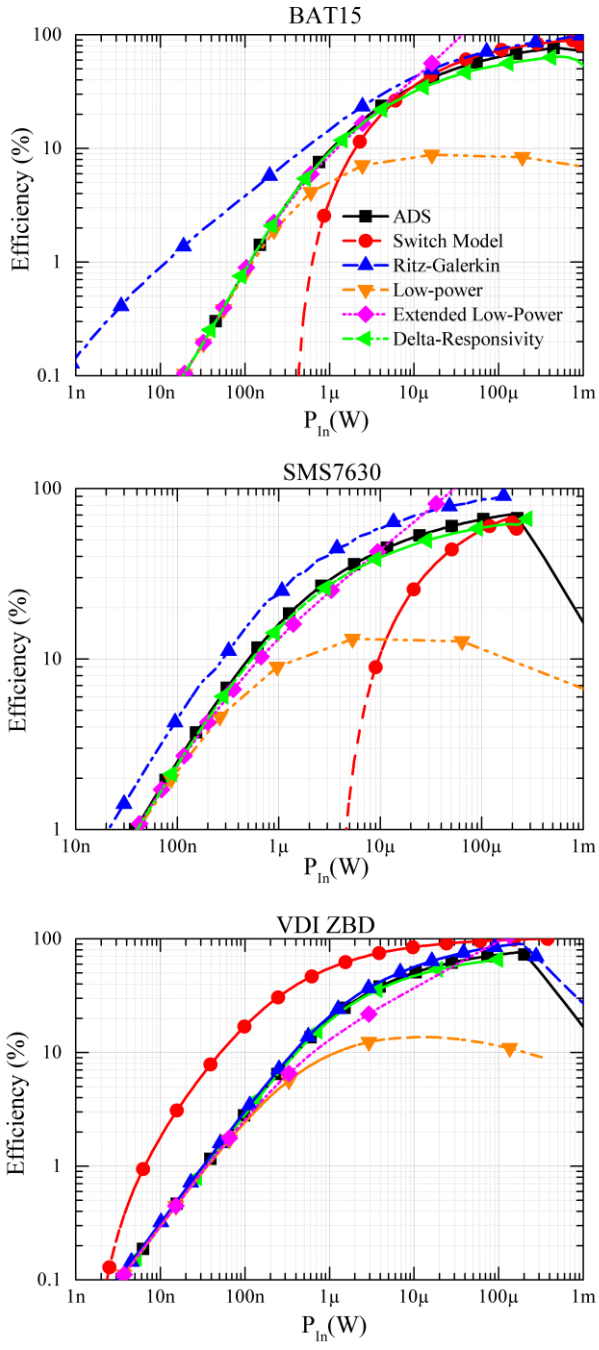

Figure 2-15: Comparison of the predictions given by the proposed methods and other already published models. Matching network insertion losses are not included as other models do not include them. f = 1.9 GHz, 5.1kΩ load.

The application of the Bode-Fano criteria for ambient microwave power harvesting has also been shown, predicting correctly which diodes may be matched to the desired frequency band of operation.

Based on the presented results, the authors suggest that in order to increase efficiency of low power microwave energy harvesters, there are mainly two paths that still need to be further investigated. The first is the use of devices with higher current responsivity than Schottky diodes, as is the case of recently published backward hetero-junction tunnel diodes [10, 13, 38]. The second path is the improvement of the matching network quality factor. As shown in [39], a power harvester working at 13.56 MHz has achieved nearly 55% of efficiency at -30 dBm input power, using quartz crystals in the matching network, although this approach results in narrower bandwidth matching networks.

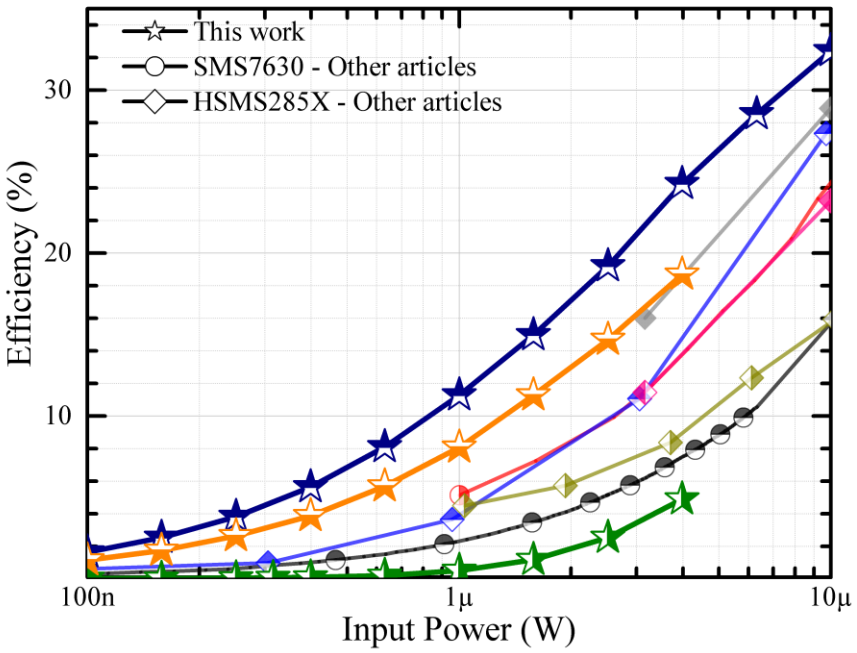

Figure 2-16: Comparison of measured rectifiers' efficiency to other state of the art microwave rectifiers. The references are given in Table 2-1.

In Figure 2-16, the prototypes' measured power conversion efficiencies are compared to some of the state-of-the-art MPH published results. Only results from rectifiers using Schottky diodes with matching network losses included in the efficiency measurements are plotted. Published papers that report results in frequencies below 1 GHz or above 4 GHz are not considered to keep parasitic losses within the same range. It may be seen that the result presented in [40] is very close

to the performance obtained by the prototype using the SMS7630 diode. This is expected as the load value is near and both diodes present similar characteristics. As far as the authors are aware, the efficiency presented by the prototype using the VDI ZBD diode is the highest published within the power range of interest using Schottky diodes for rectification, being close to the latest results presented for CMOS rectifiers [41] at the 1.9GHz frequency range.

Table 2-1: List of Rectifiers Presented in Figure 2-16

Symbol	Year	Diode	Frequency	Reference
	2015	VDI ZBD	1.9 GHz	Prototype
	2015	SMS7630	1.9 GHz	Prototype
	2015	BAT15	1.9 GHZ	Prototype
	2010	SMS7630	2.45 GHz	[42]
	2014	SMS7630	2.45 GHz	[43]
	2013	HSMS2855	2.45 GHz	[44]
	2012	HSMS285X	1.8 GHz	[45]
	2014	HSMS285X	1.8 GHz	[40]
	2014	HSMS285X	2.1 GHz	[40]

2.2.12 Acknowledgment

The authors would like to acknowledge the financial support of the Natural Sciences and Engineering Research Council of Canada (NSERC) and CREATE PERSWADE Training Program, which have partially funded the work presented in this paper. Also the samples provided by Rogers Corporation and Virginia Diodes are deeply appreciated, and were of great importance during the development of the presented work.

The authors wish to thank J. Gauthier, D. Dousset, M. Thibault, S. Dubé, T. Antonescu, and J.-S. Décarie of the Poly-Grames Research Center, Ecole Polytechnique de Montreal, for their technical assistance.

2.2.13 Appendix A

The mathematical proof of the optimum load where the maximum PCE is obtained is shown below, this is valid for the low input power range explored in this work, usually while the diode is operating in the square-law region. From (2.5) and (2.11) one can write:

$$\eta_{SL} \cdot \eta_{RFdc} = \frac{K \cdot R_L \cdot R_j^2}{\left(R_L + R_S + R_j\right)^2} \tag{2.32}$$

where $K = \left(\Re_{I0} \cdot \Delta_{\Re_{I0}}\right)^2 \cdot P_{jf0}$. The first derivative of this equation as a function of the load R_L is shown below:

$$\frac{\partial(\eta_{SL} \cdot \eta_{RFdc})}{\partial R_L} = \frac{K \cdot R_j^2 \cdot \left(R_L + R_S + R_j\right) - 2K \cdot R_L \cdot R_j^2}{\left(R_L + R_S + R_j\right)^2} \tag{2.33}$$

Making it equal to 0, one can find the values of RL where $\boldsymbol{\eta}_{\mathrm{SL}}\boldsymbol{\eta}_{\mathrm{RFdc}}$ has a maximum or a minimum:

$$\begin{aligned} & K \cdot R_j^2 \cdot \left(R_L + R_S + R_j\right) - 2K \cdot R_L \cdot R_j^2 = 0 \\ & R_j^2 \cdot R_S + R_j^3 = R_L \cdot R_j^2 \\ & R_L = R_S + R_j \end{aligned} \tag{2.34}$$

As the second derivative of $\boldsymbol{\eta}_{SL} \cdot \boldsymbol{\eta}_{RFdc}$ is always negative, this point represents the only maximum of $\boldsymbol{\eta}_{SL} \cdot \boldsymbol{\eta}_{RFdc}$, which happens when the load is equal to the diode resistance (which can be approximated by R_j at low power level).

2.2.14 Appendix B

In order to find the *z* positions where (26) has a minimum voltage amplitude or a maximum voltage amplitude, its first derivative is calculated by

$$\frac{\partial |V_l(z)|}{\partial z} = \left| \frac{V_{in}}{1 - \Gamma_2 \Gamma_3 e^{-2\gamma l}} \right| \cdot \frac{\partial \left| \left(e^{-\gamma z} + \Gamma_3 e^{\gamma z} e^{-2\gamma l} \right) \right|}{\partial z} \tag{2.35}$$

Making $C + iD = \Gamma_3 \cdot e^{-2\gamma l}$ to simplify the mathematical derivation:

$$\frac{\partial |V_l(z)|}{\partial z} = \left| \frac{V_{in}}{1 - \Gamma_2 \Gamma_3 e^{-2\gamma l}} \right| \cdot \frac{\partial \left| \left[e^{-\gamma z} + \left(C + iD\right) e^{\gamma z} \right] \right|}{\partial z} \tag{2.36}$$

One can use the points where this equation is equal to zero so to find the candidate maximum and minimum standing wave voltage amplitude positions:

$$\frac{\partial\left\|\left[e^{-\gamma z}+(C+iD)e^{\gamma z}\right]\right\|}{\partial z}=$$

$$\frac{\partial\sqrt{\left[(C+1)\cos(\beta z)-D\sin(\beta z)\right]^2}}{\partial z}+$$

$$+\frac{\partial\sqrt{\left[D\cos(\beta z)+(C-1)\sin(\beta z)\right]^2}}{\partial z}=0 \tag{2.37}$$

Expanding these equations and simplifying the resulting expression using trigonometric identities one can get:

$$C\sin(2\beta z)+D\cos(2\beta z)=0 \tag{2.38}$$

which finally results in the previously given result equal to:

$$z=\frac{\mathrm{n}\cdot\pi+\mathrm{atan}\left(-D/C\right)}{2\beta} \tag{2.39}$$

where *n* is any integer number equal or larger than zero.

CHAPITRE 3 RÉCUPÉRATION HYBRIDE COOPÉRATIVE D'ÉNERGIE AMBIANTE

3.1 Introduction

L'un des principaux obstacles à surmonter pour que la récupération d'énergie ambiante devienne une technologie utilisable dans les applications commerciales est la faible efficacité de conversion de la puissance reçue en courant-continu, qui ne permet pas de maximiser la puissance totale récupérée. L'état de l'art des circuits de REMA présentait des efficacités de conversion proches de 5% jusqu'à la publication de ce travail pour une puissance à l'entrée proche de -30 dBm et une fréquence dans la bande allant de 1 GHz - 3 GHz, comme montré dans la Figure 2-16. Cette efficacité amène à une puissance rectifiée proche de 50 nW, tout en admettant qu'une puissance continue (CW) est fournie à l'entrée du circuit de REMA, ce qui n'est pas toujours vrai dans un scénario réel, où les signaux vont plutôt présenter une amplitude variable et/ou être intermittents. La récupération d'énergie ambiante provenant d'autres sources, comme la vibration mécanique, souffre aussi d'une limitation semblable quand la puissance captée de l'environnement est très faible.

Selon le modèle mathématique présenté dans le chapitre 2, l'efficacité de la conversion de puissance RF-en-cc effectué dans une jonction non linéaire est proportionnelle à la puissance fournie à cette même jonction. Ce résultat est donné par l'équation (2-11), copiée ci-dessous :

$$\eta_{RFdc} = \frac{P_{dc}}{P_{jf\,0}} = \frac{R_j^2(I_{load})}{R_L + R_s + R_j(I_{load})} . \left(\Re_{I_0} . \Delta_{\Re_{I_0}} \right)^2 . P_{jf\,0} \tag{3.1}$$

Selon cette équation, l'augmentation de la puissance P_{jf0} fournie à la résistance de jonction devrait se traduire par une augmentation de la puissance rectifiée P_{dc}, et ce, de manière quadratique en raison d'une augmentation de l'efficacité η_{RFcc}. Soit :

$$P_{DC} = \eta_{RFdc} \cdot P_{jf\,0} = \frac{R_j^2(I_{load})}{R_L + R_s + R_j(I_{load})} \cdot \left(\Re_{I_0} . \Delta_{\Re_{I_0}} \right)^2 \cdot \left(P_{f\,0} \cdot \eta_P \cdot \eta_M \right)^2 \tag{3.2}$$

Cependant, vu que les sources distribuées dans le milieu ambiante ne sont pas connues ni contrôlées, la puissance micro-ondes disponible ne peux pas être modifiée pour les applications de REMA. Toutefois, il est néanmoins possible d'exploiter différentes sources d'énergie (non

corrélées) de manière collaborative, en combinant la puissance provenant de ces sources dans un seul élément non linéaire. L'exploitation de différentes sources avait déjà été proposée par d'autres travaux [8, 46]. Toutefois, dans ces travaux, la puissance de chaque source était rectifiée par un élément non linéaire indépendant, tandis qu'un circuit de combinaison de puissance cc était utilisé en fin de chaine, ce qu'ajoutait de pertes supplémentaires dans le circuit.

Comme cela va être démontré dans ce chapitre, lequel est aussi présenté dans le format d'article, la solution proposée profite des gains prévus par la théorie et simplifie le circuit, vu que la combinaison des puissances cc est déjà faite par l'élément non linéaire utilisé pour le redressement des signaux récupérés.

3.2 Article 2 — Hybrid Power Harvesting for Increased Power Conversion Efficiency

Carlos H. P. Lorenz, *Student Member, IEEE*, Simon Hemour, *Member, IEEE*, Weiqun Liu, Adrien Badel, Fabien Formosa, Ke Wu, *Fellow, IEEE*.

Accepté le 15 juin 2015 pour être publié dans la revue « *IEEE Microwave and Wireless Components Letters* ».

***Abstract* — This work presents a cooperative power harvesting scheme, collecting power from two or more independent ambient energy sources into a single non-linear component. It is shown that the interaction of uncorrelated signals in a nonlinear device can greatly improve the conversion efficiency of the harvester. This letter proposes and studies a hybrid power harvester working with both microwave radiation and mechanical vibration excitations. Up to 6 dB gain on the harvested power is obtained for excitations in the range of maximum -40 dBm input power, when compared to a single excitation and standalone harvester working at the same input power level.**

Index Terms — Hybrid energy harvesting, mechanical vibration, microwave power transmission, Schottky diodes, rectifier, rectenna.

Manuscript received February 09, 2015; revised April 09, 2015; accepted June 15, 2015. Date of publication August 18, 2015; date of current version October 05, 2015. This work was supported in part by the Natural Sciences and Engineering Research Council of Canada (NSERC) and CREATE PERSWADE Training Program.

Carlos H. P. Lorenz, Simon Hemour and Ke Wu are with the Poly-GRAMES research center, École Polytechnique de Montréal, Montreal (QC) Canada, H3T 1J4 (e-mail: carlos.lorenz@polymtl.ca).

Weiqun Liu, Adrien Badel and Fabien Formosa are with the SYMME research laboratory, Université de Savoie – Polytech BP 80439, Annecy Le Vieux, Cedex, France (e-mail: fabien.formosa@univ-savoie.fr).

Color versions of one or more of the figures in this letter are available online at http://IEEExplore.IEEE.org. Digital Object Identifier 10.1109/LMWC.2015.2463229

3.2.1 Introduction

The development of the internet of things (IoT), smart cities and smart houses is expected to rely on networks of dozens to millions of interconnected electronic devices and apparatus. Powering all of these devices and apparatus through cables or batteries may become an unpractical or even impossible task as some of them may be installed in inaccessible places, or too small to hold a battery, not to mention the huge quantity of those scattered elements.

As every new generation of transistor becomes more power efficient, these distributed devices will become less power hungry. Koomey's law [14] crystalizes this trend, predicting that the total energy needed per computing operation halves roughly each 18 months. Thus, in a few years, the hundreds of computations necessary for the ubiquitous/embedded sensors will require only a couple of nano joule [13, 14]. This would make microwave power harvesting a possible source of power for these distributed network devices and apparatus.

Ambient microwave power harvesters have been the subject of many recent publications. However, η_{Total}, the total harvester RF to dc power conversion efficiency, remains usually below 10% [9] at power levels below -30 dBm, as found in ambient energy harvesting applications [6].

Harvesting from multiple sources to increase the total power has already been considered [5, 46]. Niotaki *et al.* [5] presented a very interesting topology, combining dc power from solar and RF harvesting, however no efficiency improvement from energy combination has been reported to date. This letter evaluates a collaborative conversion of power using different sources, namely mechanical vibration and microwave radiation. The powers of both sources are combined using a single diode, operating in such a way that the system efficiency is increased and the topology is simplified.

3.2.2 Increasing the Conversion Efficiency

Using small signal theory, the diode's voltage-current relationship may be written in a Taylor series around the 0V bias operation point [29]:

$$I_{Rj}\left(V_j\right) = I_s \cdot \left[\frac{V_j}{N \cdot V_T} + \frac{V_j^2}{\left(N \cdot V_T\right)^2 2!} + \ldots + \frac{V_j^n}{\left(N \cdot V_T\right)^n n!} \right] \tag{3.3}$$

where I_{Rj} is the current flowing through the diode's nonlinear junction resistance; V_j is the voltage over the diode's junction; I_s is the diode's saturation current; N is the diode's ideality factor, V_T is the thermal voltage constant and n the order of the Taylor series. Assuming a voltage applied to the diode's junction, composed by two sinusoidal signals, corresponding to two different ambient energy transducers with angular frequencies equal to ω_1 and ω_2, and amplitudes equal to A and B, one can write:

$$V_j = A.\cos(\omega_1.t) + B.\cos(\omega_2.t) \tag{3.4}$$

For signals exhibiting a very small swing around the 0V bias point, one can keep only the first and second terms of equation (3.3) as a good approximation. Substituting (3.4) into (3.3) and applying some trigonometric manipulations, one can isolate the dc component of the resulting current, I_{dc}, and the current in each angular frequency, $I_{j\omega 1}$ and $I_{j\omega 2}$. Using these current components together with (3.4), the power absorbed by the diode junction at each of these frequencies, $P_{j\omega 1}$ and $P_{j\omega 2}$, may be calculated as follows,

$$I_{dc} = I_s \cdot \frac{A^2 + B^2}{4 \cdot N^2 \cdot V_T^2} \tag{3.5}$$

$$P_{j\omega 1} = \frac{I_s \cdot A^2}{2 \cdot N \cdot V_T} \tag{3.6}$$

$$P_{j\omega 2} = \frac{I_s \cdot B^2}{2 \cdot N \cdot V_T} \tag{3.7}$$

The sinusoidal signal to dc power conversion efficiency at the diode's non-linear junction, $\eta_{AC\text{-}DC}$ [9], can then be found, being described by (3.8). R_{j0} is the diode's zero-bias junction resistance, R_s is the diode's series resistance and R_L is the load's resistance. This equation gives the ratio of the total power reaching the diode's junction that is converted into dc power. As it can be seen from this equation, $\eta_{AC\text{-}DC}$ is directly proportional to the total power that is absorbed by the diode's junction.

$$\begin{aligned} \eta_{AC-DC} &= \frac{P_{DC}}{P_{j\omega 1} + P_{j\omega 2}} \\ &= \left(P_{j\omega 1} + P_{j\omega 2}\right) \cdot \left(\frac{R_{j0}}{2 \cdot N \cdot V_T}\right)^2 \frac{1}{R_{j0} + R_L + R_s} \end{aligned} \tag{3.8}$$

In other words, (3.8) indicates that the collaboration of different energy sources brings the operation point of the rectifier to a higher efficiency region. This increase in the efficiency has already been documented in multi-tone low power microwave power harvesting, as shown in [47].

3.2.3 Prototype and Measurements Results

The constructed prototype consists of a collaborative harvester, composed by a microwave signal harvester and a mechanical vibration harvester. It was optimized for excitations at the -50 dBm to -30 dBm power range. For these power levels, one can assume the two harvested powers as two sinusoidal signals arriving at the diode's junction, so the small signal approximation previously made remains valid.

The microwave rectifier operates at 2.1 GHz, and was built using a SMS7630-061 Schottky diode on a 15 mil Rogers RT/Duroid 5880 substrate. A parallel topology was chosen along with a 5.1 kΩ load, to which the dc power is delivered. This load value was chosen to optimize the source to load dc power transfer, and has a value near the diode's R_{j0} [9]. An electromagnetic cantilever type mechanical vibration harvesting system, with low dc impedance and resonant frequency at 33 Hz was added in series with the dc current path (Figure 3-1). In order to reduce the low-frequency mechanical harvester losses over R_L, a 100 µF capacitor, $C_{decoupling}$, was placed in parallel with R_L.

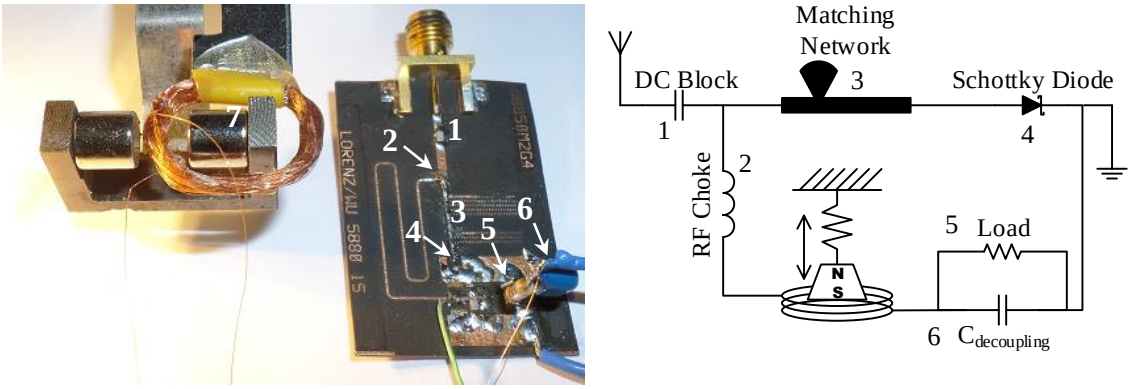

Figure 3-1: Picture and scheme of the built prototype, combining both Vibration and Microwave power harvesting.

The cantilever was excited by a shaker and monitored by an accelerometer, while the RF input was connected to a calibrated signal generator. In order to measure the power provided by the mechanical harvester to the system, the voltages at its terminals and over $R_L//C_{decoupling}$ were

monitored by an oscilloscope. The dc power supplied to the load was calculated using the dc component of the voltage over R_L.

The system was simulated using Keysight ADS Harmonic Balance. A sweep of the two input signals was done to generate a matrix of data. The vibration acceleration can be directly related to the power supplied by the mechanical harvester. Figure 3-2 shows the simulated output power for a constant -40 dBm input RF power using a lossless matching network, and varying input mechanical power. The output power is multiplied by a factor of 4 when the two input signals reach the same amplitude, meaning that the total efficiency is doubled, as expected from (3.8). The acceleration amplitude near this point, 70 m*g*, is equivalent to the one found at an external window near to a busy street [48].

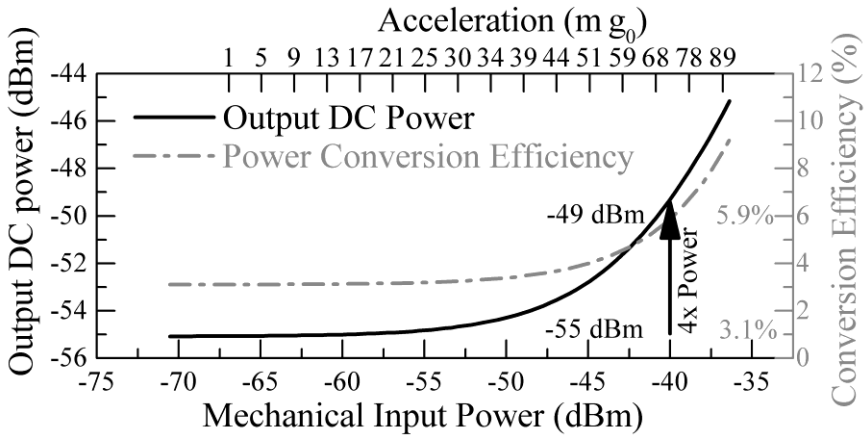

Figure 3-2: Simulated dc power delivered to the load, for a constant -40 dBm RF input power, as a function of the Mechanical input power. The top X axis shows the acceleration needed to obtain the corresponding input power from the cantilever transducer, and the right Y axis shows $\eta_{\text{AC-DC}}$ (6).

In Figure 3-3, simulation and measurement results are used in a comparison between the harvested powers when a single excitation is applied, and when both excitations are applied. An additional curve showing the direct sum of the harvested power with single excitation is given to ease the comparison. As nearly half of the input RF power is lost in diode parasitic components and matching network insertion losses (*IL*), the RF input power axis was shifted by 3dB to align the excitations where the magnitude of the power arriving at the diode's junction is equivalent for both sources. This approximation is valid while the diode's non-linear junction maintains a value

near R_{j0}, for higher powers the decrease in R_{j0} will result in a lower *IL* and diode parasitic losses [9], and matching network retuning may be necessary.

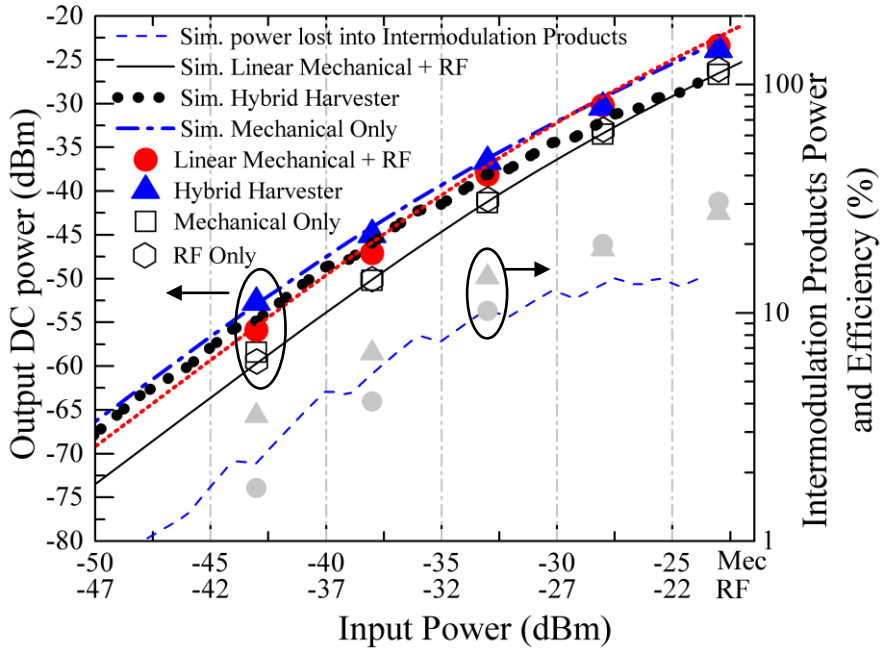

Figure 3-3: Comparison between the harvesters working only with mechanical excitation, only RF excitation or in hybrid mode, with both excitations applied at the same time. Scattered symbols (measurements) and lines (simulation) were added for comparison, the light grey symbols show the equivalent measurements power conversion efficiency. The percentage of the input power converted into intermodulation products is also shown as a dashed line.

A 6 dB increase in the total power harvested by the hybrid strategy was obtained, when compared to the single source harvesting. This gain is verified up to nearly -35 dBm input RF power. Above this threshold, the excitation cannot be considered as being small-signal anymore, and intermodulation products at the combination of the two excitation frequencies start to be generated by the non-linear diode junction. This power is then lost on parasitic effects or re-radiated by the antenna. The percentage of the total input power that is converted into intermodulation products, as a function of the input power, is shown in Figure 3-3.

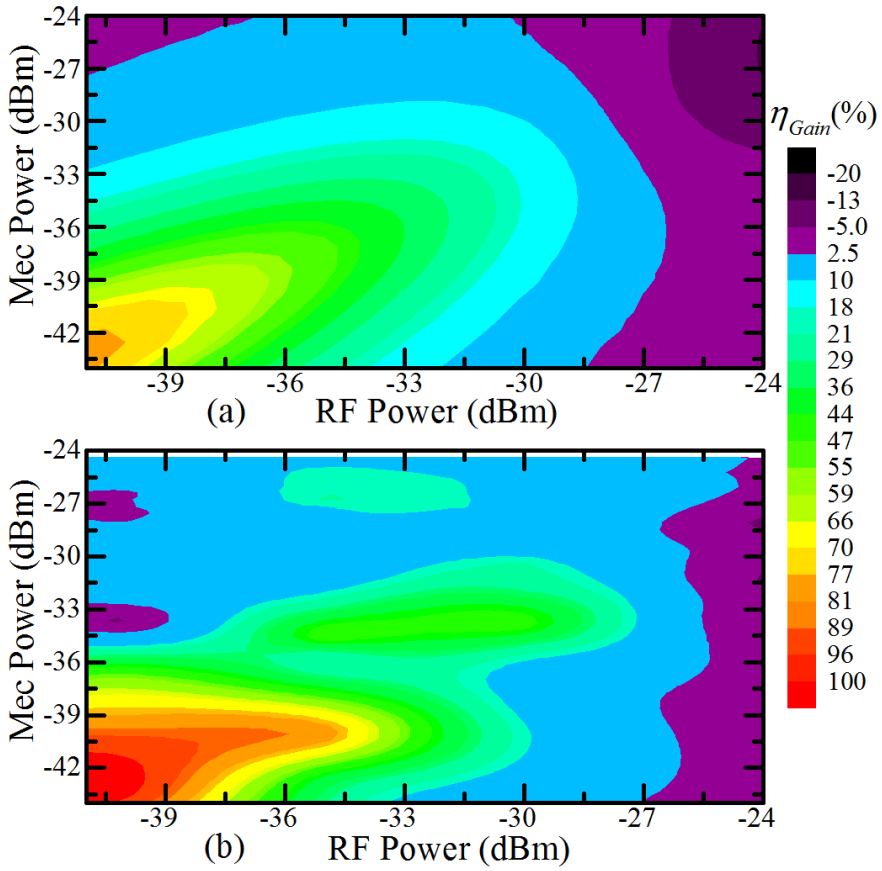

Figure 3-4: Comparison between (a) simulated and (b) measured efficiency gain, η_{Gain}. The color scale indicates the rapport between the dc power harvested by the hybrid harvester (P_{RF+MEC}), over the added dc power that would be recovered if each source was harvested by a separated circuit, multiplied by 100.

The efficiency gain obtained using the hybrid harvesting, η_{Gain}, is shown in Figure 3-4. Equation (7) describes η_{Gain}, where P_{DC_RF+MEC} is the recovered dc power using the hybrid approach, with both excitations applied at the same time, while P_{DC_RF} and P_{DC_MEC} are the recovered dc powers for separate excitations.

$$\eta_{Gain} = \frac{P_{DC\_RF+MEC}}{P_{DC\_RF} + P_{DC\_MEC}} \cdot 100 \tag{3.9}$$

The agreement between the simulation and the measurement demonstrates the relevance and the fine understanding of the proposed approach. The gain in the recovered power reaches nearly 100% for input power levels below -40 dBm, decreasing when the power increases. For

stronger input power levels, near -24 dBm, losses start to appear due to intermodulation products generation.

3.2.4 Conclusion

This work has successfully demonstrated the increase in power harvesting efficiency at power levels below -30 dBm, usually found in ambient power harvesting applications, by the use of Collaborative Hybrid Power Harvesters.

The Power Harvester proposed by this work uses two different power sources to excite a single rectification circuit, increasing the overall harvesting efficiency at low power levels. An example was presented, of a collaborative hybrid power harvester of mechanical vibration and microwave radiation, where output power gains up to nearly 100% were observed for -40 dBm and lower input powers, in accordance to the small signal theory presented in the beginning of this letter. Even though the proposed prototype uses these two power sources, the authors propose that other alternate signal harvesters could be combined to obtain a similar result.

The proposed hybrid technique presents another advantage over the separated power harvesting schemes, as the delivered dc power is already combined at the rectifying element. No extra circuitry is needed to combine both dc outputs. Hence diminishing eventual power losses that would occur during this process, simplifying the circuit and reducing its cost.

3.2.5 ACKNOWLEDGMENT

The authors would like to thank B. Besner and I. Nowlan, for allowing the use of the acoustics laboratory installations, and also the Technicians in Poly-GRAMES research center.

CHAPITRE 4 DÉPASSANT LA LIMITE D'EFFICACITÉ AVEC LES DIODES TUNNEL

4.1 Introduction

Comme indiqué dans le chapitre 2, les différentes efficacités de conversion qui prennent part dans le processus de récupération d'énergie micro-ondes ambiante peuvent être optimisées pour que le maximum ECP atteignable soit trouvé. La Figure 4-1 [9] présentée ici-bas donne un sommaire des efficacités de conversion de puissance obtenues pour plusieurs travaux scientifiques publiés dans les dernières années. Une corrélation peut être faite entre ces résultats, les résultats obtenus pour les prototypes présentés dans le chapitre 2 et les prévisions données par le modèle mathématique. En observant les résultats mesurés, on voit que la limite d'efficacité prédite par la théorie a déjà été atteinte dans la pratique. On relève tout particulièrement que dans la plage de puissance d'opération des circuits de REMA indépendamment de la technologie utilisée, cette limitation est très marquée dans la Figure 4-1 [9].

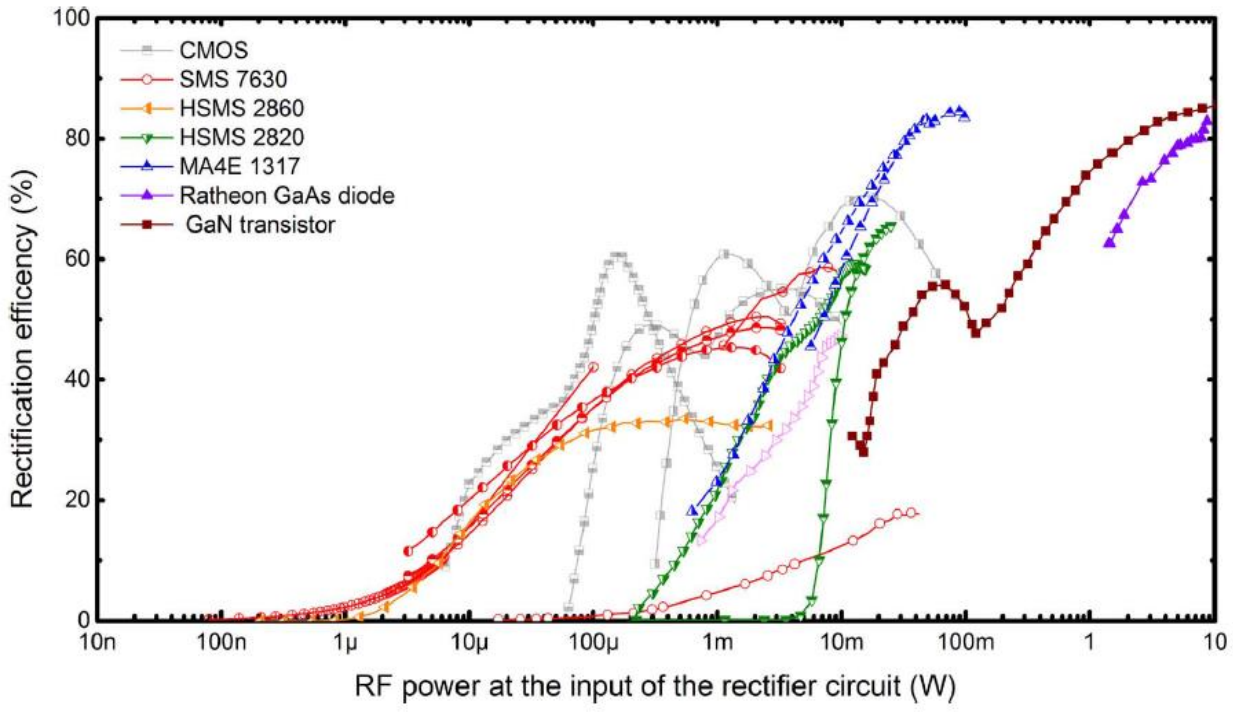

Figure 4-1: État de l'art des circuits de récupération de micro-ondes. Les couleurs et symboles indiquent le composant non linéaire utilisé dans le circuit en question [9].

Dans la Figure 4-1, les ECP semblent arriver à une limite maximale dans la plage de puissances en dessous de 3 µW (approximativement -25 dBm), indépendamment de la technologie utilisée pour le redressement (diode Schottky, CMOS, …). Comme il va en être discuté dans l'article présenté dans ce chapitre, l'origine de ce seuil d'efficacité provient du mécanisme physique qui régit le transport des électrons dans les jonctions des diodes Schottky et dans les transistors utilisés dans les composantes CMOS – les émissions thermo-ioniques.

Selon l'équation (2-11), répétée ici-bas, l'efficacité de conversion de puissance RF-cc est proportionnelle au carré de la responsivité en courant du dispositif non linéaire utilisé pour le redressement de la puissance. Dans ce chapitre, l'utilisation de diodes tunnel pour atteindre une ECP plus élevée que celle obtenue avec les diodes Schottky est étudiée. Le transport des électrons dans ces diodes, différemment des diodes Schottky, n'est pas régi par l'effet thermo-ionique. Cela permet le développement de diodes ayant une responsivité plus élevée que celle atteignable avec les diodes Schottky, permettant ainsi que des ECP plus élevées que les atteintes jusqu'à ici soient ainsi obtenues.

$$\eta_{RFDC} = \frac{P_{DC}}{P_{jf\,0}} = \frac{R_j^2(I_{load})}{R_L + R_s + R_j(I_{load})} \cdot \left(\Re_{I_0} . \Delta_{\Re_{I_0}}\right)^2 . P_{jf\,0} \tag{3.10}$$

4.2 Article 3 — Breaking the Efficiency Barrier for Ambient Microwave Power Harvesting With Heterojunction Backward Tunnel Diodes

Carlos H. P. Lorenz, *Student Member IEEE*, Simon Hemour, *Member IEEE*, Wenjun Li, Yi Xie, Jules Gauthier, *Member, IEEE*, Patrick Fay, *Senior Member IEEE*, Ke Wu, *Fellow, IEEE*

Soumis le 1er juillet 2015 à « *IEEE Transactions on Microwave Theory and Techniques* », accepté le 13 octobre 2015.

***Abstract* — Harvesting low-density ambient microwave power as an alternative power source for small ubiquitous wireless nodes has been proposed in recent papers discussing emerging technologies like the Internet of Things and Smart Cities. However a literature review of the state-of-the-art Schottky diode based microwave rectifiers shows that a maximum efficiency has been reached for such devices operating in the low-power regime, as is the case for ambient microwave power-harvesters. This work examines the underlying physical mechanisms responsible for this RF-to-dc power conversion efficiency limitation, and explores a high I-V curvature backward tunnel diode to overcome this efficiency limitation. Measurements of the 2.4 GHz RF-to-dc power conversion efficiency at -40 dBm input power demonstrates that the backward tunnel diode outperforms the HSMS-285B Schottky diode by a factor of 10.5 and the Skyworks SMS7630 by a factor of 5.5 in a lossless matching network scenario. A prototype built using a new GSG probe embedded with a matching circuit showed a total power conversion efficiency of 3.8% for -40 dBm input power and 18.2% for -30 dBm input power at 2.35 GHz.**

***Index Terms*— Backward tunnel diode, Schottky diode, microwave power harvesting, microwave power rectification, rectenna.**

4.2.1 Introduction

The way the internet is perceived by its users is going through a significant transformation. Today, nearly two billion people have access to the internet [2], using it to browse websites, play games, work, send and receive e-mails and messages, among many other on-line applications. Most of these applications, however, share a common characteristic: an end-user terminal. Nonetheless an important revolution is in progress, in which ubiquitous objects will be more and more connected to the internet or other local networks, leading to the Internet of Things (IoT) [1, 2]. Some emerging applications of this new paradigm in networking include monitoring the structural health of buildings and monuments, smart roads to help detect heavy traffic so that efficient itineraries can be suggested and traffic light timings can be optimized, remote health monitoring of patients, to cite just a few [16].

Emerging hardware technologies are being studied to enable these Smart Cities, Smart Building Automation and Monitoring, as well as Wearable Devices applications. These usually require wireless connections and small form-factor energy sources to remotely power the ubiquitous sensing and controlling devices, without the burden of a heavy and bulky battery that may be difficult to replace – as in the case of body implants and sensors embedded into building

---

Manuscript received July 1, 2015; revised September 30, 2015; accepted October 13, 2015. Date of publication November 18, 2015; date of current version December 02, 2015. This work was supported in part by the Natural Sciences and Engineering Research Council of Canada (NSERC) and CREATE PERSWADE Training Program. This paper is an expanded version from the IEEE MTT-S International Microwave Symposium, Phoenix, AZ, USA, May 17-22, 2015.

C. H. P. Lorenz, S. Hemour, J. Gauthier and K. Wu are with the Poly-Grames Research Center, École Polytechnique de Montréal, Montreal, QC H3T 1J4, Canada. (e-mail: carlos.lorenz@polymtl.ca).

W. Li, Y. Xie and P. Fay are with the Department of Electrical Engineering, University of Notre Dame, Notre Dame, IN 46556, USA. (e-mail: pfay@nd.edu).

Color versions of one or more of the figures in this paper are available online at http://ieeexplore.ieee.org.

Digital Object Identifier: 10.1109/TMTT.2015.2495356

structural parts. Resonant power transfer technology has shown to be a good alternative when a charger may be placed in close proximity to the wireless device of interest, as is the case for parked electric vehicles and even body implants that may be charged at periodic intervals [49]. However, very short operational distances between the charger and device becomes a fundamental obstacle when omnipresent, distributed sensor networks are deployed. Microwave Power Harvesting (MPH) has been proposed as an alternative wireless power source for such low power consumption and low duty cycle ubiquitous devices [8, 50, 51].

However, an overview of the state of the art in the field of microwave power harvesting suggests that a limitation in the efficiency of Schottky diode-based converters at low incident power levels has been reached [8, 9, 13]. In practice, microwave power rectifiers capable of operating below -30 dBm are needed for ambient microwave power harvesting (AMPH) as indicated in recent ambient microwave power density assessments [3, 8]. However, to date RF-to-dc conversion efficiency has not yet reached even 10% at frequencies above 1 GHz at such low-density power levels. Overcoming this performance barrier is essential for AMPH systems to become a practical reality.

Schottky diodes rely on the thermionic effect, which limits the zero-bias current responsivity $\mathcal{R}_{I0}$ to 19.34 A/W at 300K [13]. As shown in [9, 13], the rectification efficiency of microwave rectifiers operating in the diode's square-law region is directly proportional to the square of $\mathcal{R}_{I0}$. Backward tunnel diodes, which make use of quantum mechanical tunneling rather than thermionic emission, have been reported that overcome the Schottky diodes' inherent $\mathcal{R}_{I0}$, reaching values near 24 A/W for devices optimized for millimeter-wave operation [13, 38] or even as high as 35 A/W for lower-frequency devices [52]. This paper presents a deeper evaluation of the application of such diodes to overcome the low-power RF-to-dc conversion efficiency limitation observed with Schottky diode microwave rectifiers, an idea which was first introduced in [10] and is extended in this paper. A comparison between a backward diode and an HSMS-285B Schottky diode is presented, demonstrating an increase in the RF-to-dc conversion efficiency at extremely low incident power levels, as required when harvesting ambient power below -30 dBm.

4.2.2 Microwave Power Harvesting

In order to explore possible ways of increasing the power conversion efficiency PCE (3.11) of ambient microwave power harvesters, it is, first of all, necessary to understand the mechanisms

that play a role in the energy rectification process at very low input powers levels, as found in ambient microwave power harvesting scenarios. In such applications, the expected operation power range has peaks in the vicinity of -30 dBm and below, with a typical average power of -40 dBm and below [3, 8]. At such power levels the square-law microwave power rectification model presented in [9] can be used as a good approximation.

In this rectification model, the power conversion mechanism is sub-divided into different steps, each one with an intrinsic efficiency. These efficiencies combine to produce the total rectifier's PCE, as summarized below:

η_m is the matching network efficiency;

η_p is the parasitic efficiency;

η_0 is the non-linear junction RF-to-dc power conversion efficiency;

η_{dcT} is the dc power transfer efficiency, which gives the percentage of the total rectified dc power that is actually delivered to the load.

The total power conversion efficiency PCE can thus be calculated using (3.11):

$$PCE = \frac{P_{LOAD}}{P_{RF}} = \eta_m \cdot \eta_p \cdot \eta_0 \cdot \eta_{dcT} \tag{3.11}$$

where P_{LOAD} is the dc power delivered to the load and P_{RF} is the input RF power. The non-linear device characteristics influence in different ways each of these efficiencies. In the case of diodes, which are the subject of the study presented in this work, the Shockley diode model with package parasitic components is used, as shown in Figure 4-2. In this figure R_j represents the diode's non-linear junction resistance, C_j the junction capacitance, C_p the package parasitic capacitance, L_p, the package inductance and R_S the series resistance.

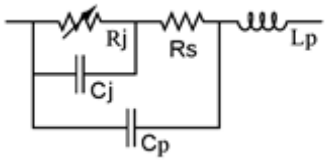

Figure 4-2: Shockley diode model with package/pads parasitic components.

Using this model, the total $\eta_0 \cdot \eta_{dcT}$ efficiency when the load connected to the diode is equal to R_{j0} is given by [9]:

$$\eta_0 \cdot \eta_{dcT} = \left(P_j \frac{\Re_{I0}^2 \cdot R_{j0}}{4} \right) \tag{3.12}$$

where P_j is the microwave power delivered to the junction resistance, R_{j0} is the junction resistance at zero-bias, and $\Re_{I0}$ is the diode zero-bias current responsivity. The parasitic efficiency can then be calculated by using [9]:

$$\eta_p = \frac{1}{\left(1+\left(\omega_0 \cdot C_{j0}\right)^2 \cdot R_s \cdot R_{j0}\right)^2} \tag{3.13}$$

where ω_0 is the angular frequency of operation.

The matching network efficiency η_m largely depends on the matching topology and circuit/component technology used to implement the matching network. However, (3.14) and (3.15) [21] can be used to estimate the relative increase or decrease of η_m achieved with different candidate diodes, provided that the quality factor of the matching network Q_m can be maintained at the same level. Such an assumption of constant Q_m is true if the source and load mismatch does not change substantially (i.e., the diode impedances under consideration are not dramatically different). Under these assumptions,

$$\eta_m = \frac{1}{1+\frac{Q_r}{Q_m}} \tag{3.14}$$

$$Q_r = \sqrt{\frac{R_{HIGH}}{R_{LOW}} - 1} \tag{3.15}$$

where Q_r is the required quality factor, which depends on the mismatch between the highest and lowest impedances (R_{HIGH} and R_{LOW}, respectively) that are to be matched. In the case of diode-based matching for AMPH, this is typically the source impedance and the diode's R_{j0}.

Using equations (3.11) through (3.15) one can understand the diode parameters that need to be optimized in order to maximize the power conversion efficiency.

As expected, equation (3.13) suggests that lowering the parasitic resistance and junction capacitance improves the parasitic efficiency. The importance of choosing devices with low parasitic capacitance is already well-known in the microwave community and will not be further discussed here.

The junction resistance R_{j0} has a more complex influence on AMPH performance. A higher R_{j0} increases the $\eta_0 \cdot \eta_{dcT}$ efficiency, assuming that the load magnitude can be adjusted to match that of the junction resistance. However η_p exhibits the opposite trend, and decreases when R_{j0} is increased. Similarly, η_m also degrades as R_{j0} increases since the losses in the matching network rise with an increased mismatch between source and diode junction resistance. The maximum PCE limitation that is reflected in the current-state-of-the-art AMPH designs [9, 13] resides in the fact that an optimum R_{j0} has been established, and for which $\eta_0 \cdot \eta_{dcT} \cdot \eta_p$ reaches its maximum for Schottky diodes.

Consequently to improve power conversion efficiency at low incident power levels, the only remaining parameter to consider is the diode's zero-bias current responsivity $\mathfrak{R}_{I0}$. However as presented in the next section, Schottky diodes' $\mathfrak{R}_{I0}$ is limited by thermionic emission over a potential barrier. This work explores and harnesses the use of another class of diodes, backward tunnel diodes, which are not governed by thermionic emission, for their use in AMPH applications.

4.2.3 Diodes for Energy Harvesting

Energy harvesting based on detection of low-level AC waveforms fundamentally relies on achieving a large second-order nonlinearity in order to maximize the RF-to-dc conversion. While large-signal rectification (i.e., switching) simply requires a strongly asymmetric I-V relationship to maximize the impedance difference between on- and off-states, harvesting energy from low-level sources that are insufficient to induce switching is more challenging. In this low-level signal regime, conversion efficiency is directly related to the square of the current responsivity $\mathfrak{R}_{I0}$ as shown in (3.12), which equals half the curvature, $\gamma = \frac{\partial^2 I}{\partial V^2} / \frac{\partial I}{\partial V}$, of the detection device at the zero-bias condition [13]. This metric can be directly assessed from the I-V characteristics of the device, and thus provides a convenient means for comparison among technologies. For thermionic devices such as Schottky and PN junctions for which the I-V relationship is of the form

$J = J_o(\exp(qV/nkT) - 1)$, one can see that $\gamma = q/nkT \approx 38.5\ V^{-1}$ at room temperature, independent of technology or the details of device design. This imposes fundamental physical limits on the ultimately achievable performance of thermionic detectors for energy harvesting applications. To circumvent this limitation, devices based on alternative physical operation principles for which γ is not limited to *q/kT* are potentially attractive. One promising physical mechanism that can be leveraged to obtain a higher curvature is interband tunneling. In contrast to Schottky diodes, PN junctions, and transistor-based passive detectors (e.g. diode-connected FETs, Schottky diodes using HEMT gates) in which carriers in a single band interact with a voltage-controlled potential barrier as the basis for detection and rectification, interband tunnel diodes are governed by the combination of the density of states and occupancy probabilities on both sides of the tunnel junction as well as the tunneling probability. In this way the density of states in both the conduction and valence bands, as well as the details of the tunnel barrier, can be used to engineer devices with increased second-order nonlinearity and thus offer the potential for improved detection and conversion efficiency. An analytical treatment of homojunction interband tunnel diodes can be found in [53]; within the simplified model used, an arbitrarily large curvature can be achieved by a proper selection of the Fermi levels within the device [53]. Fundamentally these devices can offer larger curvatures than thermionic-emission based devices because the overlap between the occupied electron and hole densities of states is "filtered" by the bandgaps at the heterojunction, leading to a truncation of the Fermi-Dirac distribution for the carriers. Devices of this type have been demonstrated experimentally as millimeter-wave detectors [54], and curvatures as high as 70 V^{-1} have been reported experimentally [52], broadly consistent with the expectations with theory. It should be noted that in order to achieve these high curvatures, a "backward" tunnel diode structure is needed, in contrast to an Esaki diode [55, 56]. In the case of an Esaki diode, extremely high doping is used on both sides of the junction, leading to low junction resistance and the onset of negative differential resistance in the forward characteristic. For detector and harvester applications, however, the negative differential resistance is not desirable (the curvature changes sign at the onset of negative differential resistance, leading to a partial cancellation of the detected signal with an increasing input power) and the second-order curvature near zero bias is smaller than with the more modestly-doped backward diode structures [53].

However, homojunction tunnel diodes such as those described above also pose some challenges in energy harvesting applications. Of particular concern for RF and microwave applications, homojunction tunnel diodes have a large capacitance per unit area (as a direct consequence of the use of heavy doping to achieve the thin depletion region and band degeneracy required to enable tunneling). This limits the frequency range of application, due to increased parasitic losses, as well as the bandwidth achievable with reactive matching networks. It has also been reported that Ge-based tunnel junctions can pose reliability and manufacturability challenges [57].

As an alternative, heterostructure backward tunnel diodes are an attractive approach. These devices maintain the fundamental operational principles of homojunction tunnel diodes (interband tunneling) and thus the possibility for high curvature, while at the same time introducing significant additional degrees of freedom in the device design to allow optimization of the device performance for specific applications. For example, devices of this type have previously been demonstrated to provide high-sensitivity, low-noise microwave and millimeter-wave detection [38, 58-60] for applications such as passive millimeter-wave imaging, with an extremely low noise equivalent power (NEP) of 0.18 $pW/Hz^{1/2}$ [38]. This record-low NEP is made possible by a combination of both extremely low device noise, in conjunction with higher curvature arising from the operational physics. To maximize performance for detection, the devices are designed to maximize the second order nonlinearity at zero bias, thereby allowing the detectors to be used without externally applied bias. This dramatically reduces 1/f noise (resulting in nearly thermal-noise-limited performance) [59, 61], and it has been shown that zero-bias second-order nonlinearity in excess of what is possible with Schottky diodes can be achieved [38]. This degree of control of the device characteristics is made possible by the substantial design flexibility in heterostructure devices. Low-level RF energy harvesters have similar requirements, i.e., strong nonlinearity near zero bias is needed for efficient RF-to-dc conversion, and thus these devices are also attractive for this application.

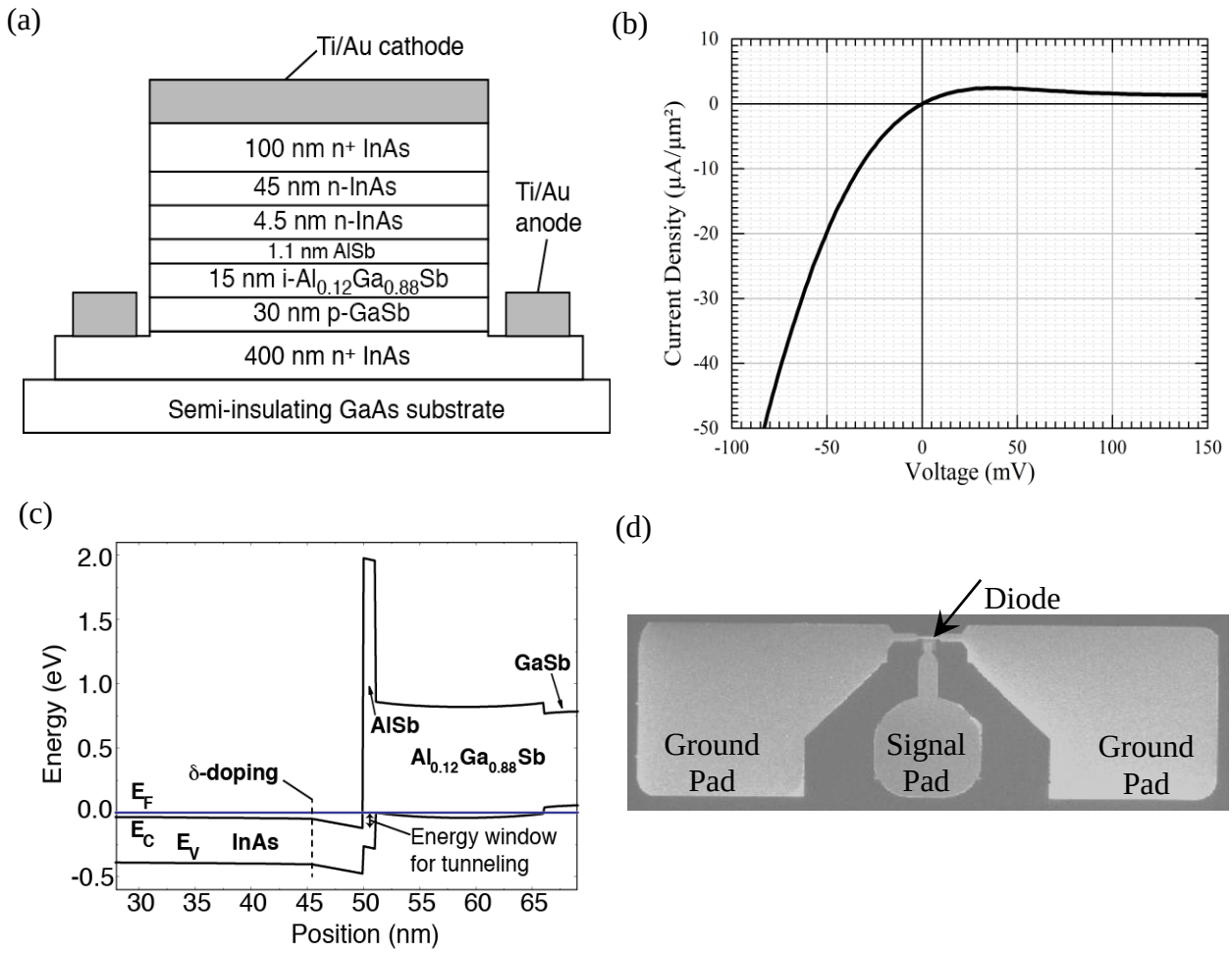

Figure 4-3: (a) Schematic cross-section diagram for the heterostructure backward diode used in this work. The energy filtering enforced by the small tunneling window results in strongly nonlinear current-voltage characteristics and high sensitivity. (b) Current Density - Voltage characteristic for the heterostructure backward diodes used for the power harvesting prototypes presented in this work. (c) Calculated energy band diagram. (d) Scanning electron micrograph of fabricated backward tunnel diode with ground-signal-ground probe pads.

Figure 4-3 (a) shows a schematic cross-sectional diagram of the nominal heterostructure backward diode used in this work; the corresponding measured Current Density-Voltage characteristics are shown in Figure 4-3 (b). As can be seen, a rectifying characteristic is obtained, with an extremely asymmetric I-V characteristic and “knee” at very low voltage, indicative of a

strong curvature. In addition, the turn-on is in the 'reverse' direction (i.e., in the opposite sense from a conventional PN junction diode), as expected for a backward diode. As discussed previously, the efficiency of a power harvester is directly related to the junction resistance and curvature. Due to the interband tunneling mechanism in heterostructure backward diodes, γ can be much larger than what is possible with conventional Schottky or other thermionic emission-based devices; optimizing a heterostructure backward tunnel diode for energy harvesting applications requires maximizing the curvature while keeping the junction resistance at an acceptably low level. The key parameters that enable control over the device performance are the anode and cathode doping concentrations (and doping profiles), the tunnel barrier thickness, and the energy band offset between the valence band in the anode and the conduction band in the cathode. As one example, Figure 4-3 (c) shows the computed energy band diagram for the backward diode structure shown in Figure 4-3 (a). The choice of an aluminum composition of 12% in the anode layer leads to a small overlap between the conduction and valence bands, and thus as shown Figure 4-3 (c), only carriers occupying a narrow range of energies can participate in tunneling through the AlSb tunnel barrier. Carriers with higher energies in either the anode or cathode are blocked by the bandgaps (i.e., are filtered) and cannot contribute to the current [53, 62]. The choice of the AlSb tunnel barrier thickness allows an independent control of the junction resistance (since to first order tunneling probability is exponential in barrier thickness) without altering the densities of states in the cathode and anode appreciably. The doping profiles in the anode and cathode are selected to enhance transmission through the structure, with a δ-doping plane incorporated into the cathode in this structure to provide a nearly flat band profile.

The device heterostructure was grown by molecular beam epitaxy on a semi-insulating GaAs substrate. Device fabrication included evaporated Ti/Au anode and cathode contacts, mesa isolation using selective wet chemical etchants [63], and passivation with benzocyclobutene. The devices had an area of approximately 0.5 μm^2; electron beam lithography was used to accurately define the device active area. Optical lithography was used to define the pads, mesas, contacts and passivation layers.

For the power harvesting experiments performed here, devices with the nominal heterostructure shown in Figure 4-3 (a) were used; this results in a measured zero-bias curvature γ=45 V^{-1}, and as will be shown, this improved curvature and low turn-on voltage result in high

power harvester efficiency even at low incident RF levels. To further increase the harvester efficiency, increased curvature is desirable. Fundamentally, increases in curvature are correlated with improved energy filtering at the tunnel junction; one promising approach for narrowing the energy window over which tunneling can occur is by modifying the composition of the AlGaSb anode (i.e., increasing the Al composition results in a smaller tunneling window). Physics-based simulations of heterostructures with the same basic form as shown in Figure 4-3 (c), except with varying $Al_xGa_{1-x}Sb$ compositions have been performed, and the junction resistance and curvature expected from these models is shown in Figure 4-4. Details of the modeling framework have been reported previously [64]. As can be seen in Figure 4-4, increasing the Al composition in the anode results in a significant increase in curvature, with curvatures approaching 90 V^{-1} possible for compositions of approximately 25%. This increased curvature arises from the more narrowly-filtered carrier energy, but as expected this narrower energy range for tunneling is also accompanied by an increase in junction resistance. Our models project a harvester efficiency $\eta_0 \cdot \eta_{dcT}$ of 63% for such a diode at -40 dBm input power, indicating that despite the promising results obtained to date and reported here, considerable additional improvements are possible. While further increases in curvature can be obtained, they come at the expense of a significant increase in junction resistance that may limit overall conversion efficiency. The junction resistance increase can be counterbalanced to some extent by increasing the diode's junction area, however at the cost of an increased junction capacitance. As a result, the optimum anode composition and junction area is also a function of the intended frequency of operation. Detailed study of these tradeoffs is the subject of ongoing work.

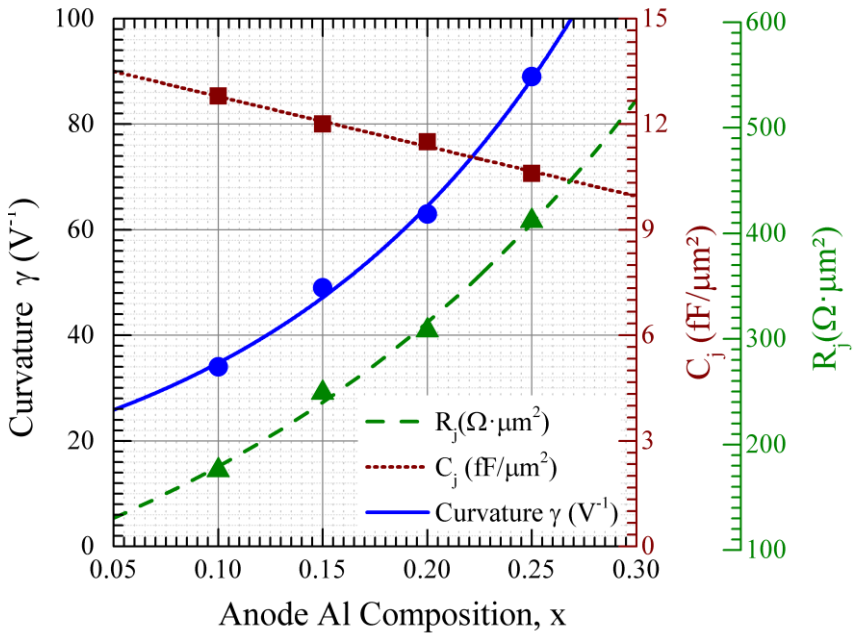

Figure 4-4: Projected curvature (γ) and junction resistance (R_j) as a function of anode composition as obtained from physics-based simulations. Discrete points have been computed using the simulations; the curves are exponential fits to the simulated data. Increased curvature as well as junction resistance result from narrowing of the tunneling window with increasing Al composition in the anode.

4.2.4 Backward Tunnel Diode Characterization

Backward tunnel diodes with 12% anode Al composition have been characterized using a 100 µm pitch GSG (Ground-Signal-Ground) probe on a Cascade Summit probe station. A Keysight PNA network analyzer was used to measure the S_{11} parameters and also as a calibrated microwave power source. The PNA network analyzer output power was calibrated at the probe K-connector interface using a power meter, and the probe insertion loss was loaded into the network analyzer to compensate for power losses inherent from the probe. In this way, the power delivered to the diode could be precisely controlled. The diode sensitivity and I-V characteristics were measured using a 6-1/2 digit HP 34401A precision multimeter, connected to the network analyzer's internal bias-T. The dc current-voltage characteristic, as well as the diode's sensitivity and reflection coefficient Γ from 500 MHz to 40 GHz were measured for an input power ranging from -30 dBm to -5 dBm, in 5 dB steps .

The diode model parameters given in Figure 4-2 were then extracted from the measurements. The nonlinear junction current-voltage equation $I_j(V_j)$ was modeled using a 7th order polynomial, given in (3.16); the coefficients were obtained through least-squares curve fitting to the measured I-V characteristics. A comparison between the modeling results and measurements is shown in Figure 4-5. The dc non-linear model has been verified between -100 mV and 200 mV; this voltage range is sufficient to cover the voltages experienced by the device in ambient energy harvesting applications.

$$I_j(V_j) = 7.99\cdot10^{-5}(V_j) - 1.73\cdot10^{-3}(V_j^{\,2}) + 1.27\cdot10^{-2}(V_j^{\,3}) + 6.76\cdot10^{-3}(V_j^{\,4}) - 0.58(V_j^{\,5}) + 2.92(V_j^{\,6}) - 4.65(V_j^{\,7}) \tag{3.16}$$

Using the $I_j(V_j)$ polynomial given in (3.16), the diode's junction resistance R_j, and current responsivity $\mathcal{R}_I$ were calculated and are shown in Figure 4-6 [18]. Having the non-linear junction behavior already defined, the measured sensitivity and reflection coefficient were used to extract the linear parasitic model parameters; these were found to be C_p = 13.7 fF, R_s = 25 Ω and L_p = 52.6 pH. Although C_j may in general be bias-dependent, for the model developed here C_j was approximated by a linear (constant) capacitance of 4.5 fF. Modeling results and measurements are compared in Figure 4-7. Although the measurements were limited to 40 GHz, the simulation results have been projected up to 100 GHz to show the expected diode behavior.

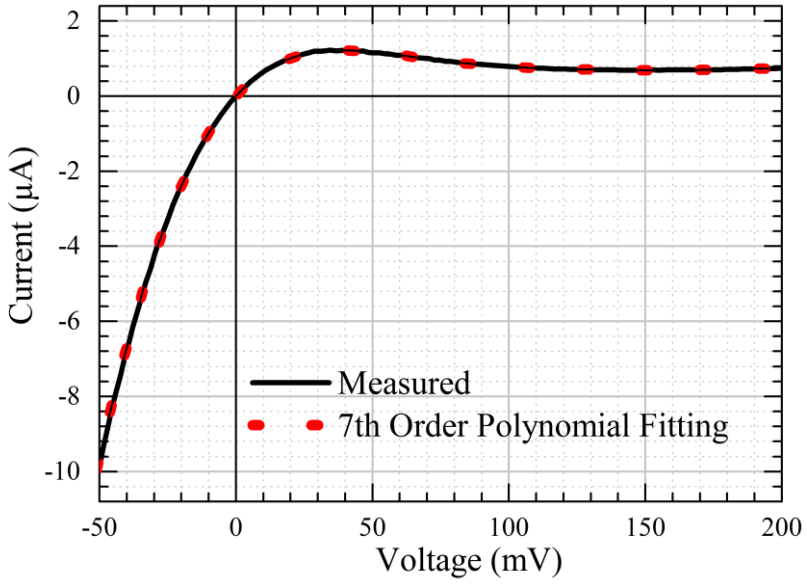

Figure 4-5: Measured and modeled backward tunnel diode I-V curve.

The modeled diode resistance and responsivity near zero-bias are shown in Figure 4-6, over the expected operating region for the AMPH application presented here. From this figure, a $\mathcal{R}_{I0}$ of 21.65 A/W and R_{j0} of 12.5 kΩ are obtained for the particular backward tunnel diode used for this work.

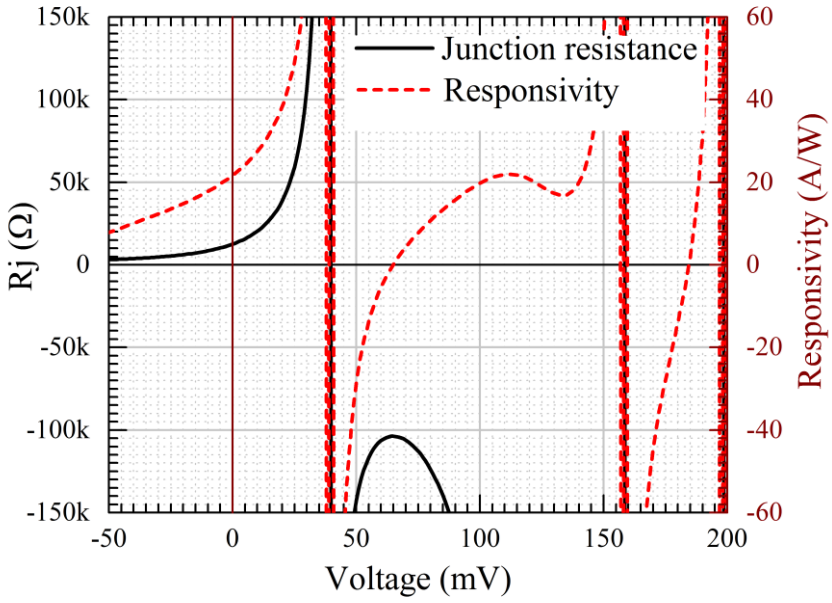

Figure 4-6: Calculated backward diode R_j and $\mathcal{R}_I$, using the 7th order polynomial fitted to the measured I-V relationship.

Assuming that the parasitic efficiency is comparable for Schottky and tunnel diodes, the increase in the diode's $\mathcal{R}_{I0}$ from 19.34 A/W in the ideal Schottky diode case to the measured tunnel diode responsivity of 21.65 A/W indicates that the efficiency at square-law power levels is expected to increase by a factor of 1.25 according to (3.12).

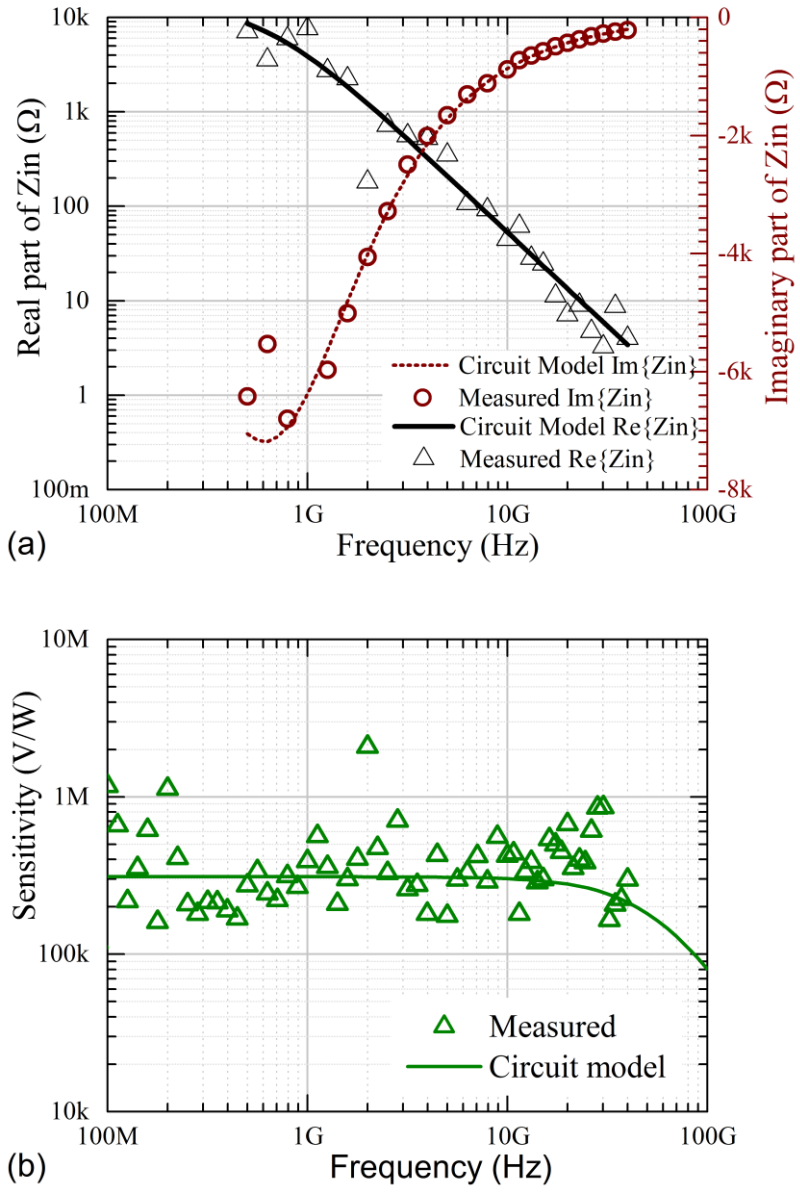

Figure 4-7: Comparison between measured and modeled backward diode RF characteristics at -30 dBm. (a) Input impedance, Z_{in}, real and imaginary components. (b) Voltage sensitivity; the simulation has been projected to 100GHz.

4.2.5 Comparison of Backward Tunnel Diode and Schottky Diode Microwave Rectifiers

Neglecting the matching losses and considering that parasitic losses are negligible at 2.45 GHz due to very low C_j, the studied backward diode has a calculated RF-to-dc power conversion

efficiency equal to 14.7% at -40 dBm input power. Two commonly used Schottky diodes in AMPH applications were also evaluated and compared to the proposed backward diode, these are the Avago HSMS-2850 and the Skyworks SMS7630 diodes. Table 4-1 compares the expected power conversion efficiencies at -40 dBm input power, 2.4 GHz center frequency, and resistive load matched to each diode's R_{j0}. The efficiencies were calculated using the backward diode model parameters presented previously, and Schottky diodes parameters from the manufacturer datasheets. This comparison highlights two important advantages that arise from the use of the backward tunnel diode in AMPH applications. The first is the discussed increase in the $\eta_0 \cdot \eta_{dcT}$ efficiency product due to the increased $\mathcal{R}_{I0}$. However another advantage that should be noted is the very high parasitic efficiency due to the low junction capacitance that results from the backward tunnel diode structure used here.

Table 4-1: Rectifier Efficiencies at -40dBm @ 2.4 GHZ

Diode	$\mathcal{R}_{I0}$ **(A/W)**	R_{j0} **kΩ**	C_{j0} **fF**	**Efficiency (%)**		
				$\eta_0 \cdot \eta_{dcT}$	η_p	**PCE**
Backward	21.65	12.5	4.5	14.7	99.7	14.6
Ideal Schottky	19.34	12.5	NA	11.7	NA	NA
HSMS285B	18.25	9.13	180	7.6	13.9	1.1
SMS7630	18.42	5.43	140	4.6	45.4	2.1

From Table 4-1, it can be seen that a large advantage is expected when using backward tunnel diode in AMPH applications; the expected PCE for the tunnel diode case is nearly 7 times the PCE of the SMS7630 diode at microwave input power levels typical of ambient harvesting applications.

In order to verify the increase in PCE predicted by the theory, both HSMS-285B and the backward diode rectification efficiencies were measured. The choice of the Schottky diode was based on the value of Rj0, which should be near to that presented by the backward diode to ensure a valid comparison.

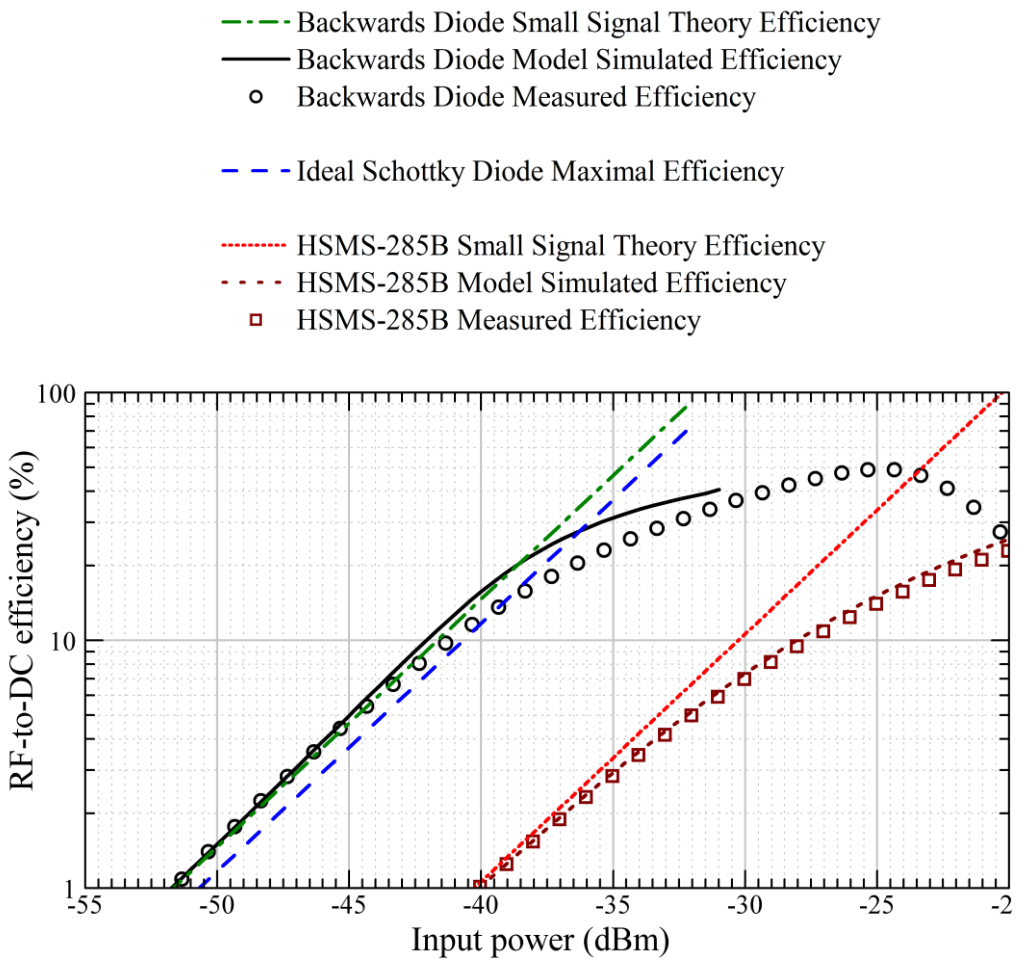

Figure 4-8: Measured, simulated and calculated efficiencies of the backward tunnel diode and HSMS-285B diode microwave rectifiers at 2.4GHz. Matching network losses have been de-embedded.

The microwave power rectification setup in our experiments consisted of a Keysight PNA Network Analyzer with an integrated bias-T, a Focus microwave tuner system used as matching network, and a 6-1/2 digit HP 34401A multimeter connected to a variable resistor, used as the dc load. The output power of the PNA was calibrated at the tuner input plane (source side) so that it could be used as the microwave power source. At the same time, the PNA was used to measure the reflection coefficient and ensure that a good matching was obtained at 2.4 GHz. A schematic diagram of the setup is shown in Figure 4-9 and a picture in Figure 4-10.

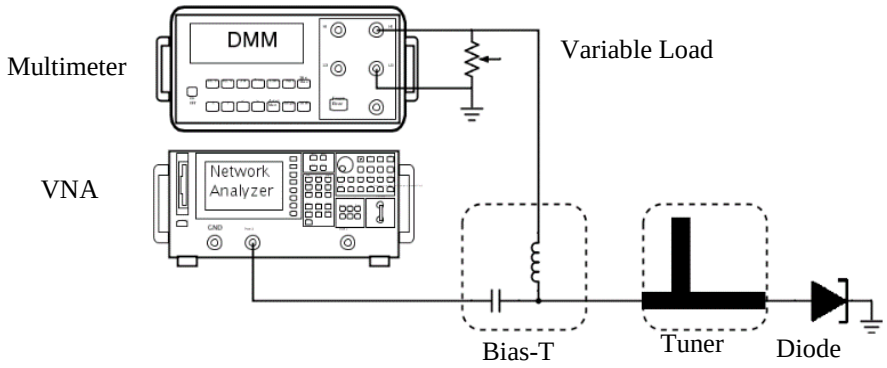

Figure 4-9: Simplified schematic of the setup used for the microwave rectifier PCE measurements.

Figure 4-10: Picture of part of the setup used to compare the PCE of the HSMS-2850 and backward tunnel diode. The picture shows the probe station and the Focus Microwaves Tuner, used as matching network.

To evaluate the power incident on the diodes, the open-circuit detector voltage was measured, using the diodes as microwave power detectors. This information together with the diode's sensitivity measured during the characterization step was then used to extract the insertion losses of the matching circuit. In this way, the rectifier's RF-to-dc conversion efficiency $\eta_0 \cdot \eta_{dcT}$ and parasitic efficiency η_P were evaluated for both diode types, independently of any losses that originated from the matching circuit implementation.

For the efficiency measurement, the variable load was adjusted to its optimum value; 13 kΩ was used for the backward diode, and 9 kΩ for the HSMS-285B diode. The measured, calculated and simulated results are given in Figure 4-8 together with an indication of the maximum efficiency that an ideal Schottky diode with no parasitic losses and the same R_{j0} as the studied backward diode could attain. The simulation tool used was the Keysight ADS harmonic balance simulator.

The results given in Figure 4-8 show the two predicted advantages of the evaluated backward diode for AMPH applications. The first is the improvement in power conversion efficiency due to the higher current responsivity. Even when compared to the ideal Schottky diode theoretical limit, the backward diode has a 25.3% higher efficiency at extremely low input power, showing a very good agreement with the previously calculated factor of 1.25. The second advantage comes from the low junction capacitance resulting from the backward diode construction. The resulting parasitic loss is extremely low at 2.4 GHz, leading to a 10.5 times higher efficiency when compared to the HSMS-285B diode at -40 dBm input power. This result too is in very good accordance with the previously calculated results given in Table 4-1.

4.2.6 Backward Tunnel Diode Rectifier Prototype

In order to demonstrate a microwave power rectifier working at AMPH input power levels, a prototype with a narrow-band matching network has been fabricated to demonstrate operation in a more realistic context, including matching network losses. An in-house GSG probe was developed so multiple backward diodes could be tested using the same matching network board so the repeatability of the predicted result could be verified.

4.2.6.1 GSG probe fabrication

The GSG probes have been developed with the goal of being embeddable to any PCB circuit. For convenience, all test and qualification measurements have been done on the same 30 mil Rogers RT/Duroid 6002 substrate. A 50 Ohm tapered coplanar line is used as a transition from the connector to the GSG probe, as seen in Figure 4-11.

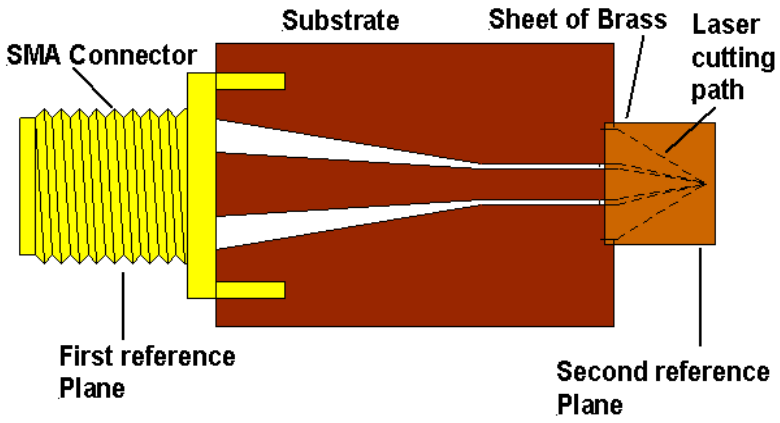

Figure 4-11: An adapter characterization is done to extract the S parameters of the probe, along with the substrate it is soldered on and the SMA connector

The GSG probe tips are realized on a thin 8 mil sheet of brass which is first welded to the PCB. The brass is then micromachined with a laser (indicated in the figure by the dotted lines) along the shape of the required tip. Alignment references are set from the sides of the transmission line to ensure the cutting contour fits the line and PCB gap.

The dimensions of the probe tip (starting pitch as well as the pitch of the tip) are determined on one side by our PCB fabrication process, which allows a minimum 5 mil gap between the ground plane and the 42 mil center conductor, and the on-wafer diode pads which have a 100 μm pitch for the diodes reported here. A photograph of the micromachined probe tips can be seen in Figure 4-14. To allow micro-positioning using standardized probe stations, a customized probe holder has been fabricated.

The scattering matrix has been extracted and validated using an adapter characterization procedure [65-67], which uses two calibration planes. The first reference plane is set with APC 3.5mm calibration standards (before the connector) and the second reference plane is set at the end of the tips, with an on-wafer SOL calibration (using Picoprobe CS5 standards). S_{21} and S_{11} are shown in Figure 4-12.

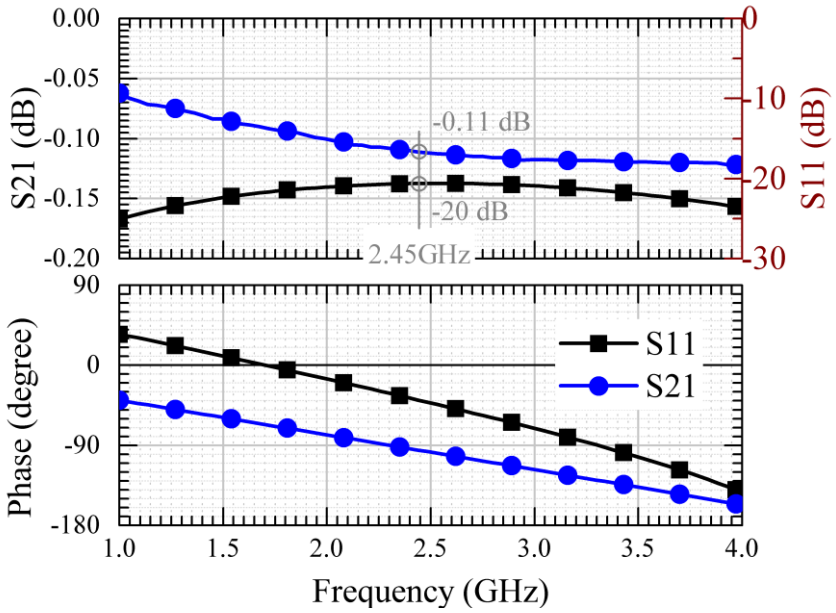

Figure 4-12: Reflection and transmission parameter of the probe extracted through an adapter characterization procedure.

4.2.6.2 Rectifier prototype measurements

The substrate used for the matching network construction is 30 mil Rogers RT/Duroid 6002. This design was based on the ideal matching network impedance given in Figure 4-13, and includes a matching network with an adjustable length short circuit stub, which was used to fine-tune the narrow band matching network. A picture of the circuit is shown in Figure 4-14.

Figure 4-13 shows the PCE as a function of the matching network output impedance. The simulation was done using the backward diode model presented previously with an L-section matching network composed of a 50 Ω series transmission line and 50 Ω short-circuited stub which is used as the dc rectified current return path. The line and stub lengths were swept from 0.05 mm up to **λ**/2. The very high initial mismatch between the 50 Ω source and the 12.5kΩ diode R_{j0} introduces almost 3 dB matching network insertion loss, resulting in a reduced peak PCE of approximately 20% at -30 dBm input power, while the lossless case presented in Figure 4-8 had a PCE near 37% at the same frequency and input power. An important remark that can be made based on the results from Figure 4-13 is that the impedance to be matched is nearly real, with very low imaginary part. This means that the proposed backward tunnel diodes may be matched to a

large bandwidth using more complex matching network structures according to the Bode-Fano criterion [27].

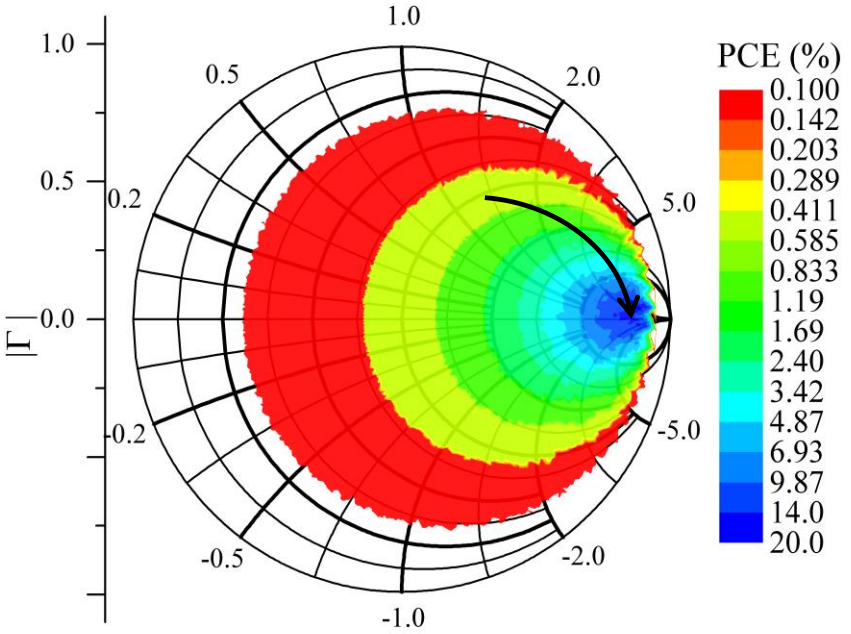

Figure 4-13: Simulated PCE for different matching networks impedances. -30 dBm input power, 2.4GHz, 13kOhm load. The arrow indicates an increasing PCE.

Due to the 3 dB matching network insertion losses resulting from the high mismatch between the source and the diode junction resistance [68], an overall rectifier efficiency at 100 nW of 3.8% has been measured. Although well below the 11.6% PCE expected from the measurements in Figure 4-8, the device technology has proved to be promising based on this first demonstration. Figure 4-15 shows the measured PCE for four different samples of the backward tunnel diode, showing the repeatability of the results across several tunnel diodes. The dc loads connected to the circuit were adjusted for each diode, in order to reach the maximum PCE. Measurements and Harmonic Balance (HB) simulation using the proposed backward tunnel diode model agree very well, indicating that the parameters extracted are in accordance with the actual diodes evaluated. The matching network was simulated using the Keysight Momentum electromagnetic fields simulator.

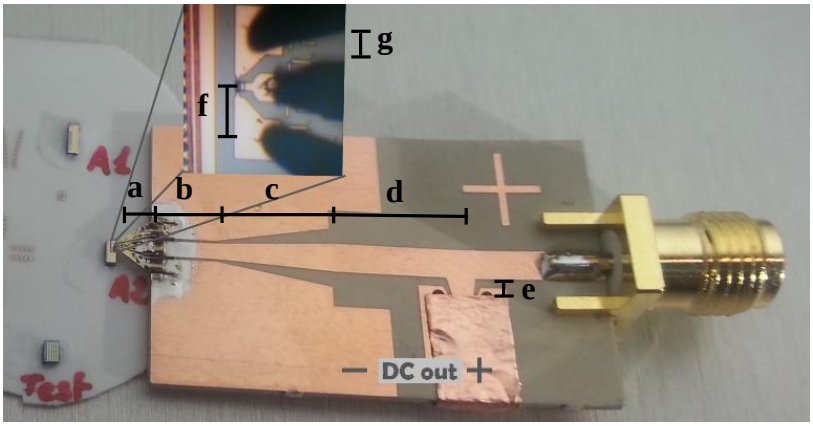

Figure 4-14: Photograph of the rectifier circuit using a backward diode. The matching network was built and integrated with an in-house GSG probe used to interface with the diode pads (inset). a = 83 mil, b = 170 mil, c = 300 mil, d = 333 mil, e = 25 mil, f = 100 µm, g = 2 mil. Width of the line in d = 75 mil, width of the line in b = 42 mil (6 mil separation between line and ground).

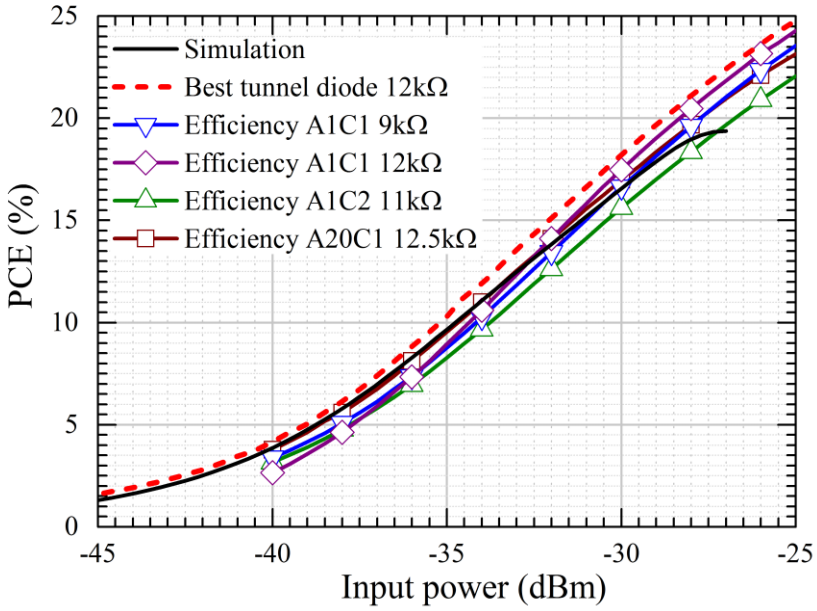

Figure 4-15: Measured efficiencies for different diode samples at optimum load, the simulated result has been added for comparison

4.2.7 Conclusion

This paper has reported and demonstrated for the first time the possibility of overcoming the microwave power harvesting rectification efficiency limit of Schottky diode rectifiers, at low

power levels typical of AMPH applications, through the use of backward tunnel diodes. A 25.3% increase in efficiency was observed when the backward diode rectifier model was compared to a theoretically ideal Schottky diode with the same R_{j0}, while a 10.5 times higher efficiency was obtained when compared to a real HSMS-285B Schottky diode, due to lower diode parasitic losses and improved intrinsic current responsivity $\mathcal{R}_{I0}$.

The rectifier's measured efficiency for three different backward diodes agreed with the simulation results and showed a good repeatability between different backward diode devices. The best measured result from Figure 4-15 is compared to other state-of-the-art published results in Figure 4-16; only diode based rectifiers operating between 1.5 GHz and 3 GHz were included in this comparison. The efficiency limitation of Schottky diode based AMPH is evident from this figure, even though different diodes, matching technologies and loads are used in the reports cited here, all of the Schottky-based rectifiers show an abrupt drop in the efficiency below approximately 10 μW input power. The presented rectifier, based on a backward tunnel diode, on the other hand demonstrates good conversion efficiency for input powers in the 1 μW range due to its low parasitic junction capacitance and increased current responsivity. The input power range for this figure has been extended to higher power levels to give the reader a good understanding of the power range where the backward tunnel diode can be used to increase microwave power transmission (MPT) and AMPH efficiency.

The backward diode rectifier efficiency roll off seen at higher powers likely originates from a larger voltage swing increasing the forward (thermionic) current, thereby limiting the efficiency. This could be addressed by using maximum power point tracking (MPPT) [69], rectification bridges using more diodes, or structural modifications to the diode design if input power is expected to reach higher values.

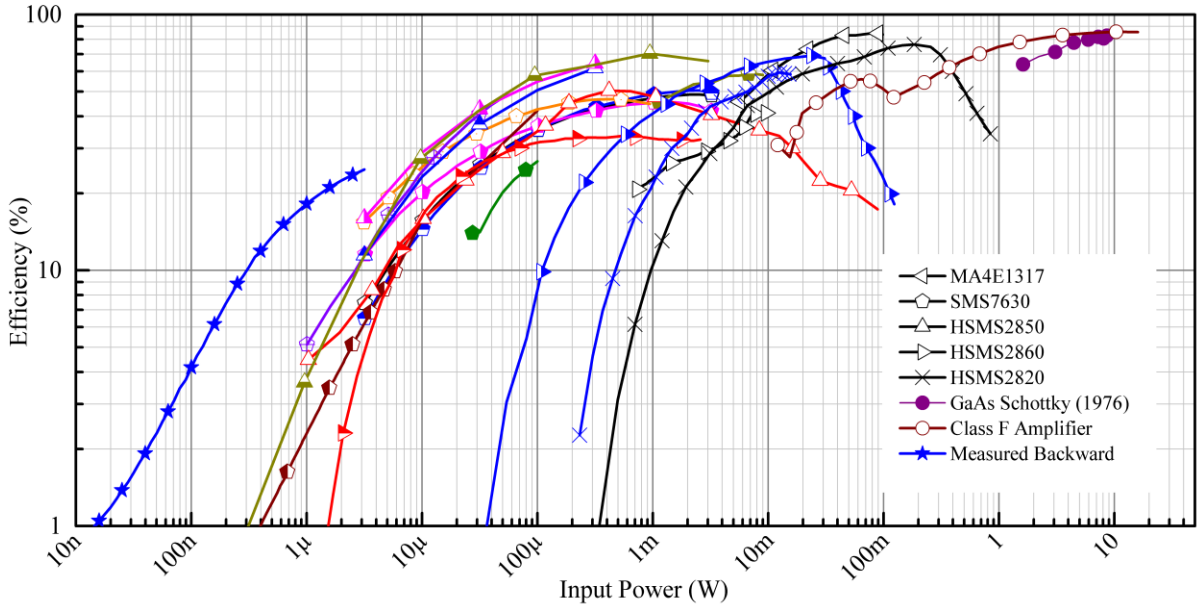

Figure 4-16: Backward tunnel diode AMPH measured result compared to the state of the art microwave power harvesters and transmitters. Historical references have been added for reference. The symbol form has been maintained between rectifiers using the same diode.

Table 4-2: References from curves given in Figure 4-16.

Symbol	Diode	Frequency	Year	Source
	Backward Diode	2.4 GHz	2015	This Work
	MA4E1317	2.45 GHz	2002	[70]
	SMS7630	1.85 GHz	2010	[71]
	SMS7630	2.45 GHz	2010	[71]
	SMS7630	1.96 GHz	2012	[72]
	SMS7630	2.45 GHz	2010	[42]
	SMS7630	2.45 GHz	2011	[73]
	SMS7630	2.45 GHz	2014	[43]
	HSMS2850	1.8 GHz	2012	[45]
	HSMS2850	2.15 GHz	2014	[40]
	HSMS2850	1.8 GHz	2014	[40]
	HSMS2850	2.45 GHz	2013	[44]
	HSMS2860	2.45 GHz	2010	[74]
	HSMS2860	1.8 GHz	2012	[45]
	HSMS2820	1.8 GHz	2012	[45]
	HSMS2820	2.45 GHz	2010	[75]
	GaAs Schottky	2.388 GHz	1976	[12]
	Class F Amplifier	2.14 GHz	2012	[76]

The results presented in this work were obtained using backward tunnel diodes optimized for low-level power detection and imaging applications. As shown in Figure 4-4, the junction composition could be further optimized to increase the diode curvature γ, and consequently its

current responsivity $\mathcal{R}_{I0}$, increasing the power conversion efficiency even more at lower input powers. The diode junction area, on the other hand, could be increased to optimize R_{j0}, which could be used to minimize matching losses, although this would also increase the junction capacitance C_j. The authors believe this increase in C_j would not be large enough to impact significantly performance in AMPH applications, since the frequencies of signals where higher power density appear are usually below 3 GHz [3, 6]. The expected improvements in AMPH for a varying backward tunnel diode anode Al composition are shown in Figure 4-17; this efficiency improvement was calculated using the simulation results given in Figure 4-4 adjusting the junction area so that a 12.5 kΩ R_{j0} was maintained. The intrinsic capacitance value remains negligible at 2.45 GHz even with an increasing anode Al composition. As a result, the power conversion efficiency is improving in the same exponential fashion as the curvature γ. This low power analysis forecasts a significant improvement of at least one order of magnitude on the efficiency for narrower tunneling window. Determining and verifying the optimum characteristics of a backward tunnel diode for AMPH remains the subject of future work.

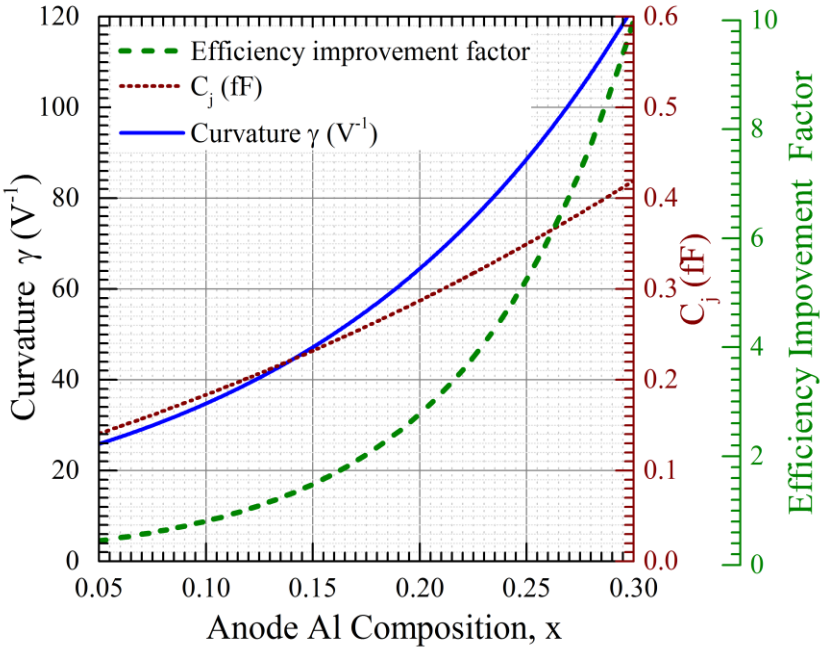

Figure 4-17: Expected power conversion efficiency improvement for different backward tunnel diode anode Al compositions, the diode junction area was calculated to mantain a 12.5 kΩ junction resistance.

4.2.8 Acknowledgment

The authors would like to thank Rogers Corporation for providing the laminates used in this project.

The authors would also like to thank the support provided by the Poly-GRAMES Research Center technical support team, who are: Traian Antonescu, Steve Dubé, Maxime Thibault, and Jean-Sébastien Décarie.

CHAPITRE 5 TRANSMISSION DE PUISSANCE PAR ONDES MILLIMETRIQUES (94 GHz)

5.1 Introduction

A la différence de la récupération d'énergie des radiofréquences ambiantes, qui peut être utilisée dans les applications avec une très faible consommation d'énergie, la transmission de puissance par micro-ondes ou même ondes millimétriques peut être utilisée dans des applications dans lesquelles le dispositif a besoin d'une puissance dans une plage allant des microwatts jusqu'à quelques watts; et qui requièrent également une source de puissance sans fil, petite et légère.

Dans le schéma classique de transmission de puissance sans fil un émetteur est intentionnellement installé pour augmenter la densité de puissance disponible pour le circuit de récupération d'énergie micro-ondes, ce qui permet que de plus hautes puissances soient fournies par le circuit de redressement de puissance. Les premières démonstrations de transmission de puissances par micro-ondes ont été effectuées par Brown et Dickinson dans les décennies de 1960 et de 1970, où jusqu'à 30 kW cc ont été récupérés par un lien de transmission de puissance par micro-ondes [11, 12].

Ce travail qui est présenté dans la suite sous le format d'article, explore l'application de la transmission de puissance par micro-ondes pour résoudre un des problèmes classiques de la conception des micro-robots : la disponibilité d'une source d'énergie fiable et de taille et poids compatibles avec les dimensions d'un micro-robot.

Les micro-robots peuvent être utilisés dans une multitude de scénarios. Mentionnons les deux exemples importants de la décontamination de régions affectées par un débordement de produits chimiques ou la fouille de décombres après un séisme ou une autre catastrophe. Dans ces deux exemples, la région affectée pourrait être illuminée par une source de micro-ondes, qui fournirait ainsi la puissance aux micro-robots dotés d'une rectenne.

Dans ce travail une rectenne a été développée à la fréquence de 94 GHz. A cette fréquence la longueur d'onde dans le vide est de seulement 3.19 mm, ce qui permet la conception d'une rectenne de dimensions très réduites. Un circuit d'adaptation d'impédances a été réalisé en technologie de guide d'ondes coplanaire, de façon à simplifier la connexion à l'antenne papillon à fentes qui a été

choisie en raison de sa caractéristique large bande et qui peut accommoder ainsi une variation de dimensions dues aux imprécisions de la fabrication. Cette antenne a aussi été sélectionnée pour son patron de rayonnement ayant une faible directivité, caractéristique nécessaire pour l'application micro-robots, puisque la position du micro-robot par rapport à la source de puissance est variable.

Toutes les simulations du circuit d'adaptation d'impédances ont été faites utilisant les logiciels HFSS pour les lignes de transmission et Keysight ADS pour les effets non linéaires. L'antenne a été développée avec le logiciel HFSS.

5.2 Article 4 — Small-Footprint Wideband 94GHz Rectifier for Swarm Micro-Robotics

Simon Hemour, *Member IEEE*, Carlos H. P. Lorenz, *Student Member IEEE*, Ke Wu, *Fellow, IEEE.*

Accepté le 1er février 2015 à la conférence « *International Microwave Symposium* 2015 », qui a eu lieu entre le 17 et le 22 Mai 2015 à Phoenix, AZ, É.-U.

***Abstract* — A very small footprint rectifier designed to support the micro-robotic applications is proposed and presented in this paper. The frequency of 94GHz has been selected as the best tradeoff between receiving antenna size and available transmitter power. To comply with the swarm micro-robotic requirements in which every part should be mass-producible and little sensitive to fabrication tolerance, a wideband planar rectenna using a single layer of metallization has been designed. The rectifier prototype exhibits a maximum efficiency of 37.7% at 90GHz measured at 3 dBm input power and a half efficiency bandwidth of 22%.**

Index Terms — Battery-less autonomous systems, Power beaming technique, Micro-robotics, Rectenna, Rectifier circuit, Self-biased system, Swarm robotics, W-band, Wireless power transmission.

5.2.1 Introduction

With the rise of low-power integrated electronics, and more specifically microcontrollers, the presence of autonomous microsystems in our life is more and more becoming a reality. Those systems – or "things" – are mainly appearing in the form of smart sensors collecting information of our environment and communicating through wireless network (Wireless Sensor Network or WSN and Internet of Things or IoT). However, similar autonomous systems, built instead with actuators, have also spawned the whole new realm of swarm micro-robotics. With a few mm^3 volume (see an example in Figure 5-1), and acting like ants or bees, the micro-robots are capable of collectively acting in a large group to accomplish tasks beyond the capability of a single robot [77]. They can be deployed in colony to explore and operate in environments which are too small

or too dangerous for people or larger robots, e. g. search and rescue in earthquake rubble, bomb disposal, inspection of radioactive hardware, etc.

Like their sensor-oriented counterparts, robotic autonomous microsystems cannot rely only on batteries, which would be incompatible with their size and life-span requirements. Instead, remote or wireless powering is needed to offer the flexibility to relocate the source of energy. Energy harvesting [13], however, would not match the degree of reliability required by the duties of micro-robots. Wireless power transmission technology, based on resonant magnetic coupling, is also to be avoided because of the poor distance-to-resonator diameter ratio [49]. Thus, and since many materials found in nature are opaque to light, the best choice tends to be found in millimeter-wave and sub-THz region.

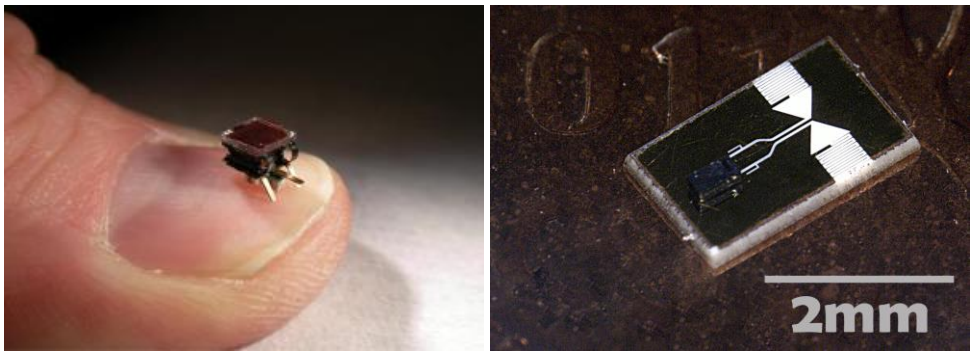

Figure 5-1: (a) Photograph of the I-SWARM micro-robot [77], (b) Proposed 94GHz rectenna.

5.2.2 Choice of Frequency and Technology

The technology that is usually chosen for the micro-robotics should comply with elementary requirements: every part of the robots should be easy-to-manufacture and accept a high-degree fabrication tolerance to enable mass-production.

In a tradeoff between receiving antenna size and ability to generate a high power at the transmitter, the 94GHz frequency of operation was selected. A wireless power beaming platform (Figure 5-2) with a 100W Klystron amplifier, which would be eventually used to evaluate energy transfer over distance, was built.

There are few works of rectifier reported in the literature working in the upper millimeter band, all using CMOS technology. In [78], an 8% RF-to-DC rectification efficiency has been obtained at 71GHz for 5 dBm input power. In [79], a 10% efficiency has been obtained at 94GHz

for 4.5 dBm input power. Both works used 65cm[1] CMOS technology. In this work, a millimeter-wave GaAs Schottky diode (Virginia diode VDI ZBD) is selected to design the proposed 94GHz rectifier energy receiver. It is expected that this diode, which was especially developed to operate above 100GHz would outclass CMOS rectifiers, especially bellow 1mW RF power.

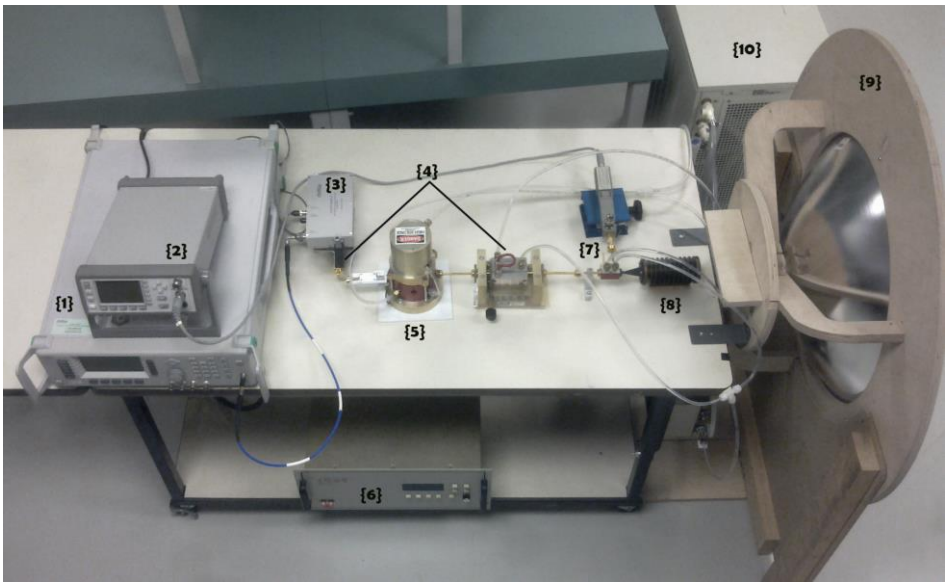

Figure 5-2: 94GHz power beaming platform. (1) 18.8GHz signal generator, (2) power meter, (3) frequency quintupler, (4) variable attenuators, (5) 100W 50dB gain klystron amplifier, (6) high voltage Klystron power supply, (7) coupler & power probe, (8) WR10 power load, (9) 43dB gain cassegrain antenna, (10) chiller and cooling systems

5.2.3 Rectenna Development

The topology of the proposed rectenna is depicted in Figure 5-3. Coplanar waveguide (CPW) technology is selected for its simple fabrication process.

[1] L'unité appropriée est *nm*, cependant le texte originel tel quel publié dans la conférence a été maintenu selon requis par le règlement de l'École Polytechnique de Montréal pour les mémoires écrites par articles.

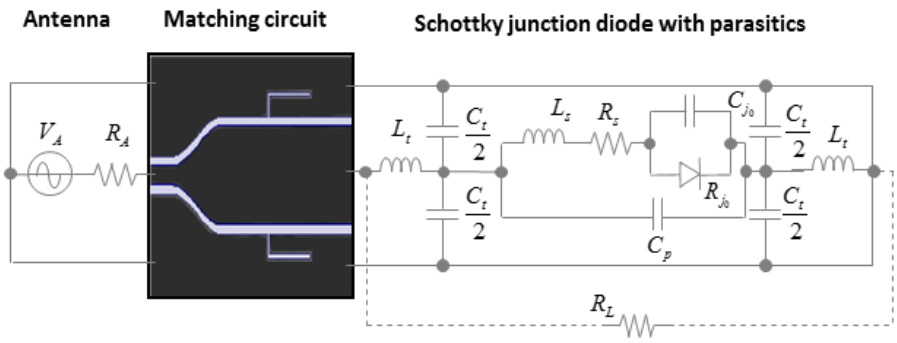

Figure 5-3: Schematic of the proposed 94GHz rectenna. The antenna is modeled as a Thevenin source, V_A and R_A being respectively the equivalent RF source and impedance of the antenna. L_T and C_T are the inductance and capacitance accounting for effects of the pad and mounting. L_S and C_P are roughly the packaging parasitics, while R_S, the series resistance, and C_{J0} are dependent on the junction properties.

5.2.3.1 Antenna design

A CPW-fed bow-tie slot antenna is selected and designed using Ansoft HFSS to receive the power beam. This type of antenna is rather large-band, which allows for good fabrication tolerances. A set of Inter Digital Capacitors at each side of the bow-tie slot is utilized to open the DC current path and include the load. As it is found in the literature [80] and verified in Figure 5-4 (b), planar antenna on high permittivity substrate tends to radiate naturally through its dielectric. The antenna is designed with a single lobe, but as it can be seen in the radiation pattern in Figure 5-4 (b), the presence of the diode and its matching network have broken the symmetry of the whole rectenna, giving rise to a second lobe. This is not a critical problem, as it adds a second direction of transmission, which may be usefull in our application, and we are not restricted by the amount of power density available at the receiving antenna.

5.2.3.2 Diode model extraction

Prior to the design, a diode sample mounted using conductive epoxy (Epo-Tech H20) on a CPW line has been characterized, the used substrate was 10mil alumina. The obtained scattering parameters have been de-embedded after a TRL calibration. Figure 5-3 shows a set of parasitic elements extracted from the mounted diode characterization. DC characterization of the I(V) curve enabled the recovery of the Shockley diode parameters (Table 5-1). The junction diode's large signal model is modeled with RJ0.

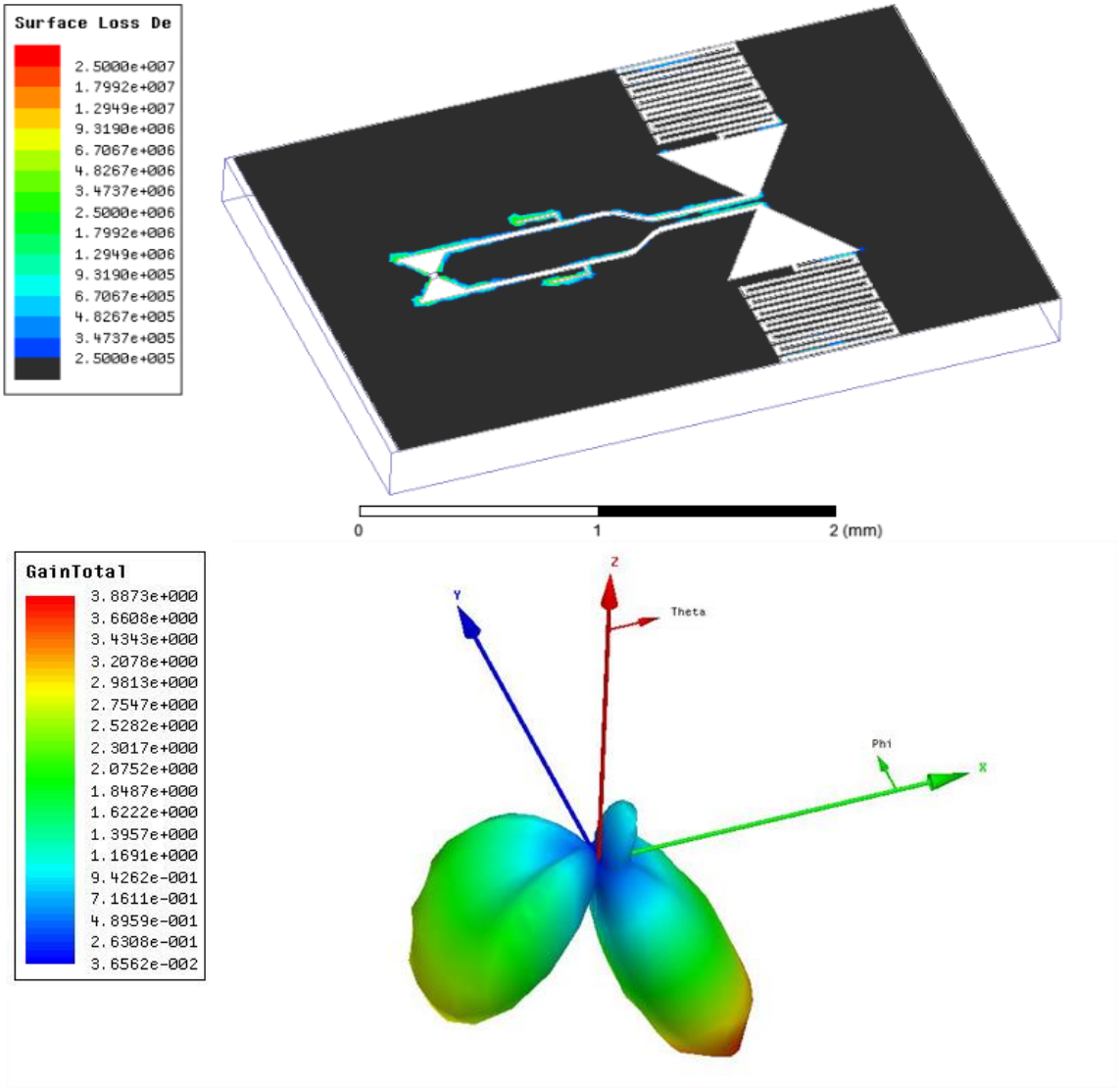

Figure 5-4: Simulation results of full-wave FDTD analysis (a) Surface losses on the rectenna in W/m² and (b) Radiation pattern of the entire rectenna (antenna & rectifier)

5.2.3.3 Rectifier circuit

A single diode topology is selected over a dual diode structure [81] or full bridge architecture [82] to reduce effects of the parasitics and size. A taper has to be included in the matching circuit, as the width of the Schottky diode die is larger than the CPW feed of the antenna. The matching network transforms the 50Ohm real impedance of the antenna into the expected 108-j11 Ohm of the diode. Figure 5-4 shows the surface losses in the rectenna. It can be seen that the losses originate mainly from the matching network. The matching efficiency computed from Harmonic Balance simulation is 65% at -10 dBm and 67.5% at -5 dBm input power levels.

Table 5-1: Diode parameters extracted from RF and DC measurements

	Is	Vj	N	I_{bv}	Rs	Cj_0
Value	5x10-6 A	0.085 V	1.1	0.1 mA	13 Ω	19 fF

5.2.4 Measurements

As it is discovered, the fabrication process in our work has introduced a 4 μm over-etching. It is seen in Figure 5-5 that the antenna resonance frequency is moved from 94GHz to 90GHz. The over-etching might tend to reduce the matching efficiency because of higher radiation losses although this effect is hard to quantify in our measurements.

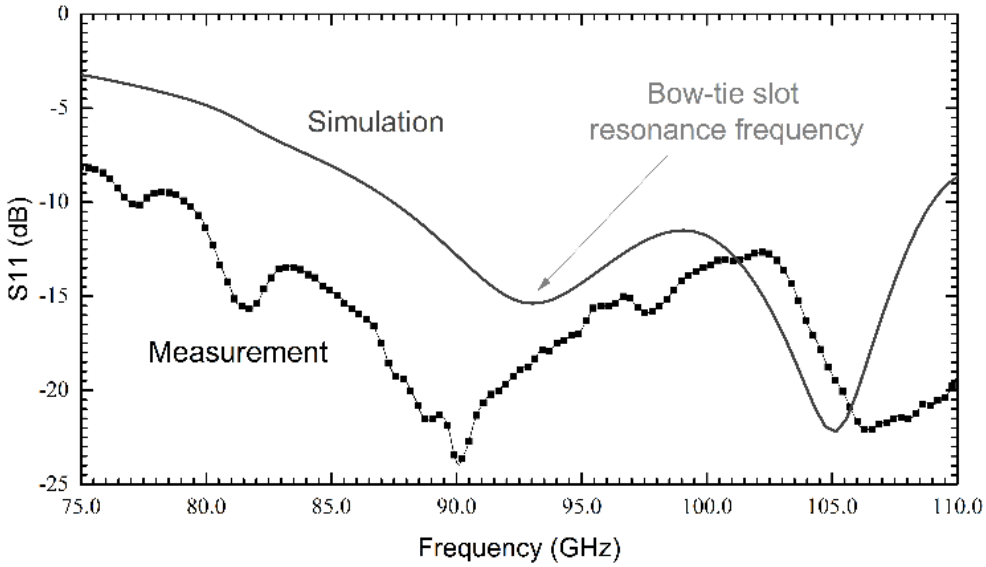

Figure 5-5: Comparison of simulation and measurement for S11 of the CPW-fed bow-tie antenna. Measurements were performed on a probe station after on-wafer Short-Open-Load calibration.

On-wafer measurements were done using a power calibrated procedure at the tips of the GSG probe [9]. A comparison of the simulated and measured rectifier circuit (without the antenna) behavior is plotted in Figure 5-6, given for an input power of -12 dBm. It suggests that in our simulation, parasitic components of the diode are overestimated, thus leading to an underestimated power conversion efficiency. In the measurement, the rectifier current is larger than expected, and in turn decreases the junction resistance, which explains why the optimum resistance is larger in the simulation than in the measurement. The frequency shift caused by the over etching is also clearly visible. The robustness of the circuit to fabrication tolerance, provided by a wideband circuit

design, is also demonstrated: Even under the over etching condition, the rectifier is still operating at 94GHz with almost 7% efficiency.

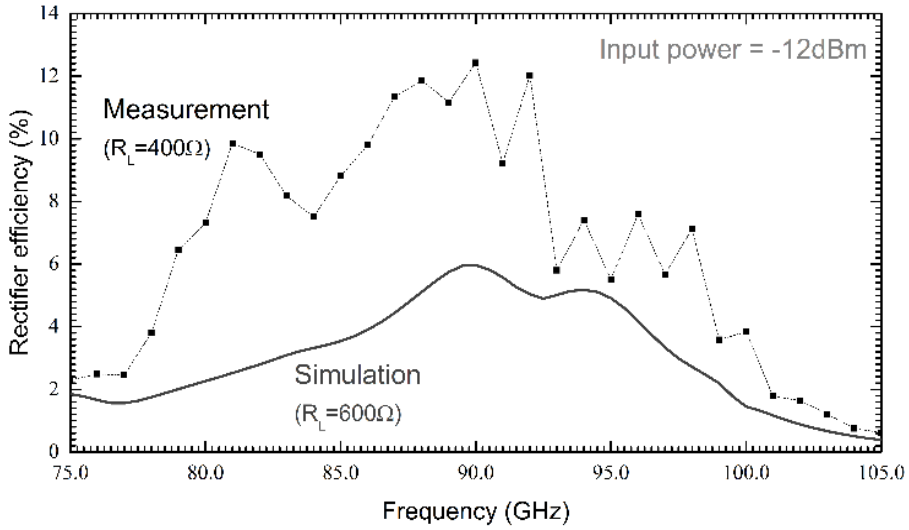

Figure 5-6: Rectifier efficiency as a function of frequency, plotted with the optimum load for an input power of -12 dBm (calibrated probe measurement). In the simulation condition, the optimum load was found to be 600 Ohm (solid line). However, due to lower parasitic in the real diode, junction current has been higher in the measurement, leading to a lower junction resistance, thus to a lower optimum load resistance, *i.e.* 400 Ohm (dotted line).

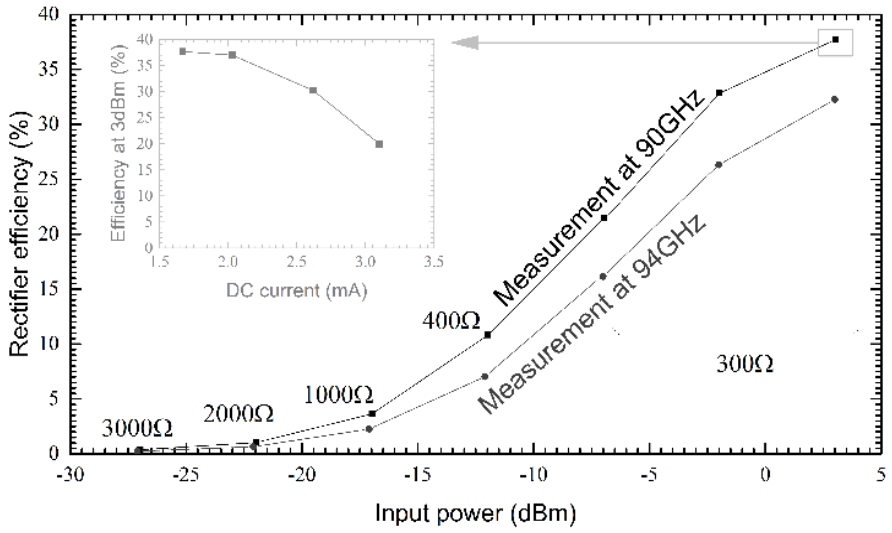

Figure 5-7: Rectifier efficiency as a function of the input power at 90GHz and 94GHz (calibrated probe measurement at the input of the rectifier circuit). The optimum resistive load is indicated for each measurement point. In the insert, the efficiency is shown as a function of DC current, for a RF signal of 3 dBm at 90GHz.

A comparison between the optimum rectification frequency, 90GHz, and 94GHz is presented in Figure 5-7, showing the benefit of the wideband design on the behavior of the rectifier circuit (no antenna) fabricated with a high tolerance, In Table 5-2 the results are summarized and compared with the previous works. The efficiency is improved by nearly four times, for a similar half efficiency bandwidth.

Table 5-2: Comparison with other related works

	[78]	[79]	**This work**
Technology	65nm CMOS	65nm CMOS	**GaAs Schottky diode**
Frequency	70-72GHz	94GHz	**94GHz**
Rectifier efficiency	8% (71GHz)	10%	**37.7% (90GHz)** **32.3% (94GHz)**
Half efficiency Bandwidth	-	24%*	**22%**
Input power	5 dBm	4.5 dBm	**3 dBm**
Rectifier area	1.09mm^2	0.095mm^2	**1.17mm^2**
Rectenna area	1.78mm^2	0.48mm^2	**5.62mm^2**

* Simulation results

5.2.5 Conclusion

We have developed a rectifier compatible with mass-production requirement and high fabrication tolerance (Half efficiency bandwidth of 22%). An unprecedented efficiency of 37.7% has been obtained at 90GHz. The rectifier presented in this work is the first iteration in our research. A further improvement includes lower area, improved efficiency using higher Schottky barrier diode, such as mixer diode, and circuit engineering in order to obtain a necessary amount of voltage to operate the microrobot of interest.

5.2.6 Acknowledgement

The authors would like to acknowledge the financial support of the Natural Sciences and Engineering Research Council of Canada (NSERC) and CREATE PERSWADE Training Program, which partially funded the work presented in this article. The authors wish to thank J. Gauthier, M. Thibault, D. Dousset, S. Dubé, T. Antonescu, and J.-S. Décarie, all with the Poly-Grames Research Center, École Polytechnique de Montréal, Montreal, QC, Canada, for their technical assistance.

CHAPITRE 6 DISCUSSION GÉNÉRALE

La récupération d'énergie micro-ondes ambiantes demeure un défi en raison des faibles densités de puissance disponibles dans l'environnement, comme rapporté par des études déjà publiées [3, 6, 8]. Dans ce travail on a présenté un modèle mathématique qui permet la compréhension des mécanismes de redressement et des pertes lors de la conversion de puissance micro-ondes en courant continu (cc). À partir de la théorie développée pour établir ce modèle, deux méthodes ont été proposées et vérifiés pour augmenter l'efficacité de conversion de puissance micro-ondes en cc dans les faibles puissances: la récupération hybride coopérative d'énergie ambiante, présentée dans le chapitre 3, et l'utilisation des diodes tunnel avec une forte responsivité en courant démontrée dans le chapitre 4.

Toutefois, la perte dans le réseau d'adaptation d'impédance reste un phénomène majeur à l'origine de la faible ECP obtenue dans les circuits de récupération d'énergie micro-ondes ambiantes. Dans le chapitre 4, nous avons vu que pour une puissance d'entrée de -40 dBm, l'efficacité atteignable sans pertes d'adaptation était estimé à 15%, alors que les mesures ont montré une efficacité proche de 4.2%. Le même effet a été constaté pour une puissance à l'entrée de -30 dBm, où le maximum atteignable était estimé à 36% et les mesures ont démontré une ECP proche de 18%. Les résultats présentés dans le chapitre 2 mettent cet effet en évidence dans la Figure 2-7, où il existe une résistance de jonction R_{j0} optimale dans un compromis entre les pertes d'insertion du réseau d'adaptation d'impédances et l'efficacité de conversion de puissance micro-ondes en cc. À ce point de fonctionnement, les pertes d'insertion du réseau d'adaptation d'impédances sont responsables à hauteur de 30% de la puissance perdue.

Ces pertes importantes dans le réseau d'adaptation d'impédances ont été étudiées dans ce chapitre avec l'aide du modèle de pertes présenté dans le Chapitre 2. Un modèle de diode à faibles pertes parasitiques a été utilisé pour étudier une nouvelle topologie de réseau d'adaptation d'impédances visant diminuer ses pertes d'insertion. Les caractéristiques de la diode sont : C_{j0} = 15.7 fF, C_p = 25.2 fF, R_s = 15 Ω, L_p =0 et N=1.1. Le courant de saturation I_s a été varié de 10 nA à 100 μA et une capacitance de 10 fF a été ajoutée en parallèle avec la diode pour prendre en compte la capacitance des plots de soudure. Tous les calculs considèrent des lignes microruban 50 Ω construites sur un substrat Rogers RT/Duroid 6002 d'une épaisseur de 30 mil.

Utilisant l'équation (2-16) pour calculer le facteur de qualité requis pour adapter une diode non polarisé avec une résistance de jonction égale à 12.5 kΩ à une source de 50 Ω, on obtient Q_r = 15.78. Cela veut dire qu'un réseau d'adaptation qui présente un facteur de qualité égal à 15.78 présenterait une perte d'insertion de 50%. Ce facteur de qualité ne semble pas difficile à obtenir ni même à dépasser, mais comme décrit par l'équation (2-22), la constante effective de pertes d'une ligne de transmission augmente quand l'onde stationnaire présente sur cette ligne a un ROS important. En raison de la grande différence entre l'impédance de la source et de la charge représentée par la diode, cette augmentation dans les pertes sur la ligne de transmission ne peut pas être négligée.

L'impédance initiale d'une telle diode est proche de l'infini, comme montré dans la Figure 6-1 ici-bas. Cela signifie que le ROS soutenu sur la ligne connectée à cette diode est très élevé.

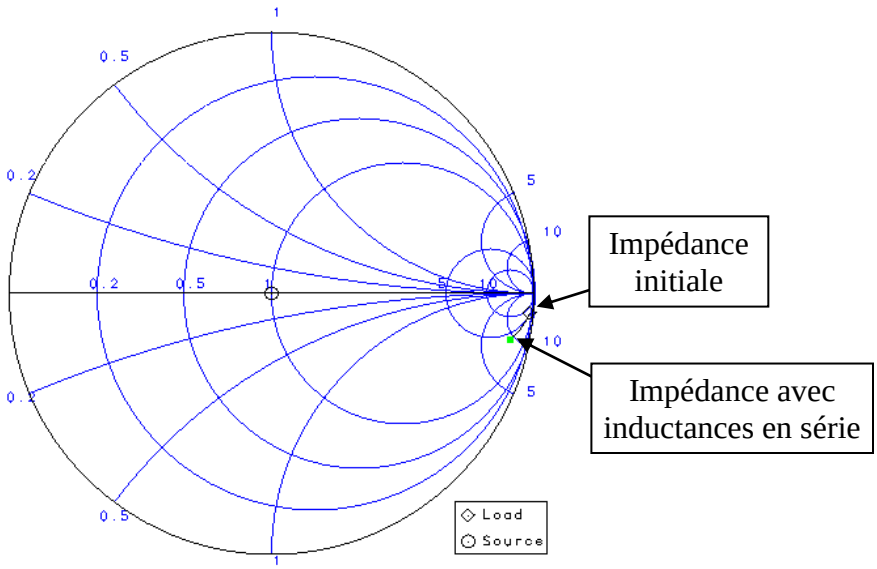

Figure 6-1: Effet de l'ajout de deux inductances de 34 nH en série avec la diode sur l'impédance d'entrée. Fréquence = 2.45 GHz.

Une façon de diminuer les pertes d'insertion de ce réseau d'adaptation d'impédances est de diminuer le ROS présent sur la ligne connectée à la diode. Pour y arriver, il faut rapprocher l'impédance à adapter du centre de l'abaque de Smith, comme montré dans la Figure 6-1. Dans cette figure deux inductances de 34 nH Coilcraft (0302CS-34NXJL_) ont été mises en série avec la diode. Le modèle réel de l'inductance, fourni par Coilcraft, a été utilisé pour prendre en compte les éléments parasites.

L'effet de l'ajout de ces inductances peut sembler négligeable sur l'abaque de Smith, cependant le coefficient de réflexion de l'impédance résultante connecté à une ligne de 50 Ω chute de 0.99 vers 0.925. Cela signifie une chute de 199 à 25.7 dans le ROS et une chute de 99 vers 12.85 dans le facteur de multiplication de l'atténuation de la ligne de transmission selon l'équation (2-22) soit une atténuation 7.7 fois plus petite. La théorie présentée dans la section 2.1.6 a été utilisée pour vérifier l'impact de l'ajout d'inductances en série avec la diode, avant de l'adapter à une source de 50 Ω avec un réseau d'adaptation d'impédances en L, comme montré dans la Figure 2-7. Les ECP calculées avec la méthode présentée dans le chapitre 2 sont données dans la Figure 6-2 ici-bas :

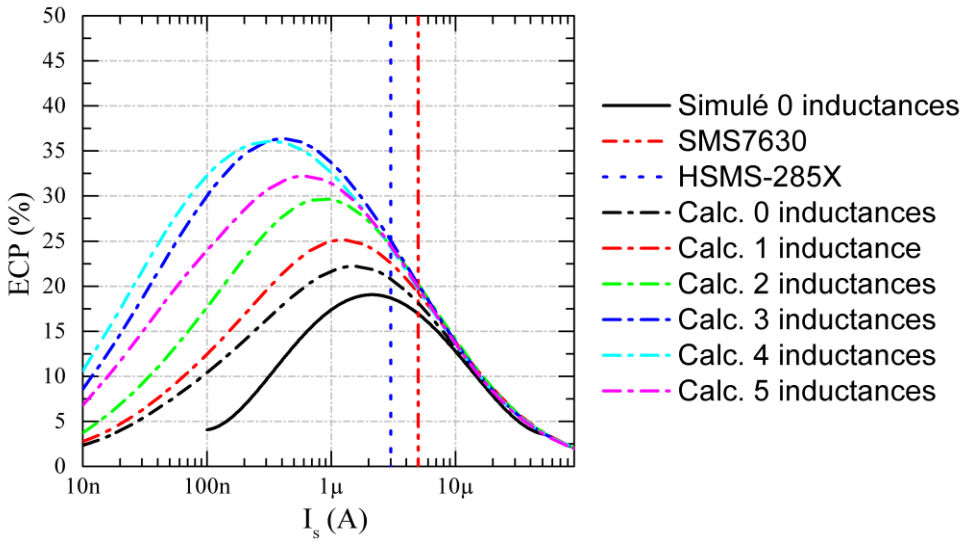

Figure 6-2: ECP calculée avec le modèle présenté dans le chapitre 2. D'inductances ont été mises en série avec la diode. La puissance à l'entrée est de -30 dBm, Fréquence = 2.45 GHz.

On voit que l'ajout des inductances permet d'augmenter l'ECP maximale qui peut être obtenue. L'ajout des inductances diminue le coefficient de réflexion au bout de la ligne de transmission série utilisée dans le réseau d'adaptation d'impédances en L, cela réduit les pertes totales dans le réseau d'adaptation d'impédances composé des inductances plus les lignes micro-ruban en L, selon la théorie présentée dans 2.2.6. L'ECP maximale monte de 22.5% pour le réseau sans inductances à 35% pour le réseau avec 3 inductances en série. L'ajout de plus de 3 inductances diminue l'ECP maximale en raison des pertes provenant de la résistance série des inductances, dans ce point, un équilibre est atteint entre la diminution du ROS sur la ligne connectée aux inductances et diode, et les pertes introduites par les inductances.

Une deuxième remarque qui peut être faite à partir des données de la Figure 6-2 est la différence de seulement 4% qu'apparaît entre les résultats simulés dans Keysight ADS et calculés pour le circuit sans diodes en série, ce qui est un très bon accord considérant les simplifications de la méthode analytique proposée.

Cette méthode a été utilisée pour améliorer la rectenne présentée dans le chapitre 4, où l'utilisation d'une diode tunnel avec une haute responsivité en courant a été étudiée pour augmenter l'ECP maximale des circuits de récupération d'énergie ambiante. Selon les simulations réalisées dans le logiciel Keysight ADS, l'ajout de deux inductances en série avec la diode (Coilcraft 03CS21N et 03CS8N3) permettrait d'augmenter l'ECP atteignable. Le circuit a été simulé avec l'aide de l'outil Momentum, lequel a été utilisé pour obtenir les paramètres S du circuit par la méthode des moments. Ces résultats ont été utilisés avec la simulation d'équilibrage harmonique pour obtenir l'ECP du circuit proposé. La topologie finale du circuit proposé est donnée dans la Figure 6-3 (Plan de masse sur la face opposée de la carte de circuit imprimée).

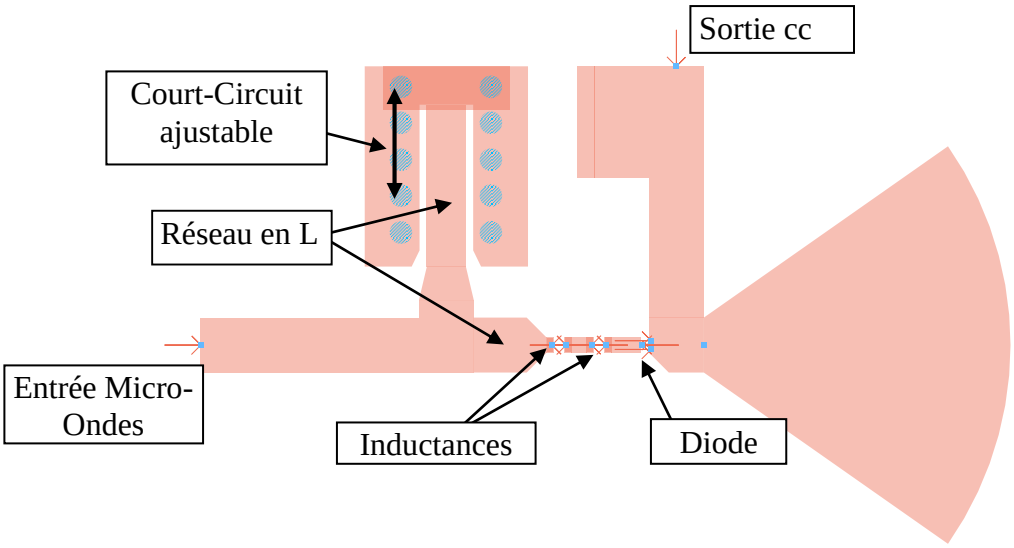

Figure 6-3: Topologie finale du circuit proposé avec le but de diminuer les pertes d'insertion du rectifieur présenté dans le chapitre 4.

Le résultat de la simulation est comparé à l'ECP maximale prévue et les résultats des mesures présentées dans l'article du chapitre 4. La méthode proposée donne un circuit qui présente de très faibles pertes d'insertion pour le réseau d'adaptation d'impédances. L'ECP prévu est proche du maximum atteignable, comme montré dans la Figure 6-4.

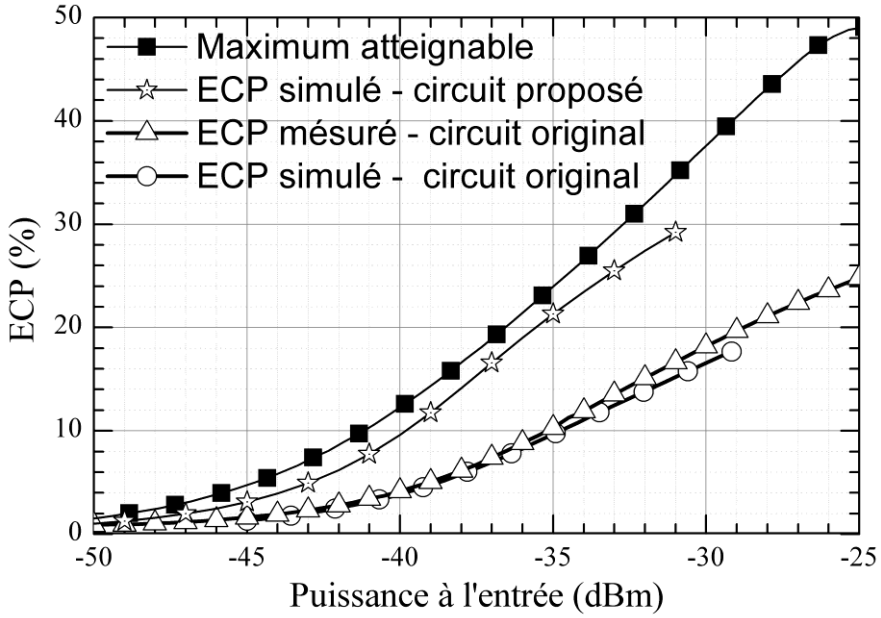

Figure 6-4: Résultat simulé pour la nouvelle méthode d'adaptation d'impédance proposée. L'ECP obtenu est très proche du maximum prévu par l'article présenté dans le chapitre 4. Fréquence simulée= 2.4 GHz, charge = 13 kΩ.

La plage des puissances simulées dans la Figure 6-4 a été limitée en raison d'une limitation du modèle de diode donné dans le chapitre 4, pour lequel la tension de jonction dépasse la plage valide à partir de -30 dBm de puissance à l'entrée.

Comme démontré, la méthode proposée peut être utilisée pour réduire les pertes d'insertion des réseaux d'adaptation d'impédances quand la différence entre la charge et la source est importante, ce qu'engendre un ROS élevé. Les composants utilisés pour réduire le ROS initial sur les éléments distribués du réseau d'adaptation d'impédances peuvent varier selon l'impédance initiale.

CHAPITRE 7 CONCLUSION ET TRAVAUX FUTURES

Ce travail a exploré la récupération d'énergie micro-ondes ambiante (REMA), débutant par la présentation d'un modèle mathématique où les mécanismes des pertes et de conversion d'énergie micro-ondes en courant continu par un circuit de redressement à diodes sont expliqués. L'efficacité totale de conversion de puissance micro-ondes en cc est divisée dans η_m, l'efficacité du réseau d'adaptation d'impédances, η_p, l'efficacité parasitique de la diode, η_{RFDC}, l'efficacité de conversion d'énergie micro-ondes en cc de la jonction non-linéaire et η_{SL}, l'efficacité de transfert de puissance de la source à la charge. Chaque efficacité est évaluée indépendamment et une méthode est proposée pour prédire l'efficacité de chaque étape. Les résultats prévus par les équations proposées ont été vérifiés et comparés aux résultats mesurés pour trois prototypes présentés dans le Chapitre 2, y incluant les pertes d'insertion calculées pour le réseau d'adaptation d'impédances.

La théorie développée pour prévoir les pertes d'insertion du réseau d'adaptation d'impédances peut facilement être utilisée pour d'autres applications où une grande différence entre l'impédance de la source et de la charge peut engendrer de pertes d'insertion importantes dans le circuit d'adaptation, comme dans la récupération d'énergie micro-ondes ambiante. La solution analytique peut facilement être mise en œuvre dans un logiciel de résolution d'équations mathématiques comme MATLAB, pour aider à choisir la topologie qui présente la plus faible perte par moyen de la méthode analytique avant de réaliser la simulation électromagnétique du circuit imprimé, laquelle peut être utilisée pour optimiser le réseau d'adaptation choisi.

Le modèle mathématique a amené à deux méthodes possibles pour augmenter l'ECP dans la plage de puissances en-dessous de -30 dBm, comme c'est généralement lecas dans les applications de REMA. La première méthode, présentée dans le chapitre 3, combine la puissance provenant de plusieurs sources dans un seul élément non-linéaire utilisé pour le redressement. Dans le travail présenté, la puissance micro-ondes reçue à 2.1 GHz a été combinée avec la puissance récupérée d'une source de vibration mécanique. L'ECP a été doublée pour des puissances à l'entrée en-dessous de -40 dBm pour chaque source, ce qui quadruplait la puissance totale récupérée par le circuit par rapport à une rectenne simple. Cette avantage diminuait progressivement pour une puissance d'entrée montant jusqu'à -24 dBm, point où la puissance perdue dans les produits d'intermodulation entre les signaux d'entrée égalait les gains de la méthode collaborative hybride

proposée. Un autre avantage de la méthode proposée est la combinaison des puissances récupérées directement par le dispositif non-linéaire utilisé dans le redressement, sans le besoin d'un circuit supplémentaire pour réaliser cette fonction, lequel rendrait le système moins efficace et augmenterait les coûts et complexité du circuit.

Ensuite, une deuxième méthode pour augmenter l'ECP a été évaluée : l'utilisation des diodes tunnel avec une responsivité en courant à zéro-biais plus élevée que celle atteignable avec les diodes Schottky, laquelle a un maximum égal à 19.4 A/W à la température ambiante. Des échantillons de diodes tunnel ayant une responsivité en courant mesurée proche de 22 A/W en température ambiante ont étés caractérisés et un modèle de diode a été créé dans le logiciel Keysight ADS. Ayant le modèle de diode en main, des prototypes ont étés construits et mesurés. L'ECP mesurée a atteint 18.2% pour une puissance de -30 dBm à l'entrée du redresseur, soit un gain de 3.6 fois par rapport au meilleur résultat publié pour les circuits de récupération de puissance micro-ondes ambiantes fonctionnant à de puissances et fréquences similaires avec des diodes Schottky. Lorsque comparé au meilleur résultat présenté dans le chapitre 2, obtenu du circuit construit avec les diodes VDI W-Band ZBD, le gain était de 1.67, ce qui peut être justifié par les très faibles pertes parasitiques présentes dans cette dernière diode. Ce chiffre est aussi en accord avec le gain prédit par le modèle mathématique si on considère que les pertes dans le réseau d'adaptation, les pertes parasitiques et les pertes dans le transfert source – charge sont proches pour les deux diodes. Selon l'équation (2-11) l'efficacité de conversion d'énergie micro-ondes en cc est proportionnelle au carré de la responsivité en courant à zéro-biais. Vu que $\mathcal{R}_{I0}$ pour la diode VDI est de 17.6 A/W, le gain calculé attendu est égal à :

$$Gain = \frac{22^2}{17.6^2} = 1.56 \tag{7.1}$$

un résultat très proche de celui mesuré considérant l'approximation faite quand on a considéré que les autres pertes sont identiques pour les deux diodes. Comme montré dans la Figure 4-17 ce gain peut encore être amélioré significativement en changeant la composition de l'anode de la diode tunnel, la confirmation expérimentale de cette prévision reste encore comme un des travaux futurs proposés par ce mémoire.

Finalement, un circuit de transmission de puissance par micro-ondes a été présenté. La transmission de puissance a lieu dans une plage de puissances plus élevée que la REMA et peut

être utilisée dans les applications où la charge a besoin des puissances plus élevées pour fonctionner. Dans ce travail une rectenne de dimensions et taille réduites a été proposée pour être utilisée comme source de puissance pour des micro-robots. Un prototype a été construit et mesuré à 94 GHz, lequel a été présenté dans le Chapitre 5.

Une faiblesse toutefois a été remarquée pour tous les circuits présentés dans ce travail et aussi dans les résultats présentés dans l'état de d'art trouvé dans les derniers articles publiés dans le domaine de la REMA. Comme présenté dans les Chapitres 2 et 4, entre 30% et 50% de la puissance reçue est dissipée dans le circuit d'adaptation d'impédances. Dans le chapitre 6 une étude est présentée où l'origine de ces pertes et un moyen pour les réduire sont discutés. Le gain attendu pour le circuit proposé dans le Chapitre 4 a été présenté dans la Figure 6-4, où on voit une hausse de l'efficacité de conversion de puissance à -30 dBm de 18.2% à 31%, très proche du maximum atteignable pour le cas d'un réseau d'adaptation d'impédances sans pertes, égal à 38%. La technique appliquée pour cet exemple pourrait aussi être utilisée pour les circuits présentés dans le Chapitre 2 de façon à augmenter les ECP obtenus. La vérification des résultats prévus par la construction des prototypes est proposée comme un des travaux futurs à réaliser.

Une dernière vérification proposée est l'étude de l'effet des pertes ohmiques et diélectriques sur le modèle d'estimation de α_r, la constante d'atténuation équivalente pour une ligne de transmission sur laquelle des ondes stationnaires sont présentes. L'évaluation indépendante des pertes ohmiques et diélectriques dans le modèle présenté dans le chapitre 2, section 2.1.6, reste encore à être faite. Dans le développement du modèle seulement le rapport d'onde stationnaire en tension a été considéré de façon générale pour corriger la constante d'atténuation totale de la ligne. Toutefois une constante d'atténuation équivalente plus précise, en prenant en compte les effets d'ondes stationnaires sur les constantes de pertes ohmiques α_c et diélectriques α_d séparément, qui ensemble composent la constante d'atténuation de la ligne de transmission α, reste encore à être étudiée.

Ce mémoire de maîtrise a exploré avec succès les fondements de la récupération d'énergie micro-ondes ambiante. Un modèle mathématique a été proposé et vérifié. À partir de la théorie décrite, deux méthodes ont étés proposées pour augmenter l'efficacité de conversion de puissance des circuits de récupération d'énergie ambiante. La vérification de ces méthodes par les prototypes

développés a confirmé l'efficacité de ces deux méthodes dans la plage de puissance où la REMA fonctionne.

RÉFÉRENCES

[1] J. Gubbi, R. Buyya, S. Marusic, and M. Palaniswami, "Internet of Things (IoT): A vision, architectural elements, and future directions," *Future Generation Computer Systems,* vol. 29, pp. 1645-1660, 2013.

[2] D. Miorandi, S. Sicari, F. De Pellegrini, and I. Chlamtac, "Internet of things: Vision, applications and research challenges," *Ad Hoc Networks,* vol. 10, pp. 1497-1516, 2012.

[3] F. Giuppi, K. Niotaki, A. Collado, and A. Georgiadis, "Challenges in energy harvesting techniques for autonomous self-powered wireless sensors," in *Microwave Conference (EuMC), 2013 European*, 2013, pp. 854-857.

[4] M. K. Hosain, A. Z. Kouzani, M. F. Samad, and S. J. Tye, "A Miniature Energy Harvesting Rectenna for Operating a Head-Mountable Deep Brain Stimulation Device," *Access, IEEE,* vol. 3, pp. 223-234, 2015.

[5] K. Niotaki, F. Giuppi, A. Georgiadis, and A. Collado, "Solar/EM energy harvester for autonomous operation of a monitoring sensor platform," *Wireless Power Transfer,* vol. 1, pp. 44-50, 2014.

[6] M. Pinuela, D. C. Yates, S. Lucyszyn, P. D. Mitcheson, C. Wang, F. Hu, *et al.* (2012, 14/06/2014). *London RF Survey*. Available: http://www.londonrfsurvey.org/

[7] M. Pinuela, P. D. Mitcheson, and S. Lucyszyn, "Ambient RF Energy Harvesting in Urban and Semi-Urban Environments," *IEEE Transactions on Microwave Theory and Techniques,* vol. 61, pp. 2715-26, 2013.

[8] K. Sangkil, R. Vyas, J. Bito, K. Niotaki, A. Collado, A. Georgiadis, *et al.*, "Ambient RF Energy-Harvesting Technologies for Self-Sustainable Standalone Wireless Sensor Platforms," *Proceedings of the IEEE,* vol. 102, pp. 1649-1666, 2014.

[9] S. Hemour, Y. P. Zhao, C. H. P. Lorenz, D. Houssameddine, Y. S. Gui, C. M. Hu, *et al.*, "Towards Low-Power High-Efficiency RF and Microwave Energy Harvesting," *IEEE Transactions on Microwave Theory and Techniques,* vol. 62, pp. 965-976, Apr 2014.

[10] C. H. P. Lorenz, S. Hemour, W. Li, Y. Xie, J. Gauthier, P. Fay, *et al.*, "Overcoming the Efficiency Limitation of Low Microwave Power Harvesting with Backward Tunnel Diodes " in *Microwave Symposium (IMS), 2015 IEEE MTT-S International*, Phoenix, AZ, USA, 2015, pp. 1-4.

[11] W. C. Brown, "Experimental airborne microwave supported platform," Rome Air Development Center, Rome, NY 1965.

[12] R. M. Dickinson, "Performance of a high-power, 2.388-GHz receiving array in wireless power transmission over 1.54 km," in *1976 IEEE MTT-S International Microwave Symposium, 14-16 June 1976*, New York, NY, USA, 1976, pp. 139-41.

[13] S. Hemour and K. Wu, "Radio-Frequency Rectifier for Electromagnetic Energy Harvesting: Development Path and Future Outlook," *Proceedings of the Ieee,* vol. 102, pp. 1667-1691, Nov 2014.

[14] J. G. Koomey, S. Berard, M. Sanchez, and H. Wong, "Implications of Historical Trends in the Electrical Efficiency of Computing," *Annals of the History of Computing, IEEE,* vol. 33, pp. 46-54, 2011.

[15] J. G. Koomey, H. S. Matthews, and E. Williams, "Smart everything: Will intelligent systems reduce resource use?," *Annual Review of Environment and Resources,* vol. 38, p. 311, 2013.

[16] Libelium. (2015, 15/06/2015). *50 Sensor Applications for a Smarter World*. Available: http://www.libelium.com/top_50_iot_sensor_applications_ranking/

[17] T. W. Yoo and K. Chang, "Theoretical and Experimental Development of 10 and 35 Ghz Rectennas," *Ieee Transactions on Microwave Theory and Techniques,* vol. 40, pp. 1259-1266, Jun 1992.

[18] H. C. Torrey, C. A. Whitmer, and S. A. Goudsmit, *Crystal rectifiers*, 1st ed. New York,: McGraw-Hill Book Co., 1948.

[19] J. Guo and X. Zhu, "An improved analytical model for RF-DC conversion efficiency in microwave rectifiers," in *2012 IEEE MTT-S International Microwave Symposium, IMS 2012, June 17, 2012 - June 22, 2012*, Montreal, QC, Canada, 2012, pp. 1-3.

[20] Skyworks. (03/03/2015). *SMS7630 Datasheet*. Available: www.skyworksinc.com/products_opendocument.asp?did=331

[21] A. M. Niknejad, *Electromagnetics for high-speed analog and digital communication circuits*: Cambridge University Press, 2007.

[22] P. Vizmuller, *RF design guide: systems, circuits, and equations* vol. 1: Artech House, 1995.

[23] A. R. Djordjevic, A. G. Zajic, D. V. Tosic, and T. Hoang, "A note on the modeling of transmission-line losses," *Microwave Theory and Techniques, IEEE Transactions on,* vol. 51, pp. 483-486, 2003.

[24] G. L. Ragan, *Microwave transmission circuits* vol. 9: published and distributed by Boston Technical Publishers, 1964.

[25] J. E. Zúñiga-Juárez, J. A. Reynoso-Hernández, M. del Carmen Maya-Sánchez, and R. S. Murphy-Arteaga, "A New Analytical Method to Calculate the Characteristic Impedance ZC of Uniform Transmission Lines," *Computación y Sistemas,* vol. 16, pp. 277-285, 2012.

[26] H. W. Bode, *Network Analysis and Feedback Amplifier Design*: Van Nostrand, 1945.

[27] R. M. Fano, "Theoretical limitations on the broadband matching of arbitrary impedances," *Journal of the Franklin Institute,* vol. 249, pp. 57-83, 1950.

[28] D. M. Pozar, *Microwave and RF wireless systems*. New York: John Wiley, 2001.

[29] S. A. Maas, *Microwave mixers*, 2nd ed. Boston, MA: Artech House, 1993.

[30] Infineon. (03/03/2015). *BAT15 Datasheet*. Available: http://www.infineon.com/dgdl/Infineon-BAT15SERIES-DS-v01_01-en.pdf?fileId=db3a304314dca3890114ff6b74ca0b48

[31] Avago. (03/03/2015). *HSMS-286X Datasheet*. Available: http://www.avagotech.com/docs/AV02-1388EN

[32] Avago. (03/03/2015). *HSMS-285X Datasheet*. Available: http://www.avagotech.com/docs/AV02-1377EN

[33] V. Diodes. (03/03/2015). *VDI Zero-Bias Detector diode Datasheet*. Available: http://vadiodes.com/images/pdfs/ZBD_20120727_Revision.pdf

[34] J. Hesler and B. Gelmont, "A discussion of power coupling bandwidth limitations of planar Schottky diodes at submillimeter wavelengths," in *Proceedings of the Nineteenth International Symposium on Space Terahertz Technology*, 1998, pp. 173-180.

[35] B. S. Yarman, *Design of ultra wideband antenna matching networks : via simplified real frequency technique*. Dordrecht: Springer, 2008.

[36] B. S. Yarman, *Design of ultra wideband power transfer networks*: John Wiley & Sons, 2010.

[37] R. G. Harrison, "Full nonlinear analysis of detector circuits using Ritz-Galerkin theory," in *Microwave Symposium Digest, 1992., IEEE MTT-S International*, 1992, pp. 267-270.

[38] Z. Zhang, R. Rajavel, P. Deelman, and P. Fay, "Sub-Micron Area Heterojunction Backward Diode Millimeter-Wave Detectors With 0.18 Noise Equivalent Power," *Microwave and Wireless Components Letters, IEEE,* vol. 21, pp. 267-269, 2011.

[39] A. Nimo, D. Grgic, T. Ungan, and L. M. Reindl, "A new family of passive wireless RF harvesters based on R-C-Quartz oscillators," in *Microwave Conference (EuMC), 2013 European*, 2013, pp. 511-514.

[40] Z. Liu, Z. Zhong, and Y.-X. Guo, "High-efficiency triple-band ambient RF energy harvesting for wireless body sensor network," in *RF and Wireless Technologies for Biomedical and Healthcare Applications (IMWS-Bio), 2014 IEEE MTT-S International Microwave Workshop Series on*, 2014, pp. 1-3.

[41] C. Valenta and G. Durgin, "Harvesting Wireless Power: Survey of Energy-Harvester Conversion Efficiency in Far-Field, Wireless Power Transfer Systems," *Microwave Magazine, IEEE,* vol. 15, pp. 108-120, 2014.

[42] G. Andia Vera, A. Georgiadis, A. Collado, and S. Via, "Design of a 2.45 GHz rectenna for electromagnetic (EM) energy scavenging," in *Radio and Wireless Symposium (RWS), 2010 IEEE*, 2010, pp. 61-64.

[43] W. Haboubi, H. Takhedmit, J.-D. Lan Sun Luk, S.-E. Adami, B. Allard, F. Costa, *et al.*, "An Efficient Dual-Circularly Polarized Rectenna for RF Energy Harvesting in the 2.45 GHz Ism Band," *Progress In Electromagnetics Research,* vol. 148, pp. 31-39, 2014.

[44] B. R. Franciscatto, V. Freitas, J.-M. Duchamp, C. Defay, and T. P. Vuong, "High-efficiency rectifier circuit at 2.45 GHz for low-input-power RF energy harvesting," in *Microwave Conference (EuMC), 2013 European*, 2013, pp. 507-510.

[45] V. Marian, B. Allard, C. Vollaire, and J. Verdier, "Strategy for Microwave Energy Harvesting From Ambient Field or a Feeding Source," *IEEE Transactions on Power Electronics*, vol. 27, pp. 4481-4491, Nov 2012.

[46] G. Marrocco, L. Mattioni, and C. Calabrese, "Multiport sensor RFIDs for wireless passive sensing of objects—Basic theory and early results," *Antennas and Propagation, IEEE Transactions on,* vol. 56, pp. 2691-2702, 2008.

[47] J. A. Hagerty, F. B. Helmbrecht, W. H. McCalpin, R. Zane, and Z. B. Popovic, "Recycling ambient microwave energy with broad-band rectenna arrays," *IEEE Transactions on Microwave Theory and Techniques,* vol. 52, pp. 1014-24, 2004.

[48] S. J. Roundy, "Energy scavenging for wireless sensor nodes with a focus on vibration to electricity conversion," Ph.D. dissertation, Mechanical Engineering, University of California, Berkeley, 2003.

[49] W. Wang, S. Hemour, and K. Wu, "Coupled resonance energy transfer over gigahertz frequency range using ceramic filled cavity for medical implanted sensors," *Microwave Theory and Techniques, IEEE Transactions on,* vol. 62, pp. 956-964, 2014.

[50] Z. Popovic, "Cut the cord: Low-power far-field wireless powering," *Microwave Magazine, IEEE,* vol. 14, pp. 55-62, 2013.

[51] D. Masotti, A. Costanzo, P. Francia, M. Filippi, and A. Romani, "A Load-Modulated Rectifier for RF Micropower Harvesting With Start-Up Strategies," *Microwave Theory and Techniques, IEEE Transactions on,* vol. 62, pp. 994-1004, 2014.

[52] J. Karlovský, "The curvature coefficient of germanium tunnel and backward diodes," *Solid-State Electronics,* vol. 10, pp. 1109-1111, 1967.

[53] S. M. Sze and K. K. Ng, *Physics of semiconductor devices*: John Wiley & Sons, 2006.

[54] C. Burrus, "Backward diodes for low-level millimeter-wave detection," *Microwave Theory and Techniques, IEEE Transactions on,* vol. 11, pp. 357-362, 1963.

[55] L. Esaki, "New phenomenon in narrow germanium p− n junctions," *Physical Review,* vol. 109, p. 603, 1958.

[56] L. Esaki, "Discovery of the tunnel diode," *Electron Devices, IEEE Transactions on,* vol. 23, pp. 644-647, 1976.

[57] R. Meyers, P. Fay, J. Schulman, S. Thomas III, D. Chow, J. Zinck, *et al.*, "Bias and temperature dependence of Sb-based heterostructure millimeter-wave detectors with improved sensitivity," *Electron Device Letters, IEEE,* vol. 25, pp. 4-6, 2004.

[58] J. Schulman, E. Croke, D. Chow, H. Dunlap, K. Holabird, M. Morgan, *et al.*, "Quantum tunneling Sb-heterostructure millimeter-wave diodes," in *Electron Devices Meeting, 2001. IEDM'01. Technical Digest. International*, 2001, pp. 35.1. 1-35.1. 3.

[59] H. Moyer, J. Schulman, J. Lynch, J. Schaffner, M. Sokolich, Y. Royter, *et al.*, "W-band Sb-diode detector MMICs for passive millimeter wave imaging," *Microwave and Wireless Components Letters, IEEE,* vol. 18, pp. 686-688, 2008.

[60] N. Su, R. Rajavel, P. Deelman, J. N. Schulman, and P. Fay, "Sb-heterostructure millimeter-wave detectors with reduced capacitance and noise equivalent power," *Electron Device Letters, IEEE,* vol. 29, pp. 536-539, 2008.

[61] J. J. Lynch, H. P. Moyer, J. H. Schaffner, Y. Royter, M. Sokolich, B. Hughes, *et al.*, "Passive millimeter-wave imaging module with preamplified zero-bias detection," *Microwave Theory and Techniques, IEEE Transactions on,* vol. 56, pp. 1592-1600, 2008.

[62] J. Schulman and D. Chow, "Sb-heterostructure interband backward diodes," *Electron Device Letters, IEEE,* vol. 21, pp. 353-355, 2000.

[63] N. Su, Y. Tang, Z. Zhang, T. Kuech, and P. Fay, "Observation and control of electrochemical etching effects in the fabrication of InAs⁄ AlSb⁄ GaSb heterostructure devices," *Journal of Vacuum Science & Technology B*, vol. 26, pp. 1025-1029, 2008.

[64] M. Shams, I. Bin, Y. Xie, Y. Lu, and P. Fay, "An accurate interband tunneling model for InAs/GaSb heterostructure devices," *physica status solidi (c)*, vol. 10, pp. 740-743, 2013.

[65] Keysight. (2002, 29/06/2015). *[VBA Sample Program] Adapter Characterization. User Manual No. 16000-95024*. Available: http://www.keysight.com/main/editorial.jspx?cc=VN&lc=vie&ckey=85082&nid=-11143.0.00&id=85082

[66] Agilent. (29/06/2015). *Measuring Noninsertable Devices. Product Note No. 8510-13*. Available: http://cp.literature.agilent.com/litweb/pdf/5956-4373E.pdf

[67] J. Randa, W. Wiatr, and R. L. Billinger, "Comparison of adapter characterization methods," *Microwave Theory and Techniques, IEEE Transactions on*, vol. 47, pp. 2613-2620, 1999.

[68] C. H. P. Lorenz, S. Hemour, and K. Wu, "Modeling and Influence of Matching Network Insertion Losses on Ambient Microwave Power Harvester," presented at the Conference on Numerical Electromagnetic and Multiphysics Modeling and Optimization (NEMO), 2015 IEEE MTT-S International, Ottawa (ON) Canada, 2015.

[69] A. Dolgov, R. Zane, and Z. Popovic, "Power management system for online low power RF energy harvesting optimization," *Circuits and Systems I: Regular Papers, IEEE Transactions on*, vol. 57, pp. 1802-1811, 2010.

[70] Y.-H. Suh and K. Chang, "A high-efficiency dual-frequency rectenna for 2.45- and 5.8-GHz wireless power transmission," *IEEE Transactions on Microwave Theory and Techniques*, vol. 50, pp. 1784-1789, 2002.

[71] C. M. Ghiglino, "Ultra-wideband (UWB) rectenna design for electromagnetic energy harvesting," *Masters theses, Dept. Teoria del Senyal i Comun., Escola Técnica Superior d'Enginyeria de Telecomun. de Barcelona, Catalunya, Spain,* 2010.

[72] E. Falkenstein, M. Roberg, and Z. Popović, "Low-power wireless power delivery," *Microwave Theory and Techniques, IEEE Transactions on*, vol. 60, pp. 2277-2286, 2012.

[73] K. Lui, A. Vilches, and C. Toumazou, "Ultra-efficient microwave harvesting system for battery-less micropower microcontroller platform," *IET microwaves, antennas & propagation*, vol. 5, pp. 811-817, 2011.

[74] S. Riviere, F. Alicalapa, A. Douyere, and J.-D. Lan Sun Luk, "A compact rectenna device at low power level," *Progress In Electromagnetics Research C*, vol. 16, pp. 137-146, 2010.

[75] H. Takhedmit, B. Merabet, L. Cirio, B. Allard, F. Costa, C. Vollaire, *et al.*, "A 2.45-GHz dual-diode RF-to-dc rectifier for rectenna applications," in *Microwave Conference (EuMC), 2010 European*, 2010, pp. 37-40.

[76] M. Roberg, T. Reveyrand, I. Ramos, E. A. Falkenstein, and Z. Popovic, "High-efficiency harmonically terminated diode and transistor rectifiers," *IEEE Transactions on Microwave Theory and Techniques*, vol. 60, pp. 4043-4052, 2012.

[77] R. Casanova, A. Arbat, O. Alonso, A. Sanuy, J. Canals, and A. Dieguez, "An Optically Programmable SoC for an Autonomous Mobile mm-Sized Microrobot," *Circuits and Systems I: Regular Papers, IEEE Transactions on,* vol. 58, pp. 2673-2685, 2011.

[78] H. Gao, M. K. Matters-Kammerer, P. Harpe, D. Milosevic, U. Johannsen, A. van Roermund, *et al.*, "A 71GHz RF energy harvesting tag with 8% efficiency for wireless temperature sensors in 65nm CMOS," in *Radio Frequency Integrated Circuits Symposium (RFIC), 2013 IEEE*, 2013, pp. 403-406.

[79] N. Weissman, S. Jameson, and E. Socher, "W-Band CMOS on-chip energy harvester and rectenna," in *Microwave Symposium (IMS), 2014 IEEE MTT-S International*, 2014, pp. 1-3.

[80] D. B. Rutledge, D. P. Neikirk, and D. P. Kasilingam, "Integrated circuit antennas," *Infrared and millimeter waves,* vol. 10, pp. 1-90, 1983.

[81] S. Ladan, S. Hemour, and K. Wu, "Towards millimeter-wave high-efficiency rectification for wireless energy harvesting," in *Wireless Symposium (IWS), 2013 IEEE International*, 2013, pp. 1-4.

[82] A. Boaventura, A. Collado, N. B. Carvalho, and A. Georgiadis, "Optimum behavior: Wireless power transmission system design through behavioral models and efficient synthesis techniques," *Microwave Magazine, IEEE,* vol. 14, pp. 26-35, 2013.